UC Riverside
UC Riverside Electronic Theses and Dissertations

Title

Scalable Synthesis of Monolayer Graphene and Graphene Oxide Films by CVD

Permalink

Author

Ruiz, Isaac

Publication Date

2015

Peer reviewed|Thesis/dissertation

UNIVERSITY OF CALIFORNIA
RIVERSIDE

Scalable Synthesis of Monolayer Graphene and Graphene Oxide Sheets by
Chemical Vapor Deposition

Doctor of Philosophy

in

Electrical Engineering

by

Isaac Ruiz

June 2015

Dissertation Committee:
        Dr. Mihrimah Ozkan, Chairperson
        Dr. Cengiz S. Ozkan
        Dr. Elaine Haberer
        Dr. Sandeep Kumar

The Dissertation of Isaac Ruiz is approved:

_____

_____

_____

_____

Committee Chairperson

University of California, Riverside

Acknowledgements

Dedications

I'd like to dedicate this to my parents, sister and my wife.

ABSTRACT OF THE DISSERTATION

Towards the Scalable Synthesis of Graphene and Graphene Oxide Sheets by
Chemical Vapor Deposition

by

Isaac Ruiz

Doctor of Philosophy, Graduate Program in Electrical Engineering
University of California Riverside, June 2015
Dr. Mihrimah Ozkan, Chairperson

Over the last decade, graphene has generated immense excitement in the

scientific and engineering community due to its extraordinary properties

stemming from its 2 dimensional structure. As research in graphene has begun

to taper off and demand for its applications begins to increase, the challenge of

synthesizing large uniform sheets of graphene for mass production has begun to

be undertaken. To date, one of the most promising methods of fabricating large,

uniform, single layer, high quality graphene is on Cu foils by chemical vapor

deposition. In this work, some of the inherit synthesis problems of graphene on

Cu foils by CVD are studied and solved. The first problem examined is the

formation of contamination on the surface of graphene grown inside quartz tubes.

This contamination, commonly referred to as "the white dots", has been the

subject of much confusion and speculation, with its source being unknown and

it's composition never thoroughly studied, until it is presented here along with a

simple solution to avoid the contamination. The second problem address in this dissertation is that of rapid synthesis of uniform, single layer graphene sheets by CVD. While much work has been focused on recipe optimization in order to produce high quality graphene sheets, here another approach is taken. Using a generic recipe which will saturate the Cu substrate with graphene quickly, emphasis on Cu foil preparation is taken in order to produce high quality, uniform single layer graphene sheets in as little as a 60 second growth time. The surface morphology of the foils, which allow the self-limiting growth of graphene on the Cu foils is examined and shown to be implementable on inexpensive Cu foils. This allows for the potential to synthesize large sheets of uniform single layer graphene rapidly and inexpensively, with a relatively low initial capital investment. Finally, a new method for synthesizing graphene oxide by chemical vapor deposition s introduced. This method is the first to be able to produce uniform single layer sheets of graphene oxide, which is scalable for semiconducting applications. This opens up the possibility for tunable functionalization of the graphene oxide and potential for band gap introduction in graphene.

Table of Contents

List of Figures

higher energy transitions to the lower energy vacancy and in the process emits an X-ray, whose energy is then measured by a photodetector. (42)

Introduction

The isolation of a 2 dimensional (2D) film was the culmination in the evolution of nanomaterials, which had begun 20 years earlier.   Interestingly enough, Carbon's allotropes have played an important part in story of nanomaterials and have spurred much excitement with each new discovery. While Carbon itself has played a vital role throughout human history, including being the "element of life" due to its ability to bond with other elements in almost unlimited ways, it is fascinating that researchers are still finding new ways for Carbon to bond to itself.   And even more important is that each new Carbon allotrope has displayed extraordinary properties, repeatedly breaking new records for its properties and being hailed as the world's newest "Wonder Material". The latest of these materials is graphene, and as the world's first 2D material, graphene has sparked the same immense interest that its predecessors have. With the massive excitement has come great hopes for graphene's future applications[1].

In order to understand the promise that nanomaterials have to offer, we must first define what constitutes a nanomaterials. An n-Dimensional (nD) material, where n=0,1,2 or 3, refers to the number of dimensions not confined by 100 nm or less. A 0D material is confined in all three dimensions, with some examples including quantum dots or other nanoparticles. 1D materials are not confined in only 1 dimension or alternatively confined in 2 dimensions, with examples of 1D materials including nanotubes, nanowires and nanorods. Finally,

2D materials are only confined in 1 dimension, thus usually appear as flat sheets, with the most famous examples of 2D materials being monoatomic layers of atoms and nanofilms. A 3D material is a material in which is it not confined by 100 nm or less in any dimension, thus it is considered a bulk nanomaterial. Bulk nanomaterials typically exhibit nano-crystalline structures or are made up by multiple nD materials, such as bundles of 1D material or certain arrangements of 0D materials. Illustrations of 0D, 1D, 2D and 3D nanomaterials are shown in Figure 1. For any of 0D, 1D or 2D materials the crystal structure can be either crystalline or amorphous.
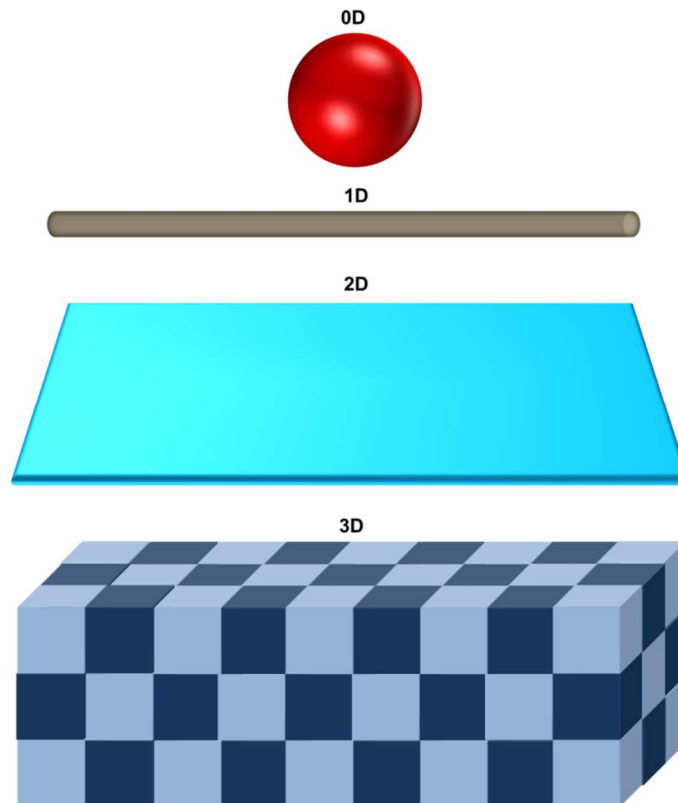
Figure I.1: Illustration of possible 0D, 1D, 2D and 3D nanomaterial configurations.

It is primarily through the confinement and/or delocalization of the electrons in these materials that the materials quantum behavior begins become apparent. For 0D materials the electrons are completely confined, 1D and 2D nanomaterials have their electrons both confined and delocalized and 3D materials have the electrons only fully delocalized. The quantum behavior created by confinement is caused by the same effect seen in the elementary "Particle in a Box" example in elementary quantum mechanics. In the simplest case an electron is confined in 1 dimension (such as in a 2D nanomaterial) between two infinite potentials. In this infinite potential well the electron is confined within a length, a, as shown in figure I.2. Classically the electron would exhibit a continuous energy spectrum, however using Schrödinger's equation to solve for the energies of the confined electron, (equation I.1), the electron energies will instead be at discrete energy levels. The discrete energy levels are dependent on the electron confinement, where greater confinement creates wider distance between the energy levels.

$$i\hbar\frac{\partial\Psi(x,t)}{\partial t} = -\frac{\hbar^2}{2m}\frac{\partial^2\Psi(x,t)}{\partial x^2} + U(x)\Psi(x,t) \qquad \text{Equation 1}$$

Solving for the wave function, Ψ, in the infinite well problem using Schrödinger's equation and solving for the energy will demonstrate the effect that quantum confinement has on the discrete energy spectra. The solution to Schrodinger's yields equation 2, where k=nπ/a, where n=1,2,3,…, due to the

$$\Psi(x) = \sin\left(\frac{n\pi}{a}x\right) \qquad \text{Equation 2}$$

3
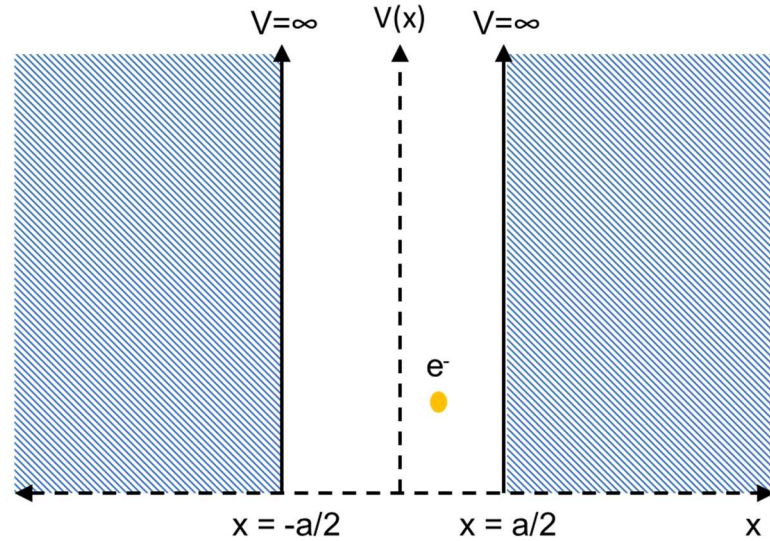
Figure I.2: *Infinite Potential Well*

boundary conditions. After normalizing the solution wave function and inserting it

back into Schrödinger's equation, the energy can be solved for. The energies

are given by equation 3,

$$E_n = \frac{n^2 \hbar^2 \pi^2}{2ma^2}$$
<div align="right">Equation 3</div>

and are dependent on the potential well width, a, and the energy level n. Figure

I.3 shows the first few wave functions of the along with their energy levels. Many

of the common and useful results in quantum mechanics can be learned from

this problem but the one of interest here is the energy dependence on the

confinement. As the confinement length, a, gets smaller the energy levels begin

to get further away from each other as n increases. If the confinement gets larger

the energy levels begin to get closer together until eventually they are close

enough to be indistinguishable, as is the case in classical mechanics. These results are easily extended to 2 and 3 dimensional confinement.

$$\Psi_5(x) = \sqrt{\frac{2}{a}} \sin\left(\frac{5\pi}{a} x\right) \qquad \text{n=5}$$

$$\Psi_4(x) = \sqrt{\frac{2}{a}} \sin\left(\frac{4\pi}{a} x\right) \qquad \text{n=4}$$

$$\Psi_3(x) = \sqrt{\frac{2}{a}} \sin\left(\frac{3\pi}{a} x\right) \qquad \text{n=3}$$

$$\Psi_2(x) = \sqrt{\frac{2}{a}} \sin\left(\frac{2\pi}{a} x\right) \qquad \text{n=2}$$

$$\Psi_1(x) = \sqrt{\frac{2}{a}} \sin\left(\frac{\pi}{a} x\right) \qquad \text{n=1}$$

x = -a/2   x = a/2   x
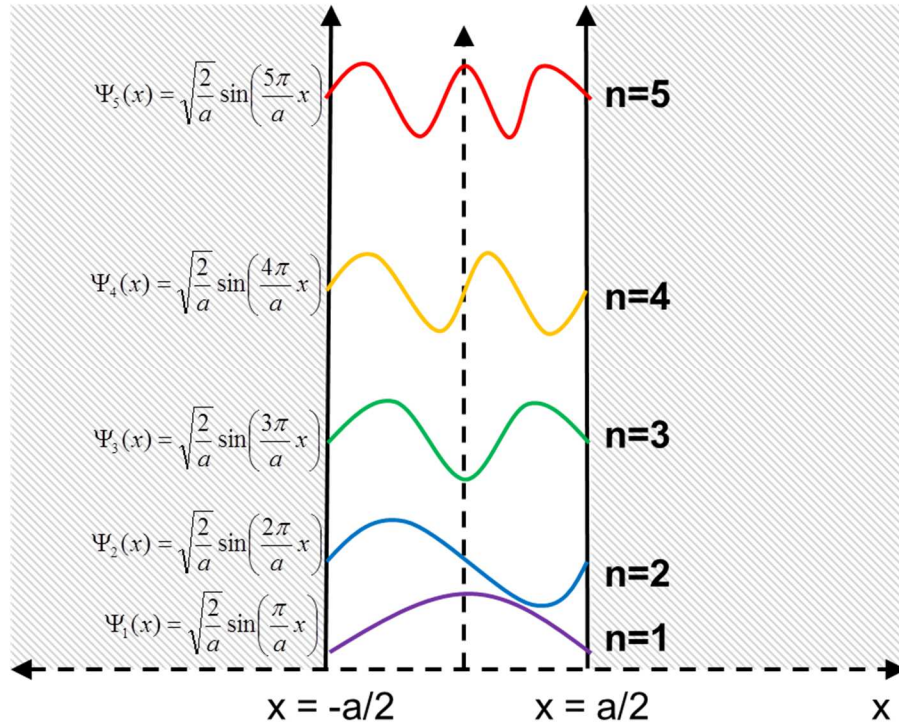
Figure I.3 Wave function solutions to Infinite potential well.

Although this problem is an elementary result in quantum mechanics, it serves to show the how nano-confinement of materials cause them to behave differently than bulk materials. Nanomaterials are governed by the laws of quantum mechanics, while typical bulk materials are primarily governed by classical physics and statistical mechanics. Just as the formulation of quantum mechanics revealed new physics, insights and excitement in science, so has the discovery of nanomaterials. Over the past 30 years, nanomaterials have begun to emerge and display extraordinary promise with their unique properties. It can

be argued that no nanomaterials have generated as much excitement as the newest allotropes of carbon, fullerene (Bucky ball), carbon nanotubes and graphene. These materials themselves tell a certain thread of the history of nanomaterials and their progress into the future[2,-5].

Previously it was believed that the only three carbon allotropes were graphite, diamond and amorphous carbon. However in 1985 the first fullerene particle, C_{60}, was discovered, at Rice University by Smalley, Curl and Kroto, and it kick started an avalanche of a whole new class of carbon allotropes. The round symmetrical C_{60} fullerene was named after architect Buckminster Fuller who was known for his spherical architectural designs. C_{60} is made up of 32 facets consisting of 20 hexagons and 12 pentagons, with carbon atoms at the vertice. At the time of its discovery it was the largest and most symmetrical molecule, and in 1996 it earned its discoverers the Noble Prize in Chemistry. However C_{60}, was just the beginning, as future work produced various other symmetrical carbon molecules, including C_{70}, C_{76} and C_{84}. Fullerene didn't initially create great promise other than a mild curiosity because it was difficult to produce in large quantities; however when an arc discharge method was discovered to produce large quantities of the materials, then fullerene research and its applications began to quickly rise[6-8].

One of the very interesting properties that fullerenes had is that they could form crystal structures very similarly to how atoms arrange themselves. They bond like individual graphite layers do, through van der Walls forces in a regular

crystal arrangement and are as chemically stable as graphite. An even more exciting result from these fullerene crystals was found when the fullerenes were doped with certain chemicals. It was shown that the fullerene crystals exhibit superconductivity when doped with K and showed similar behavior when doped with certain other elements. Now almost 30 years after their discovery, fullerenes have found applications in lubricants, as a biopharmaceutical drug delivery molecule and in semiconducting industry as a next generation photoresist.

Along with the arc discharge formation of Bucky balls, there was a separate carbon allotrope that went unnoticed or was ignored initially, carbon nanotubes. The discovery of carbon nanotubes (CNT's) is itself deserving of a Noble prize however it never did win one. In 1991, in the soot of the arc discharge chamber, Sumio Iijima, discovered the first CNT's, while later that same year a new method for producing CNT films by chemical vapor deposition was discovered. The excitement over the CNT's finally took off when MIT, and other groups published the first theoretical results about the electrical properties of single wall carbon nanotubes. The results were almost too good to be true. CNT's were later found not only have great electrical properties but also thermal, optical and mechanical properties. This is a theme that would be echoed in future graphene allotrope discoveries.

Just as carbon Bucky balls came in different varieties, so do CNT's. CNT's can vary in diameter, chirality, and number of walls, with each component

altering the physical properties of the nanotubes. Even just within single wall

CNT's their properties vary depending on their chirality and diameter. Single wall

CNT's are arguably the most interesting of the CNT types because they have

shown great versatility in their properties while also displaying extraordinary (too

good to be true) properties. Figure I.6 shows the crystal lattice of a flat sheet of

graphene, which can be rolled up to make single wall CNT's. The graphene

crystal has 2 lattice vectors a_1 and a_2, with the chiral (roll) vector, C_h, being equal

to equation 4, where n and m are positive integer values[9,10].

$$C_h = na_1 + ma_2$$
Equation 4

The chiral vector, C_h, points in the direction in which the tube will be rolled

into while the length determines the circumference of the tube, thus also

determining the diameter. The unlimited combinations for n and m, give rise to

unlimited combinations of CNT structures. The three parent single wall CNT's

and are named zig zag, arm chair and chiral CNT's. Zig zag CNT's are the

simplest to construct. They're C_h vector only consist of the component vector a_1,

with n equal to any integer value, while m is equal to 0. They are referred to as

zig zag CNT's because parallel to the circumference of the nanotube the crystal

structure follows a zig zag path. Armchair CNT's has lattice vector components

that are equal, where n=m. When following the crystal lattice parallel to the

direction of the circumference of the nanotube, the crystal structure follows an

armchair path all the way around. Another way to think about it is that the zig

zag structure will run parallel to the tube length. The third case is any case other

than the one previously described, where the lattice constants are (m,n). The zig zag path will follow some orientation to the tube length at some angle not equal to 0 or 90 degrees. The chirality of the single wall CNT's is very important because it is what determines the type of properties it will have[9,10].

Soon after they were discovered some theoretical modeling of single wall CNT's (SWCNT's) showed them to have great electrical properties such as very high carrier mobility. When initially experimentally tested the mobility values of SWCNT's were only about 200 cm^2/Vs, which was less than promising. However with higher quality and longer CNT's mobility values have more recently exceeded over 10,000 cm^2/Vs. However that wasn't the extent of CNT's capabilities. As mentioned before CNT's come in an unlimited number of chirality's, which can itself alter the electrical properties. One of the most unique results about SWCNT chirality is that it can alter whether a CNT's electrical properties are metallic or semiconducting. When 2(n + m) is an integer multiple of 3 then the SWCNT will be metallic, while all other cases will produce semiconducting SWCNT's, with a bang gap, E_g, dependent on n and m values. This allows for great versatility of electrical behavior between different CNT architectures[10].

Another property that caught researcher's and the public's attention was CNT's mechanical strength. At the time of their discovery and first measurements of their mechanical properties it was found that CNT's were the strongest materials ever measured. Young's modulus values have been

measured over 1TPa but vary depending on CNT size and number of walls. Tensile strengths were also found to be as high as 63 GPa, again varying depending on tube size and wall count. These properties created a lot of excitement over their applications as a building material and many believed carbon nanotubes were the future of nanotechnology9,10.

After over 20 years since carbon nanotubes first discovery, they have not yielded the results that everyone had expected of them. Even with their superior electrical, thermal and mechanical properties intense research and effort to bring them to a realizable market has plagued CNT's severely. 3 major problems have limited CNT's from emerging into the market. The most difficult obstacle has been price. Although the price per gram of CNT's has fallen drastically from over $1000 per gram to now below $50 per gram, it is still exceedingly higher than where it needs to be to make it a viable wide use material. The second problem is the difficult or lack of control of CNT chirality synthesis. It has proven to be exceedingly difficult repeatedly grow large amounts of specific types of CNT's. For example when growing CNT's by chemical vapor deposition (CVD), many types of CNT's will be formed and will vary by length, wall count, diameter and chirality. There are methods available to separate different tubes but they can be time consuming and again not yield large amounts of specific CNT's. Finally the problem of physically manipulating and arranging the nanotubes has been a difficult problem to overcome. Because of their nano-size it has proved to be

exceedingly difficult to arrange the tubes into large arrays that would make them useful.

One example for the limited applicability of CNT's is the problem with horizontally aligning the nanotubes across wafers in order to be used as a field emission (FET) channel. CNT's have great potential as post a post Si age material however no practical method at this point can implement CNT's into large scale semiconducting manufacturing processes. Ideally a method for growing uniform horizontally aligned CNT's on insulating substrates would have been developed in order to be quickly implement CNT's into the current fab process; however the results have not been fruitful yet. Another example is for use as a building material. The problem for implementing in large scale has been very limited up to this point. Although it has found applications as a fabric and alloying material, for use as a bulletproof protective vest and for use in making sports gear strong, it has not been able to be produced in large enough quantities to be used for building bridges, skyscrapers or anything substantial. Again the problem is the relatively small yields that current synthesis methods provide (arc discharge, CVD, solution based) and the cost per gram. Although in the future some of these problems may be solved, as of right now there doesn't seem be any immediate solution to these problems on the visible horizon.

Finally we reach the newest carbon allotrope graphene, which will the focus of this dissertation. Over the last 10 years the same excitement that CNT's experienced the proceeding decade has captured scientist and engineers about

graphene. Graphene, "the mother of all graphitic materials", shares some similar properties and traits that Fullerene and CNT's have while also surpassing some of their properties.   However it is its unique 2D nature, which makes it isotropic that may be the difference between realizable applications or just a unique scientific curiosity.

In the proceeding chapter the detailed origins of graphene's extraordinary electrical, mechanical, thermal and optical properties will be discussed. Followed by the characterization methods for graphene in chapter 2. Chapter 3 will focus on reducing contamination of graphene grown by chemical vapor deposition on Cu foils. Chapter 4 will focus on the effect that different Cu foil manufacturers and Cu surface morphology have on the formation of a self-limiting single layer graphene films as well as a method for producing rapid synthesis of high quality single layer graphene films on inexpensive Cu foils. Finally Chapter 5 will discuss a novel method to synthesize monolayer graphene oxide films by chemical vapor deposition.

References

1. Geim, A. K., & Novoselov, K. S. (2007). The rise of graphene. Nature materials, 6(3), 183-191.

2. Dai, H., Wong, E. W., & Lieber, C. M. (1996). Probing electrical transport in nanomaterials: conductivity of individual carbon nanotubes. Science, 272(5261), 523-526.

3. Ross, F. M., Tersoff, J., & Tromp, R. M. (1998). Coarsening of self-assembled Ge quantum dots on Si (001). Physical Review Letters, 80(5), 984.

4. Wolkin, M. V., Jorne, J., Fauchet, P. M., Allan, G., & Delerue, C. (1999). Electronic states and luminescence in porous silicon quantum dots: the role of oxygen. Physical Review Letters, 82(1), 197.

5. Morales, A. M., & Lieber, C. M. (1998). A laser ablation method for the synthesis of crystalline semiconductor nanowires. Science, 279(5348), 208-211.

6. Mintmire, J. W., Dunlap, B. I., & White, C. T. (1992). Are fullerene tubules metallic?. Physical Review Letters, 68(5), 631.

7. José-Yacamán, M., Miki-Yoshida, M., Rendon, L., & Santiesteban, J. G. (1993). Catalytic growth of carbon microtubules with fullerene structure. Applied physics letters, 62(2), 202-204.

8. Iijima, S., & Ichihashi, T. (1993). Single-shell carbon nanotubes of 1-nm diameter.

9. Saito, R., Dresselhaus, G., & Dresselhaus, M. S. (1998). Physical properties of carbon nanotubes (Vol. 35, pp. 73-81). London: Imperial college press.

Chapter 1

Introduction to Graphene

Although graphene is perhaps the most simple carbon allotrope to visualize, it has been up until recently the most difficult to isolate experimentally. Although the properties of a single layer of graphite has been studied since at least the mid 20th century, it wasn't until the 21st century that the theory of the material could be tested experimentally. In only the first decade since graphene's first isolation, the potential for the application of graphene is staggeringly obvious due to its extraordinary properties. It is important to note that many of these properties are not only predicted theoretically but also tested experimentally. In this chapter the basic structure of graphene will be introduced, along with its history, properties and potential applications.

1.1 Crystal Structure of Graphene

Graphene, quite simply put, is a single layer of sp^2 bonded carbon atoms arranged hexagonally as shown in figure 1.1. An alternative way to think about graphene is to consider it a single layer of graphite, which is comprised on van der waals bonded stacks of graphene. In graphite the distance between layers is approximately 3.354 Angstroms, and the energy needed to separate two graphene layers from each other has been calculated to be 61 meV per carbon atom. The carbon-carbon bonds are σ bonds, while leaving behind a free P$_z$

orbital electron or dangling π bond, on the outer plane. It is these sp^2 bonds that allow graphene to have such strong mechanical properties, while the dangling π bonds allow for the incredible electrical, optical and thermal properties. Later in this chapter we will go in more detail about graphene's properties and how they're related to its crystal structure and free π orbital.
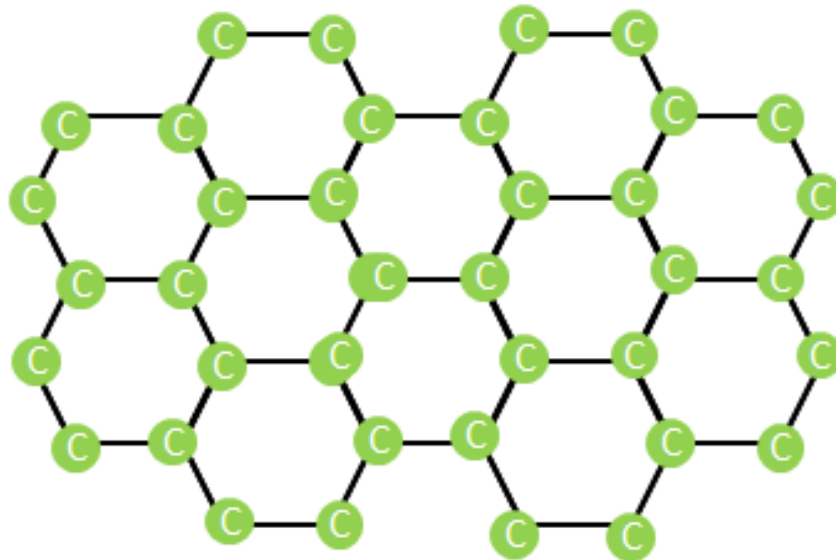
Figure 1.1: *Hexagonal/Honeycomb Arrangement of Carbon Atoms*

In figure 1.2 graphene's unit cell and reciprocal lattice are shown. It is worth noting that the unit vectors for graphene crystal are the same as shown previously for carbon nanotubes. It is worth noting that the honey comb arrangement of carbon atoms are not a Bravais lattice. The unit cells are marks by red arrows and dashed lines and it is shown to be a rhombic unit cell, with two atoms per unit cell, atoms A and B. The black arrows are the lattice vectors, $\mathbf{a_1}$

and **a₂**, while δᵢ, indicates the distance between its nearest neighbors, which for this case is 1.42 Angstroms. The lattice vectors **a₁** and **a₂** are given by equations 1.1. In these equations a is the bond length between carbon atoms, which again is 1.42 Angstroms.
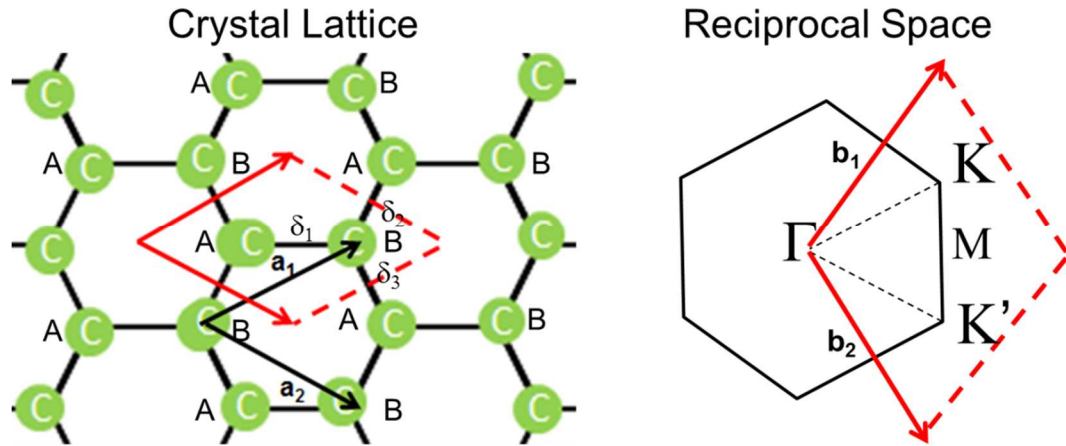
Figure 1.2: *Graphene honeycomb arrangement, with unit cell (red) and unit vectors (black) and its reciprocal space representation with important gamma, M and K points labeled in the Brillouin zone.*

$$a_1 = \frac{3a}{2}\left(\hat{x} + \frac{1}{\sqrt{3}}\hat{y}\right); \quad a_2 = \frac{3a}{2}\left(\hat{x} - \frac{1}{\sqrt{3}}\hat{y}\right) \qquad \text{Equations 1.1}$$

Also in figure 1.2 the reciprocal lattice is shown, which displays a hexagonal Brillouin zone and its lattice vectors, **b₁** and **b₂**, and again a rhombic unit cell in red. Some of the Brillouin zones most important points are also shown in figure 1.2. The Γ point is located in the center of the Brillouin zone while the

K and M points are at the corners and the midpoint between the corners, respectively. K' is considered an equivalent point to K and are known as the Dirac points, which is where the famous Dirac cones are centered about. Equation 1.2 shows the reciprocal lattice vectors **b₁** and **b₂**.

$$b_1 = \frac{2\pi}{3a}\left(\hat{x} + \sqrt{3}\,\hat{y}\right); \quad b_2 = \frac{2\pi}{3a}\left(\hat{x} - \sqrt{3}\,\hat{y}\right) \qquad \text{Equations 1.2}$$

1.2 History of Graphene

Although graphene has garnered the most excitement over the last ten years, since it was first isolated by the Manchester group using mechanical exfoliation, its history can be traced by over 150 years. As far back as the 1840's intercalation of graphite with various molecules had been demonstrated, which would increase the inter planer distance between the graphite layers. This would in turn cause a decoupling of the layers, which were shown to display very fascinating properties such as superconductivity. Into the mid and late 1800's graphite oxide was produced, which allowed for easy exfoliation of graphite oxide layers[1].

Starting in the 1930's the theoretical study of the electrical properties of individual graphite layers was carried out and it was shown that conductions within the plane was much greater than conduction between the planes. The conduction of a graphene film was predicted to be as much as 100 times greater than that of graphite. At that time however it was also believed that a single

atomic layer of graphite could not exist in nature nature due to thermal fluctuations, which would destroy long range order, essentially causing the single atomic layer to melt.   It was also believed that during the formation of graphene the perimeter to area ratios would favor the formation of other carbon allotropes over graphene.

In the 1960's and 1970's experimental work was being conducted to create small flakes of few layer graphite and graphite oxide.   In 1962, Boehm created thin lamellar flakes from chemical reduction of GO with very small amounts of oxygen and hydrogen. Measurements to determine the thickness of the GO layers were estimated to be 0.46 nm (only a slight deviation from current studies, 0.4 nm). Although it is believed that the measurements could have had large errors. Although Boehm later claimed that the thinnest of these sheets were single layer carbon, in reality it is believed that he was in fact measuring graphene oxide single layers.   In the 1970's, Blakely and etc., did a series of experiments on the surface segregation of mono and few layer carbon from transition metal substrates. These transition metals included Ni, Pt, Pd and Co. When the carbon was dissolved into these metals at high temperature, it was found that metal and carbon would separate, forming thin layers of carbon on the surface. LEED, Auger and STM were layer used to determine that these layers were in fact single and multiple layer graphene structures. Further experiments continued throughout that decade using SiC melts and were able to experimentally determine the C-C bond lengths in graphene[1].

Which now brings us to modern birth of the graphene revolution in the early 2000's. Initial work on micromechanical exfoliation was begun in 1999. Through lithographic patterning and plasma etching of highly oriented pyrolytic graphite (HOPG) was formed into multiple layer graphene. Finally in 2004, Geim, Novoselov, and etc., (Manchester) used the now infamous "Scotch Tape" method to exfoliate small flakes graphene onto a SiO2 substrate. On SiO2/Si substrates even single layer graphene is visible under an optical microscope and if the flake large enough even visible to the naked eye. Figure 1.4 shows what a typical exfoliated graphene flake looks like. It is typically nonuniform, consisting of varying layers and sometimes a single layer. On SiO2/Si substrates, the electric-field effects could now be studied, for which Geim and Novoselov would later win the Nobel Prize in Physics for[2].

Figure 1.3: *Mechanically exfoliated graphene on SiO$_2$ substrate.*

From 2004 and onward graphene has seen an influx of researchers trying to probe its intrinsic properties and it has not disappointed. Research articles have skyrocketed over the last decade in not just graphene, but other 2D materials as well such as hexagonal boron nitride, MoS_2, and other single layer dichalcogenides. Although this new class of materials can still be considered in its infancy, they hold a very high promise for potential for use in actual applications. Some of the unique properties of graphene and its potential applications will be discussed in the following sections.

1.3 Extraordinary Properties of Graphene

Repeatedly graphene has shown to be beyond extraordinary in almost every one of its physical properties. Not only has it repeatedly shown to experimentally display great properties in various aspects such as electrical, physical, chemical, optical and thermally but it has consistently been shown to have the best properties of all currently tested materials. This ranges from having the highest electrical and thermal conductivities, being the most transparent material and even being the world's strongest material. It is no wonder that it was labeled the "Wonder Material" of the 21st century. The following section will give a brief overview of some of the properties of graphene.

1.3.1 Electrical Properties

As mentioned earlier, graphene's electrical properties were expected to be much better than graphite's, according to theoretical calculations. However once graphene was experimentally isolated, it immediately confirmed these predictions, yielding very high conductivity and high carrier mobility. Graphene's electrical properties can be explained with by solving for the dispersion relationship of an infinite graphene film using the nearest neighbor tight binding model (NNTB). Here the Hamiltonian matrix is solved for, and then the eigenvectors and eigenvalues are determined and allow for the determination of the energy dispersion relationship as shown in equation 1.3.

$$E(\mathbf{k}) = \pm\gamma\sqrt{1 + \cos\left(\frac{\sqrt{3}a}{2}k_x\right)\cos\left(\frac{a}{2}k_y\right) + 4\cos^2\left(\frac{a}{2}k_y\right)} \qquad \text{Equation 1.3}$$

Figure 1.4 3D plot of graphene's energy dispersion relationship. Typical values used in equation 1.3 for γ are between 2.7 eV and 3.3 eV, however a commonly used value which was derived experimentally is 3.1 eV. Again, a is just the bond length between carbon atoms, which has a value of 1.42 Angstroms. The dispersion relation shown here are plotted in the brillouin zone. The dispersion relationship is symmetrical across the k_x-k_y plane where E is equal to zero. The most famous feature of the graphene dispersion relationship is the famous Dirac cones at the K points. The Dirac cones and Dirac points are one of the fundamental reasons for graphene's phenomenal electrical properties.

Graphene Dispersion Plot
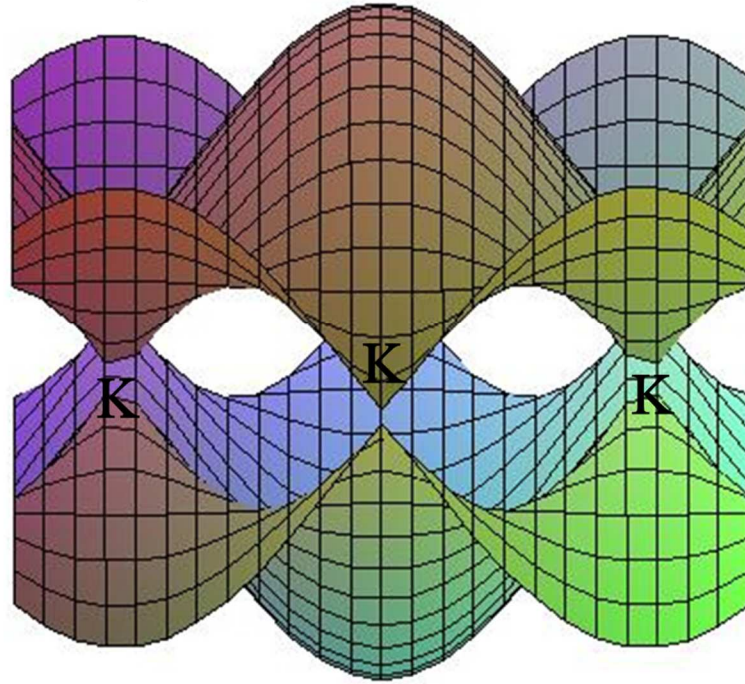
Figure 1.4: *3D plot of graphene's energy dispersion relationship.*

Figure 1.5 displays a closer look at the one of the Dirac cones at a low energy. The first noticeable feature is apparent lack of band gap between the lower valence band cone and the upper conduction band cone. This means that graphene is not semiconducting, but since E=0, there is singularity it is also not metallic, thus graphene has been labeled as a semimetal since it is a combination of both. The second important feature is the linearity of the Dirac cones at these low energies. The linearity of of the dispersion around the K points at these low energies is given by equation 1.4. The linear dispersion gives

$$E(k) = \hbar v_f \sqrt{k_x^2 + k_y^2} \qquad\qquad \text{Equation 1.4}$$
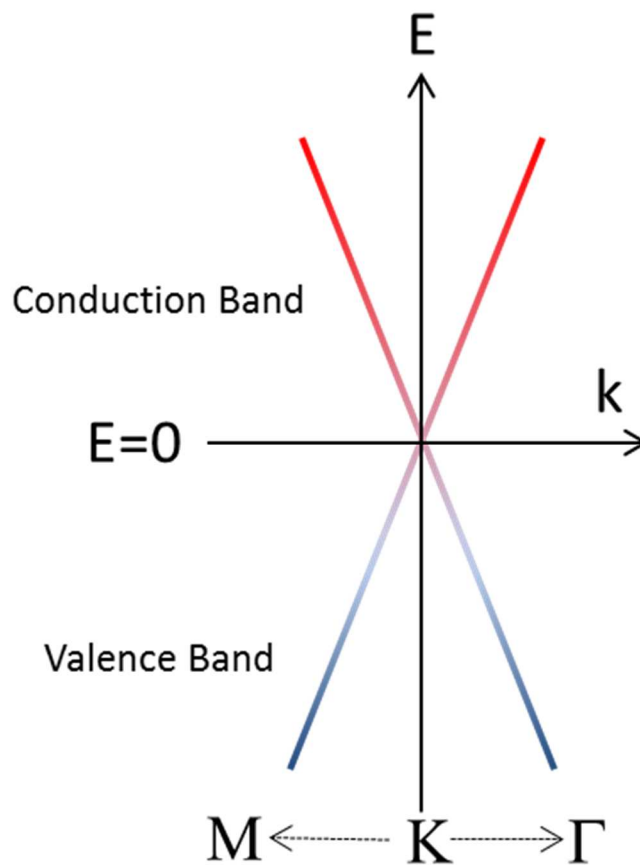
Figure 1.5: *Linear Dispersion near the K point.*

rise to very high Fermi velocities. The Fermi velocity is expected to be up to 10^6

m/s. Because of this graphene has been shown to have carrier mobilities of up

to 200,000 cm^2/Vs, and even higher, which is a record high and almost two

orders of magnitude of silicons, which is only about 1,400 cm^2/Vs. Graphene

also has the lowest resistivity of any material ever measured,at about 1.0 x 10^{-8}

Ωm. Gold and copper, the next two lowest resistivity materials have values of

1.59 x 10^{-8} Ωm and 1.68 x 10^{-8} Ωm, respectively. Other remarkable electrical

properties that have been measured have been room temperature quantum Hall

effect and spin coherence of up to several microns, which makes it a very promising material for spintronics for future applications.

Unfortunately the same dispersion relation that gives rise to graphenes extraordinary properties also limits graphene in future potential applications due to its lack of band gap. Fortunately there are methods to induce a band gap in graphene. One such method is substitutional doping with elements such as nitrogen or boron. However this method has shown to only induce very small band gaps with (meV), with doping concentrations of up to 25%, which drastically affect the graphene's mobility and resistivity. Another more promising method is by confining graphene even further in a second dimension to create a nanoribbon structure. By confining the graphene width to 20 nm or less a band gap is induced and is dependent on the graphene ribbon width. This would allow for exact tailoring of the graphene band gap, which is highly desirable in semiconducting applications. With the rise of extreme ultra violet (EUV) lithography sources, patterning at lengths of 20 nm or less should be common practice within a few years. Thus in the future it is not difficult to imagine wafer scale patterning of graphene films into graphene nanomesh structures used for logic devices, with only minimal degradation of its mobility and resistivity[3,4].

1.3.2 Optical Properties

The optical properties of graphene are also promising for future applications. Because graphene is only one atomic layer thick it is almost

entirely transparent for a very wide range of frequencies. Of course as you begin to stack more and more layers of graphene and form bilayer, tri layer and other multilayer, the transparency begins to reduce. Pristine single layer graphene is 2.3% transparent to red light. Interestingly enough the transparency is equal to πa, where a is the fine structure constant.
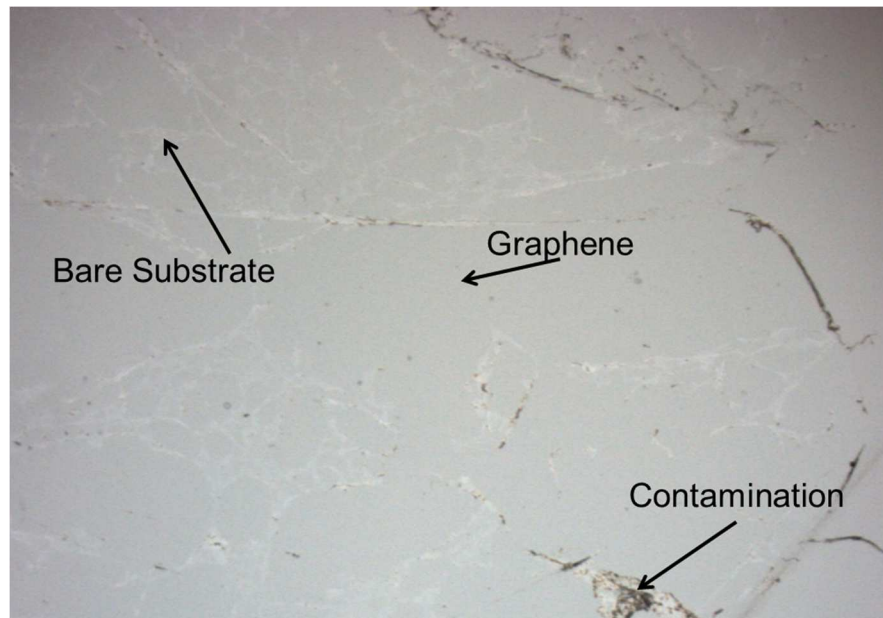
Figure 1.6: *Damaged graphene film on glass substrate. White light regions are bare area, dark areas are rolled up graphene films and contamination and grey areas are uniform single layer graphene films.*

In figure 1.6 shows an optical image of some damaged graphene grown by chemical vapor deposition was transferred onto a glass slide. The graphene grown by this method ended up with tears along the Cu grain boundaries resulting in a non-continuous graphene film on the slide. Thus here it the

comparison between the opacity of the glass and the graphene can be made by comparing the contrast between the two regions. The very light grey regions are the bare glass substrate, while the slightly darker grey regions are the single layer graphene films. The darker regions and lines are either contamination from the polymer used during the transfer or rolled up graphene residue caused by improper transfer preparation. As can be seen there is only the slightest contrast between the bare substrate and the graphene films.   This image was taken using white light. If it was taken using a red light source then the contrast would be even less obvious.

Graphene's high opacity and electrical properties make it an ideal material to be used as a transparent conductor. This lends itself to be useful in solar cell applications or as an electronic screen electrode, since it would allow for much brighter screens since so little will be absorbed by the glass, plastic outer covering.   Along with its high opacity graphene has also been shown to be a nonlinear optical materials and displays a non-linear Kerr effect, which could be used for soliton photonics in the future[5,6].

1.3.3 Mechanical Properties

Although graphene is the world's thinnest materials it is also, surprisingly, been measured to be the world's strongest material. Graphene has been measured to have a tensile of strength of up to 130 GPa. For reference, that's makes it about 200 times stronger than steel. However, although it is remarkably

strong it is also extremely flexible. It has a spring constant that has been measured between 1-5 N/m and a Young's modulus of 0.5 TPa. One of the most famous examples to illustrate graphene's strength is to compare it to a sheet of cellophane. If a sheet of graphene was as thick as cellophane and proportionally had the same mechanical properties then it would be able to hold and withstand a pencil with an elephant balanced on top of it without tearing the graphene sheet. The source of graphene's immense mechanical strength stems from its sp^2 carbon-carbon bonds which are some of nature's strongest.

Along with being strong and flexible, it is also very light. It was worked out that a football field sized sheet of graphene were fabricated it would weigh less than 1 gram. All of these properties make it an ideal material for sci-fi inspired projects, such as a space elevator. However in reality a single sheet of graphene is actually very fragile and cannot realistically be handled without being destroyed or damaged. Maybe in the future graphene compounds or twisted graphene ropes, where the collective strength of a very large amounts of graphene sheets can handle very large strains and stress[7].

1.3.4 Thermal Properties

Graphene's thermal properties have proven to be just as remarkable as the previously mentioned properties. As of this moment it has shown to be the be the best thermal conductor, showing thermal conductivity just as good as diamonds and better than carbon nanotubes. Initial experiments using a micro-

Raman to measure the thermal conductivity of suspended graphene, showed

conductivity values, K, of around 3000 W/mK. This is comparable to the thermal

conductivities of diamond and much higher than the thermal conductivity of silver,

which is 430 W/mK. However further experiments have measured conductivities

to range between 1500-5000 W/mK. Figure 1.7 shows the typical experimental

set up of the Raman measuring the thermal conductivity of a suspended

graphene sheet.
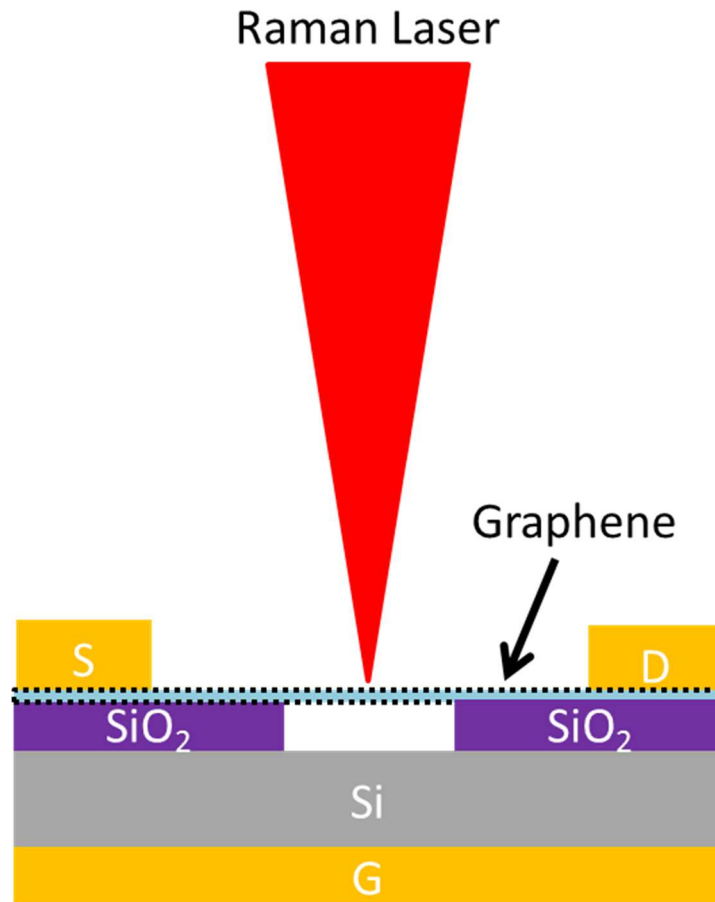
Figure 1.7: *Schematic of suspended graphene Micro-Raman*

measurement for thermal conductivity, K value calculation.

Along with high thermal conductivities comes low thermal resistivity. Graphene's thermal resistivity has been measured to be around 10^{-8}, where the exact value is dependent on the measurement condition. Free standing graphene will have the lowest resistivity values, while graphene on a substrate such as silicon dioxide will have higher thermal resistivity values[8].

1.3.5 Chemical Properties

Because of graphene's surface dangling π-bonds, it has a tendency to have a very reactive surface, along with very reactive edges. This allows for the alteration of some of its properties by simply functionalizing the surface with certain elements or molecules. This allows for tailoring of the electrical properties of graphene; however having a reactive surface can also serve in applications for detection. When a molecule attaches itself to the surface of a graphene sheet its conductivity is altered and can be measured by a change in current. This makes it an ideal material for chemical sensing. Considering that graphene is not a carcinogen like its nanotube counterpart, it may also be ideal in medical sensing, as it is expected to be completely safe for in-vivo applications.

Another useful property that graphene has displayed is that it is impermeable to gases. It has been demonstrated to be useful as a protective coating on metals to prevent oxidation or corrosion. For example on foils that have single layer graphene deposited on them by chemical vapor deposition, it has been demonstrated that leaving them exposed to air at room temperature or

even at slightly elevated temperatures, does not result in the oxidation of the metal. This has some obvious applications in systems in which oxidation or other corrosion are not desired. Depositing the graphene by CVD is not necessary either as the CVD process may damage the material that it is intended to be protected. An alternative would be the synthesis of a graphene paint or coating that consist of flakes of graphene, that can be easily spray coated onto any desired surface[2].

References

1. Boehm, H. P. (1994). Some aspects of the surface chemistry of carbon blacks and other carbons. Carbon, 32(5), 759-769.

2. Geim, A. K., & Novoselov, K. S. (2007). The rise of graphene. Nature materials, 6(3), 183-191.

3. Novoselov, K. S. A., Geim, A. K., Morozov, S., Jiang, D., Katsnelson, M., Grigorieva, I., ... & Firsov, A. (2005). Two-dimensional gas of massless Dirac fermions in graphene. nature, 438(7065), 197-200.

4. Gogotsi, Y. (2011). Controlling graphene properties through chemistry. The Journal of Physical Chemistry Letters, 2(19), 2509-2510.

5. Mikhailov, S. A. (2009). Non-linear graphene optics for terahertz applications. Microelectronics Journal, 40(4), 712-715.

6. Grigorenko, A. N., Polini, M., & Novoselov, K. S. (2012). Graphene plasmonics. Nature photonics, 6(11), 749-758.

7. Liu, F., Ming, P., & Li, J. (2007). Ab initio calculation of ideal strength and phonon instability of graphene under tension. Physical Review B, 76(6), 064120.

8. Balandin, A. A., Ghosh, S., Bao, W., Calizo, I., Teweldebrhan, D., Miao, F., & Lau, C. N. (2008). Superior thermal conductivity of single-layer graphene. Nano letters, 8(3), 902-907.

Chapter 2

Characterization of Graphene

One of the more difficult problems with graphene early on was its characterization. Although bulk graphite is dark in color as soon as you begin to reach a few atomic layers the film begins to become very transparent as mentioned in the previous chapter. Simple characterization of graphene was a difficult challenge early on because it is such a thin material. Even now SEM cannot always provide very much useful information for large uniform graphene films. However now as the field is more mature there are plenty of techniques available for graphene characterization. Here we will discuss several microscopy and spectroscopy techniques used for characterization of graphene films.

2.1 Optical Microscopy

Optical Microscopy is perhaps one of the most simple methods to observe small samples by magnifying the images several 1000 times.

Optical microscopy is one of the most inexpensive methods to look at thin graphene films and get a rough idea of the quality. Although we are limited about what kind of information we can get about a graphene film it is still none the less useful to observe it under an optical microscope. Since is about 99.7% transparent and is atomically thin, there are several challenges to being able to observe it. Fortunately it was quickly discovered that graphene could be

observed when placed on a Si wafer with a 300 nm thick SiO_2 layer. There

interference of the white light between the graphene and the SiO_2 allowed for

enough contrast to allow easy visualization of the graphene film as shown in

figure 2.1. As also seen in figure 2.1, the substrate also allows for contrast

between varying graphene thicknesses. The exfoliated graphene sample shows

a flake consisting of a single layer (very light purple), few layer (purple-dark

purple) and bulk layer(blue). The contrast allows for quick characterization of the

film uniformity, contamination deposition and thickness.

Figure 2.1: *Graphene flakes on 300 nm SiO_2/Si. The flakes range from single*

layer (light pink), few layer (purple) and multilayer (blue)

Unfortunately optical microscopy does have some limitations. First and

foremost for uniform graphene films it cannot distinguish graphene grain size like

it has commonly been used for other materials such as metals. Even is the

grains are very large they are still impossible to distinguish because there is no

visible contrast between the grain boundary and the graphene crystal. This is

due to grain boundary being atomically thin, consisting of only a few atoms. The

lack of grain boundary is visible in figure 2.2. Figure 2.2 a) is an optical image of

graphene on a 300 nm SiO_2/Si substrate, in where during the synthesis process

several grain grains were just beginning to coalesce, but have not done so

completely. Figure 2.2 b) is an optical image conducted after the film of similar

grain size has coalesced to form a uniform single layer graphene film. Besides

some surface contamination (light blue dots) there is no indication of any

graphene boundaries.
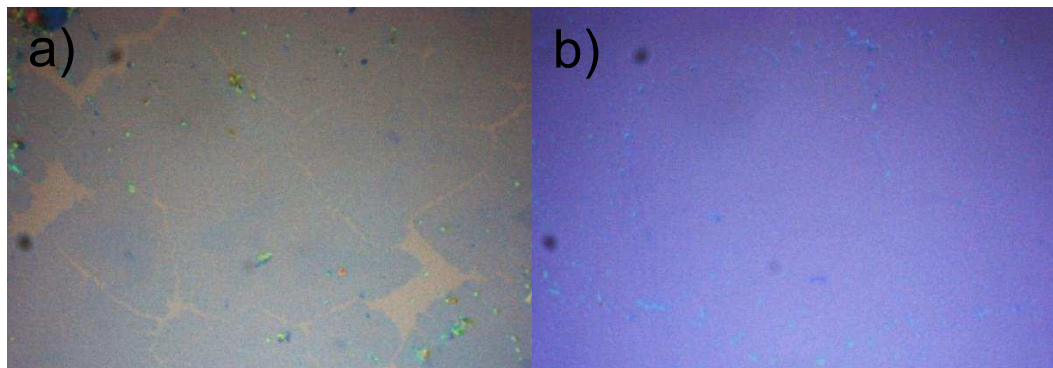
Figure 2.2: 100X Optical images. *a) graphene grains coalescing to form a film.*
b) Uniform graphene film where no grain boundaries are visible.

Another limitation for optical microscopy of graphene films is that they may

not always be transferred onto a 300 nm SiO_2 substrate, which means it may not

always be visible. Figure 2.3 shows two contrasting examples of graphene

deposited on two different metal foils by CVD. Figure 2.3 a) shows graphene

synthesized on a Cu foil and there is no sign of any graphene on the surface

although it is known that it is there. The only morphology we can gather from the optical microscopy is that of the Cu foil itself but nothing about the graphene. However in figure 2.3 b) varying graphene thickness are grown across the Ni foil surface. In this case the non-uniformity of the graphene film (varying thickness's) can be seen on the Ni surface. This does allow for some information to be obtained in a similar fashion as we obtain from the SiO_2 substrate but again it will suffer the same drawbacks. Fortunately, most device applications do not require graphene to remain on the metal foils and they must be transferred to another substrate. Unfortunately this limits when we can begin to characterize the material quality until the stages post synthesis which could be costly is the quality is poor and ends up wasting resources.
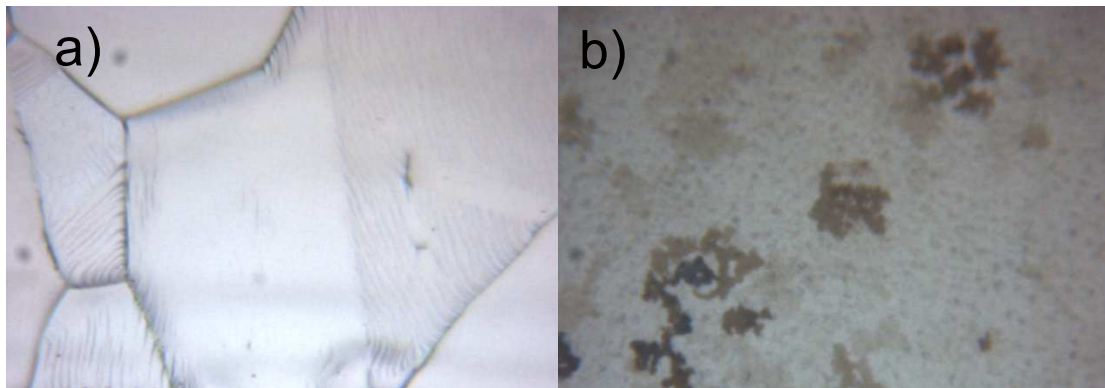
Figure 2.3: a) Single layer graphene on Cu foil and b) few layer graphene on Ni foil. There is almost no contrast between the graphene and the Cu foil, making it invisible using optical microscopy.

2.2 Scanning Electron Microscopy

Scanning electron microscopy (SEM) operates with very similar operating principles of optical microscopy but instead of a light beam a electron beam is used. Since the wavelength electrons can be much higher than that of visible light, the resolution of SEM is much higher of that of optical microscopes, allowing for very high magnification of samples.

SEM offers many of the same benefits of optical microscopy but can delve into much more detail due to the higher magnifications possible, up to 1,000,000 times magnification. However the higher magnification is not the only benefit of SEM, the contrast that it offers between the graphene and substrate can help image the graphene films more clearly than optical microscopy can. In figure 2.4 an example of how both the high magnification and the contrast offered by an SEM helps achieve characterization not possible with optical microscopy. One clear advantage of SEM is that the graphene can be characterized on any substrate and does not need to transferred to any special substrate make the contrast greater. In the case of figure 2.4 the graphene was grown directly on Cu foil and then characterized by SEM. It was though that the graphene was a continuous uniform film and figures 2.4 a) and b) at magnifications of about 1000X and 2000X, respectively, seem to indicate this. However upon closer inspection at a higher magnifications figure 2.4 c) and d) show that the film is not continuous. This can be seen by the light contrasting lines and cracks in the films, which is bare Cu, while the dark film regions are in fact single layer

graphene. During the course of this graphene deposition the graphene film did not complete full coverage across the foil. These very fine details would not be seen using optical microscopy even when it had been transferred onto a SiO_2 substrate. The fact that the film quality in terms of uniformity and continuity can be characterized before any transferring is a very large advantage compared to optical microscopy since for large scale manufacturing, transferring a poor quality material and then finding faults in it later through other characterization can be very costly and time consuming.
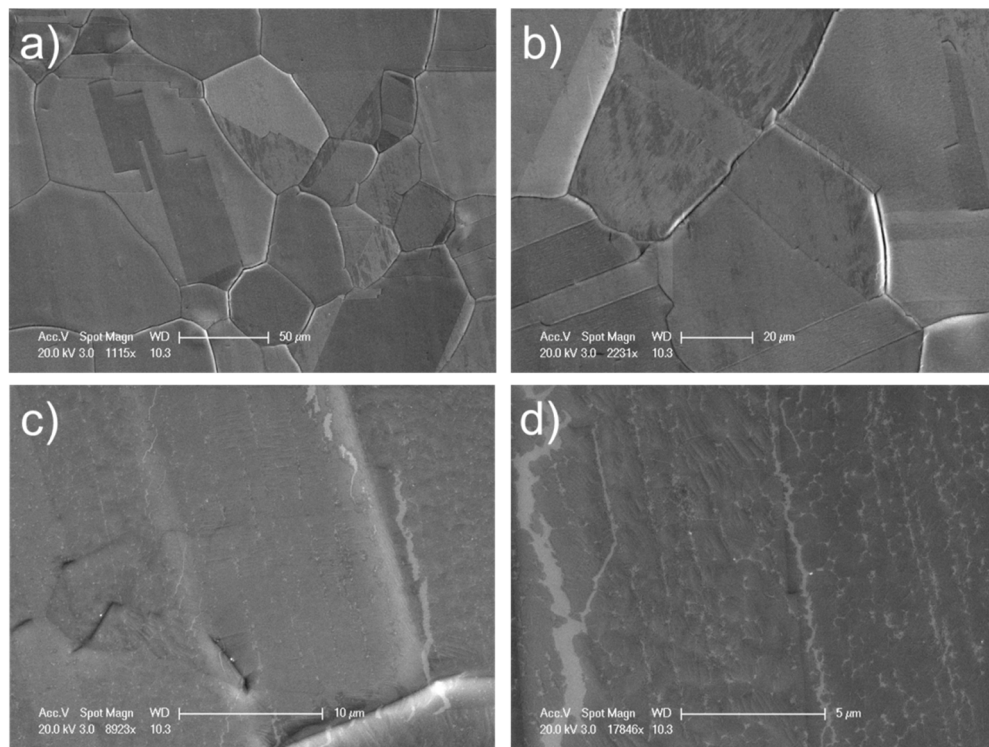
Figure 2.4: *SEM image of graphene on Cu foil. a) and b) are low magnification images showing what appears to be a uniform complete film on the surface. c) and d) show higher magnifications showing that in fact the film is not uniform and complete but actually has holes and empty regions.*

In order to get an even greater appreciation of the capabilities of SEM to characterize graphene, figure 2.5 is presented. Here individual graphene grains of about 10 microns in size are clearly visible on the Cu foil surface. The shape of the domains appear to be star-like in this case. From this sort of image information such as domain size and domain density can be measured and calculated. This is very useful information when trying to quantify graphene quality. Unfortunately, information such as grain size and domain density cannot be determined with uniform graphene sheets, because the SEM resolution is not high enough and the grain boundaries of the graphene sheets are only a few atoms large.
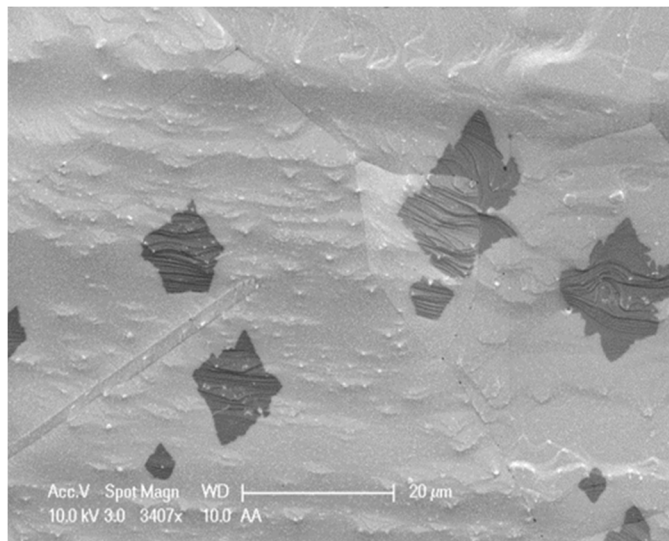
Figure 2.5: *Graphene domains on copper foil. The star shaped graphene domains show a high contrast against the Cu foil surface.*

Figure 2.6 below shows that SEM can also distinguish between single, and multilayer graphene as well as graphene and other 2D materials. Figure 2.6

a) shows a non uniform graphene film consisting of a single layer , bilayer and tri layer sheets. The contrast from the SEM can easily distinguish between the three thicknesses as well contamination that has formed between the grain boundaries. The contamination shown here helps distinguish the grain boundaries of the graphene film, but without the contamination it would not be visible. In figure 2.6 b) a non-continuous sheet of graphene was transferred onto a SiO_2 substrate, followed by exfoliated MoS_2 flakes transferred on top of the graphene. The bare substrate appears as a light grey regions, the graphene as the grey regions and the MoS_2 as the dark regions. The SEM can easily distinguish between all 3 materials and offers a very large contrast. This is very useful when dealing with multilayers, and stacked heterojunctions.
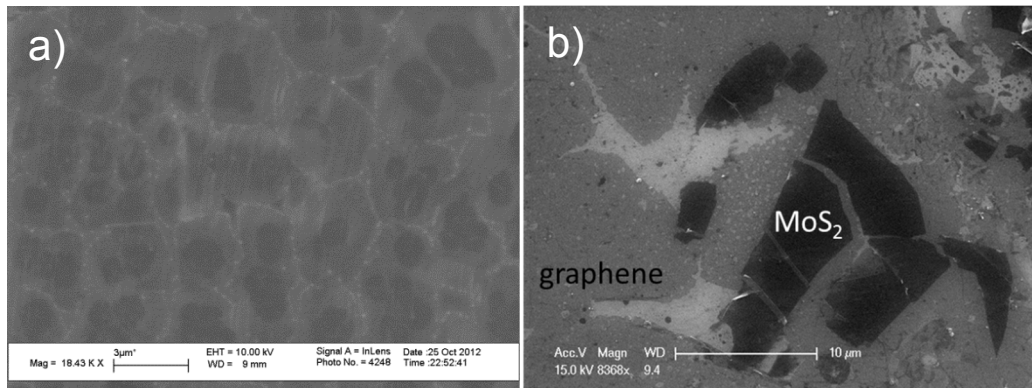
Figure 2.6: *SEM images of a) single, bi and tri -layer graphene domains on Cu foil and b) graphene film and MoS_2 flakes on a SiO_2 substrate.*

2.3 Energy Dispersive X-ray Spectroscopy

Energy Dispersive X-Ray Spectroscopy (EDS or EDX) is one of the most common spectroscopy techniques that can be implemented with a SEM system. EDS can help determine the atomic make up of a material. In the case of 2D atomic materials such as graphene it can be useful for confirming the chemical makeup of a film which consists of several other materials and not just graphene as will be the case later in this dissertation. This includes the case of where the graphene is already covered in another film and may not be easily visible by SEM or optical microscopy.

EDS measurement principle can be easily understood with a basic understanding of the basic Bohr model of the atom as presented in figure 2.7.
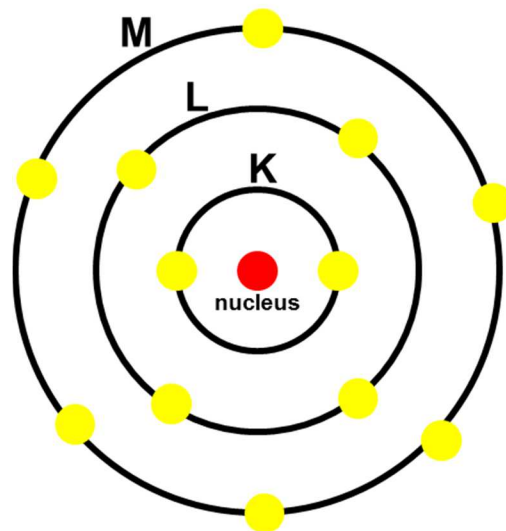
Figure 2.7: *Bohr Atomic Model, with a positive nucleus (red), surrounded by electrons (yellow) in discrete energy levels. The energy levels are unique to each atomic structure.*

The Bohr model of the atom is one of the earliest and simplest models there is in quantum mechanics. As shown in figure 2.7 the atom consist of a positive nucleus (red) surrounded by negatively charged electrons (yellow), each within their specified energy orbitals with discrete energies. These discrete energies are unique to each atomic structure as well as the amount of electrons in the energy orbitals. This allows us to be able to identify the atomic make up of a material by simply measuring the energy of the electrons transitions.

Figure 2.8 shows how EDS measurements are typically taken in a typical SEM with EDS measurement capabilities. For EDS the systems must be able to measure X-ray emissions from the samples, so a detector must be placed in the unit. As shown in figure 2.8 a), an electron beam is incident onto the sample, where it interacts with multiple individual atoms. If the electron energy is high enough then the energy provided will be enough to eject an electron from one of the inner orbitals (L or K), leaving behind an empty energy level as seen in 2.8 b). An electron from a higher energy level will then fall to the lower energy state filling that energy level while leaving behind vacancy. During this transmission a an X-ray photon will be emitted, where a detector will measure the photons energy. During this process other electrons transitions will also occur, but the transition energies are unique to each atomic number. This allows for the determination of the atomic make up of many materials. Typically however, there are limitations of how low of atomic number EDS can detect. This of course depends on individual tool capabilities. Although this is also ideal for surface

characterization it is also possible to detect the chemical make up at below the surface with high enough electron energy, but there are limitations of how deep the measurement can be taken, without damaging the sample.
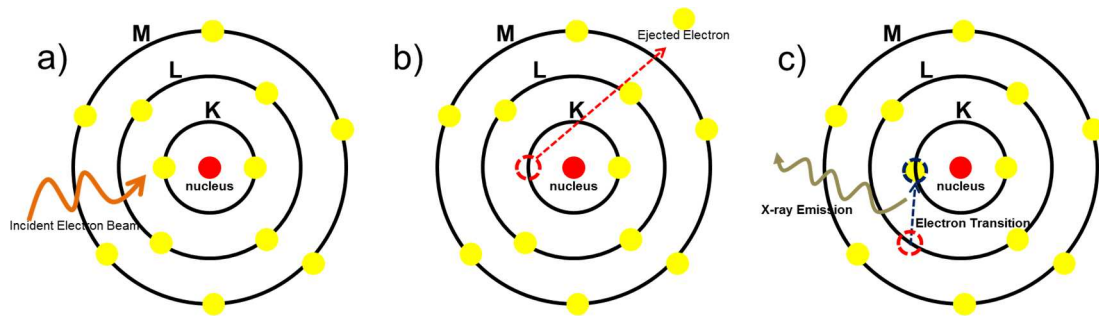
Figure 2.8: *EDS measurement principle schematic. a) Incident electron beam bombards an atom. b) electron beam energy was high enough to eject a core electron at a lower energy level and leaves behind a vacancy. c) An electron a higher energy transitions to the lower energy vacancy and in the process emits an X-ray, whose energy is then measured by a photodetector.*

The typical output of an EDS measurement can be displayed in several ways. In figure 2.9 the two most useful methods are shown. In this EDS graphene was synthesized concurrently with silica particles on a Cu foil. In order to understand whether the graphene film beneath the silica was continuous EDS measurements where conducted. The spectra on the left in figure 2.8 displays the energy peaks, which show the corresponding atomic make up at one particular point on the sample. Here it is shown that the film consist of carbon, silicon and oxygen. Unfortunately this does not yield as too much information but it is enough to clearly identify the what the chemical makeup of the material is.

The image in the right figure is a mapping of the surface, where EDS is taken

across the surface of the sample at multiple points. This allows for a 2D plot of

surface based on the atomic make up. In 2.8 the carbon counts are displayed

where the brighter regions indicate strong carbon peaks and the dark regions

indicate no carbon. This allows us to determine that the graphene film is not

continuous underneath the silica particles as there are many dark regions

between the bright regions.
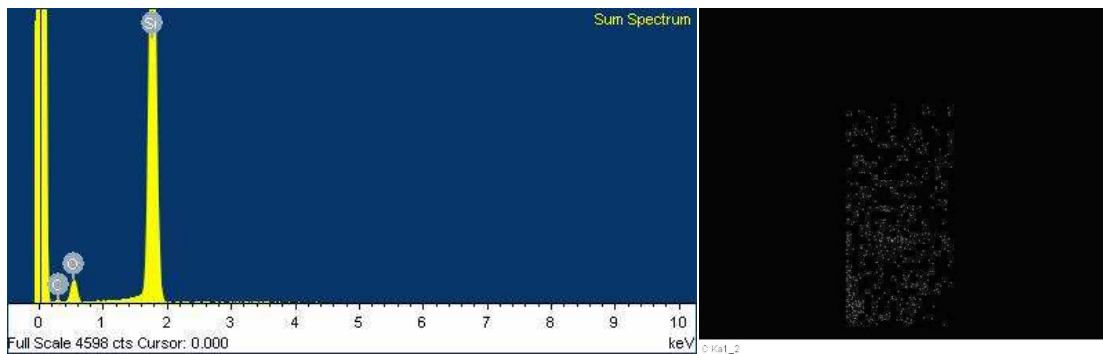
Figure 2.9: *Typical EDS out results. Left shows the spectrum of the EDS*

energies with the peaks labeled with they're corresponding atomic counterpart.

Right shows an EDS map of the Carbon makeup of the film.

2.4 Raman Spectroscopy

Raman Spectroscopy is perhaps one of the most pivotal spectroscopy

methods for 2D material characterization, but especially so for graphene. Raman

spectroscopy takes into account the unique transition energies found in

molecules or structures after being illuminated by coherent monochromatic light.

Figure 2.10 shows the mechanism   which allows for the Raman scattering to

occur. A material is illuminated with laser light with enough power to excite the atoms from a ground state to a low energy state to a higher energy state as shown in figure 2.10. In the case of Raman scattering two transitions may take place. In the first case, shown in the left figure 2.10, the incident light with wavelength, ν, excites the material from the ground state to the discrete energy level A. Then through spontaneous emission there is a transition between energy band A to energy band E, where E is greater than the ground state. This results in a photon being emitted of wavelength, ν_-, which has a lower photon energy than the incident beam ν. This sort of transition is known as a Stokes transition. The second type of Raman scattering is shown in the right of figure 2.10. With the molecule or material already at an energy state E, which is greater than the ground state, the incident photons with energy ν, pumps the energy to a state B > A and then spontaneously fall to an energy state lower than E (in this case the ground state), emitting a photon of wavelength ν_+, which has a higher photon energy than ν. The emission of the ν_- and ν_+ frequencies are known as the side bands and these energies are unique to each atomic structure. This allows for each material to have a unique Raman figure print, which allows for characterization of a myriad of materials. Typically the data which is plotted is the difference between the incident beam wavelength and the side band wavelengths. This difference is known as a Raman shift and every material has its own characteristic Raman shift spectrum, which can reveal much information about the crystallinity, quality, and atomic make up.

$\nu > \nu_-$

-------------------------------- B

-------------------------------- A

Incident Pump | Stokes Transition

ν | ν_- E

Ground State

$\nu < \nu_+$

-------------------------------- B

-------------------------------- A

Incident Pump | Anti Stokes Transition

ν | ν_+ E

Ground State
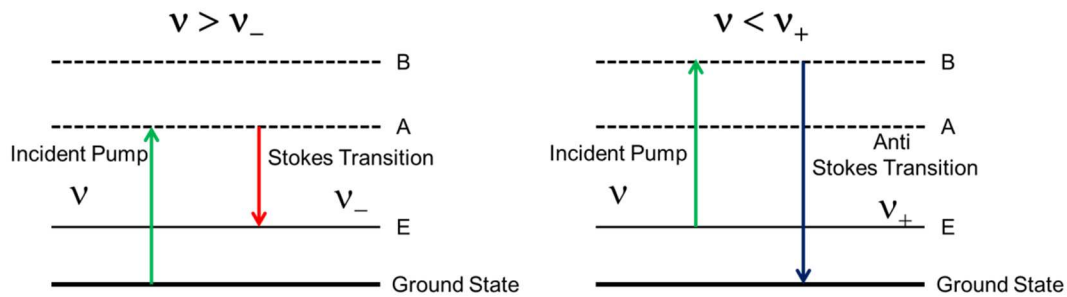
Figure 2.10: *Raman scattering diagram. (left) When the incident pump laser energy is greater than the Raman scattered light then the transition is a Stokes transition. When the scattered Raman light energy is greater than the pump laser energy then this is considered an anti-Stokes transition (right).*

In the case of graphene Raman spectroscopy offers a multitude of information. The Raman spectra of sp^2 bonded graphitic nanostructures are typically characterized by a handful of prominent peaks. The signature peak is the G band, which is centered around 1585 cm^{-1}, for graphene, graphite and carbon nanotubes. A second signature Raman peak is known as the G' band (also referred to as the 2D in earlier literature, although this is incorrect because there is a separate 2D band), which is typically centered around 2700 cm^{-1} for graphene but is dependent on laser excitation energy and number of layers. This peak is seen in all sp^2 carbons but the location and structure can vary largely. Finally the third signature band is the D band, known as the disorder peak, which is centered around 1350 cm^{-1} but again will vary depending of excitation wavelength. The D band comes about from disorder or non-symmetrical edge

defects. There are other bands such as the D', D+D', 2D and G+D' bands, which will not be discussed in much detail.

Figure 2.11 shows the Raman spectra of single layer graphene and bilayer graphene and how they differ. The Raman spectra can give a lot of information about the graphene quality and uniformity. For example, in order to distinguish between single layer and bi layer graphene, one can take a look at the intensity ratios of the G and G' bands, $I_G/I_{G'}$. Typically it has been shown that single layer graphene will have an, $I_G/I_{G'}$ ratio of about 1/3, while bilayer graphene will have a , $I_G/I_{G'}$ ratio of 1. These values will vary slightly dependent on the substrate, laser energy and material quality but for the most part they hold pretty
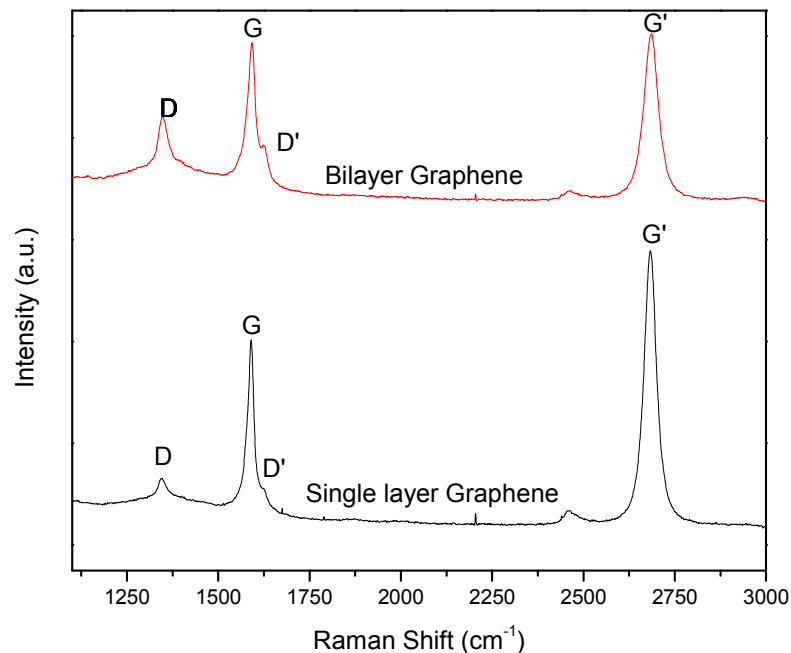
Figure 2.11: *Raman Spectra of single layer graphene and bilayer graphene, with its most important Raman peaks highlighted.*

well. Figure 2.10 shows that this is in fact the case with the bilayer graphene showing a $I_G/I_{G'}$ ratio close to one and the single layer graphene showing a $I_G/I_{G'}$ ratio of about 0.5.

Another way to determine the number of graphene layers, is by observing the width of the G' band. The G' band can be de-convoluted into Lorentzian several Lorentzian curves. When more layers are added more Lorentzian curves are make up the G' band, which end up broadening the full width at half max (FWHM) of the G' band. Along with the broadening of the G' band, single layer graphene will exhibit a higher intensity G' band, than a bilayer graphene sheet. The intensity of the G' band diminished with the number of layers added. Also, the stacking order of multiple graphene layers can be determined by the number of Lorentz peaks that make up the G' band. It gets very complicated for layers of 3 sheets or more as it takes up to 15 Lorentz peaks to create the G' band.

For the D band, the two important characteristics are the intensity and the band width. A higher intensity D peak indicates that the film quality is poor, while a low or non-existent D band indicates a high quality material. As can be seen in figure 2.11 the bilayer graphene film has a higher D peak than the single layer sheet indicating that it is of worse quality; however both films exhibit large D peaks so both would be considered of poor quality. It has also been shown that the crystalline size of a graphene film can be predicted by measuring the I_D/I_G ratio and using equation 2.4.1. Here, L_a is the lattice length and λ, is the incident laser wavelength. However this is limited by laser spot size and will not work for

crystalline sizes greater than the laser spot size. Another defect peak that is also labeled in figure 2.11 is the D' peak. This is considered a secondary defect peak and is typically centered around 1620 cm^{-1}. This peak is typically appears when there is a large amount of edge defects and is usually a good indication of a non-continuous film.

$$L_a(nm) = (2.4x10^{-10})\lambda^4 \left(\frac{I_D}{I_G}\right)^{-1}$$

Equation 2.4.1

Along with gathering Raman spectra, 2 dimensional Raman maps can be plotted to give a good visual indication of the film. In Raman mapping a sample is placed on a electronically controlled stage which can be shifted along the x and y axis. Raman spectra are taken across the sample while the stage rasters in a particular geometry, usually a square or rectangular shape. After all the Raman spectra are taken then the map can be generated in a variety of manners. The most typical mapping configuration is the mapping of a peak intensity, such as that shown in figure 2.12, which maps the peak intensity of the G peak of two graphene grains. Typically this information is not much useful other than to just confirn the presence of a certain molecule. Other popular mapping configurations for graphene include mapping the peak ratios, such as the peak ratio of G to G', which can be used to provide a map of single and multilayer regions. This is particualry useful to determine the uniformity of a graphene film and yields much more information than a single G, or G' peak intensity map[1-5].
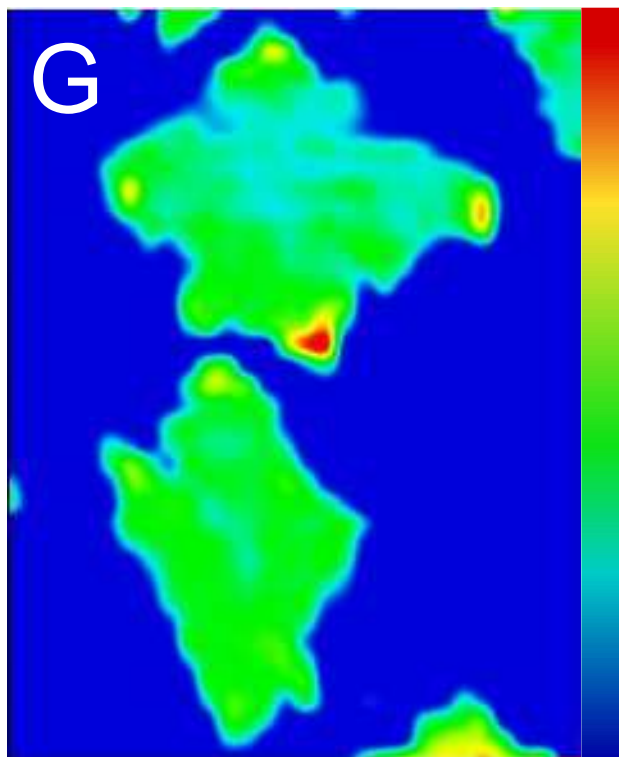
Figure 2.12: *Raman intensity mapping of G peak of graphene domains grown by chemical vapor deposition.*

2.5 Atomic Force Microscopy

Atomic force microscopy (AFM) is perhaps the most efficient and reliable tool to determine the thickness of atomically thin films. Figure 2.13 shows a schematic of how AFM works. Although it has several modes of operation the most simple operation mode to understand is the contact mode measurement. During this measurement a cantilever with a fine tip is scanned across the

surface, while the movement of the cantilever is measured with a laser beam with

reflect off the back of the cantilever. As it moves across a sample with various
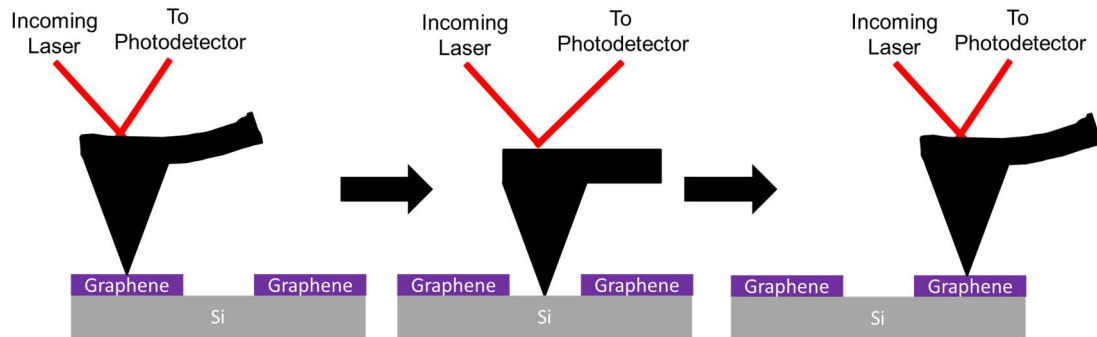
Figure 2.13: *Schematic demonstrating atomic force microscope cantilever scanning across graphene/Si substrate.*

features on the surface, the height of the features can be determined by the AFM

software which can in turn produce a 2D height profile of the sample scanned as

shown in figure 2.14. The challenge with 2D materials is that the height

difference between the 2D material and the substrate is typically less than 1nm

so careful consideration should be taken in tuning the cantilever in order to not

produce results with large errors.

Figure 2.14: 2 dimensional height map of monolayer film acquired by atomic force microscope.

References

1. Dresselhaus, M. S., Jorio, A., Hofmann, M., Dresselhaus, G., & Saito, R. (2010). Perspectives on carbon nanotubes and graphene Raman spectroscopy. Nano letters, 10(3), 751-758.

2. Berciaud, S., Ryu, S., Brus, L. E., & Heinz, T. F. (2008). Probing the intrinsic properties of exfoliated graphene: Raman spectroscopy of free-standing monolayers. Nano letters, 9(1), 346-352.

3. Calizo, I., Ghosh, S., Bao, W., Miao, F., Lau, C. N., & Balandin, A. A. (2009). Raman nanometrology of graphene: Temperature and substrate effects. Solid State Communications, 149(27), 1132-1135.

4. Graf, D., Molitor, F., Ensslin, K., Stampfer, C., Jungen, A., Hierold, C., & Wirtz, L. (2007). Spatially resolved Raman spectroscopy of single-and few-layer graphene. Nano letters, 7(2), 238-242.

5. Ferrari, A. C. (2007). Raman spectroscopy of graphene and graphite: disorder, electron–phonon coupling, doping and nonadiabatic effects. Solid state communications, 143(1), 47-57.

Chapter 3:

Silica Contamination of Graphene

One of the most promising methods to date for graphene large scale synthesis is by chemical vapor deposition (CVD) of carbon sources on catalytical transition metal substrates. Copper as a metal catalyst is ideal due to its low diffusion of carbon which self-limits the growth of graphene to single layer; however, although CVD is suited for large scale growth of graphene it leaves much to be desired in terms of graphene quality resulting in poor device performance when compared to exfoliated graphene. One culprit responsible for the low graphene quality is contamination which occurs during the graphene synthesis on the surface of the copper catalyst foil. The phase transition of quartz at 573° C allows copper and hydrocarbon to diffuse into the quartz tube, which causes silicate to precipitate onto the copper foil during the CVD process. Here the contamination from quartz tubes commonly used for the CVD furnaces is revealed and the effects on the graphene quality are studied. Scanning Electron Microscopy is used to image the contamination on the Cu surface and Energy Dispersive X-ray Spectroscopy is utilized to identify and trace the potential source of the contamination. Raman Spectroscopy and Mapping is used to demonstrate the effect of the contamination due to the quartz tube on the graphene quality by showing an increase in the D peak and the development of the D' peak. A simple method of avoiding growth substrate exposure to turbulent flow during the

growth is reported and verified to be an effective way of eliminating contaminations from the quartz tube.

3.1 Contamination of Graphene Synthesized on Cu

The first isolation of graphene by the Manchester group in 2004 sparked an explosion of interest in the science and engineering community due to its unique electrical, optical, thermal and mechanical properties, which stem from its unique 2D structure[1-5]. Graphene and other 2D materials are expected to transform the semiconducting industry and bring about a new era of thin film electronics [6-8]. The difficult challenge at hand lies in being able to produce the highest and largest quality atomically thin films for a relatively low cost. At the present moment the best quality graphene thus far has been by the scotch tape method[9], however this method is not scalable for industry use, which is why much attention has been focused on graphene synthesized of metals substrates by chemical vapor deposition (CVD).

Graphene synthesized by CVD has been demonstrated on a variety of different foils including Ni, Pt, Ir, Au, and Ru, but the arguably one the most promising (and studied) substrates is Cu due to its self-limiting growth of single layer graphene [10-13]. To date the quality of CVD graphene has left much to be desired in terms of quality and performance compared to exfoliated graphene, with CVD graphene routinely measuring up to several orders of magnitude lower than exfoliated graphene[14]. The low mobilities of CVD graphene are due in part to several different reasons including, polycrystalline nature, crystallite size,

grain boundary defects, wrinkles, non-uniform layers and contamination, which can all occur due to either the growth conditions or transfer methods from the metal substrate to a SiO_2 substrate[15-17]. In order for CVD graphene to increase in quality and performance all of these defects must be minimized if it is ever expected to be comparable to exfoliated graphene.

Enlargement of the grain size of as-grown CVD graphene can minimize the effects of grain boundary. Large single-crystal hexagonal single-layer graphene with millimeter-scale sizing has been synthesized on commercial polycrystalline copper foils with a comparable mobility to exfoliated graphene flakes [18, 19]. Electropolishing of copper foils before CVD growth has been verified to be effective of removing wrinkles and non-uniform layers [18-21].Dot like contamination of the graphene grown on copper foil has been reported and observed in previous papers [22-25], especially for large area growth on Cu foil, which can be seen in scanning electron microscope images (SEM) appearing on graphene while still on Cu and also after being transferred to other substrates such as SiO_2. However, besides tube cleaning after each growth, no effective ways of minimizing the dots contaminations have been reported yet. Here the source of the contamination, the effect of graphene mobility and a simple solution to avoid the contamination is reported. A significant increase in mobility for graphene without this type of contamination is demonstrated when compared to highly contaminated graphene samples.

3.2 Synthesis of Graphene and Dot Contamination by CVD

Prior to the growth a sheet of Cu foil is placed flat onto a clean quartz slide and then loaded into the hot-wall CVD quartz tube furnace. Graphene was synthesized by chemical vapor deposition on a thin copper foil at a temperature of 1000° C, at 2 Torr using a mixture of CH_4 and H_2 gas at a ratio of 1:40. The top side of the copper foil is directly exposed to the rest of the environment during the growth process, while the bottom side is isolated to direct exposure to the environment due to the contact with the quartz slide as demonstrated by Figure 3.1. Graphene is grown on a Cu foil by CVD which introduces contaminates onto the exposed top side graphene/Cu substrate but not the bottom side. After the growth the Graphene/Cu foil is then cut and separated by either top side growth or bottom side growth by etching opposing sides of the Cu foil and transferring the graphene onto SiO_2 substrates.

Although the bottom side of the copper foil is not exposed directly to the CVD environment, graphene will form on both the top side and bottom side of the copper foil. The direct contact of the bottom side copper foil is not enough to inhibit the gas flow and growth of graphene on its surface, however it is enough to prevent the formation of contaminates and defects, which are prevalent on the top side of the graphene surface.
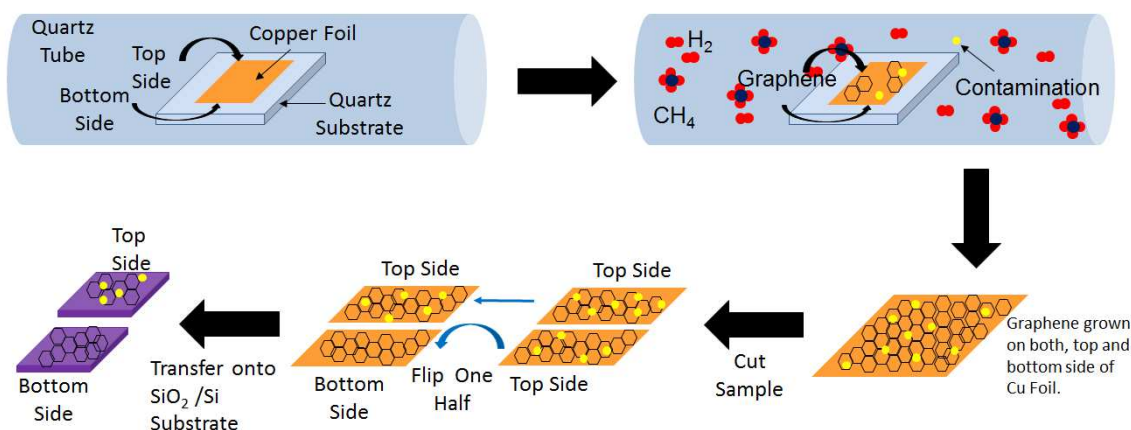
Figure 3.1: *Experimental procedure of graphene growth and comparison between the contaminated top side versus the contamination resistant bottom side after transfer*

After graphene synthesis the graphene/Cu foil was then removed from the furnace and carefully handled as to not intentionally damage or contaminate either side. The Cu foil was then cut into several pieces and opposing top and bottom sides would be coated in PMMA (Poly(methyl methacrylate)) and then separately etched in $FeCl_3$ solution and then transferred onto 300 nm SiO_2/Si substrates for further characterization. Some of the graphene was left directly on the Cu foil for direct optical and SEM imaging.

3.3 Characterization of Opposing Graphene

Once the graphene is transferred onto a SiO_2 substrate it is apparent there is a distinct difference between the top side versus the bottom side growth, when contamination levels are observable. Figure 3.2a and 3.2b show optical

57

images of a heavily contaminated top side graphene compared to a pristine

bottom side growth, respectively, done in a single growth. Figure 3.2a shows

distinct light blue and white discoloration with small regions of what appear to be

pristine graphene, while figure 3.2b shows a very uniform pristine looking

graphene layer. The black Raman spectra shown in figure 3.2g taken from a

heavily contaminated region, indicated by the black square in figure 3.2a, shows

a greater D peak intensity at 1342 cm^{-1}, compared to the other Raman spectra

displayed in figure 3.2g taken from the clean top side region (indicated by red

box figure 3.2a) and the clean bottom side region (indicated by blue box in Figure

3.2b). This indicates higher disorder and/or defects for the contaminated top side

compared to the clean bottom side. The overall Intensity of the contaminated

region is also is also smaller for the contaminated region indicating that there is

less graphene in these regions or that it is being covered up by the

contamination.

The ratio of the G peak intensity (1586 cm^{-1}) and the D peak intensity is

frequently used to indirectly determine the amount of defects present in graphene

due to the ratio is related to the graphene crystallite size [26]. Figures 3.2c and

3.2d display the G to D intensity peak ratio Raman Mappings of the top and

bottom side graphene regions respectively, which further confirm that the top

side graphene is much more contaminated since it's I_G/I_D much smaller across

the sample compared to the bottom side graphene [27, 28]. Even the regions

which look clean optically on the contaminated top side have high I_G/I_D values

compared to the bottom side graphene. Furthermore Figures 3.2e and 3.2f show
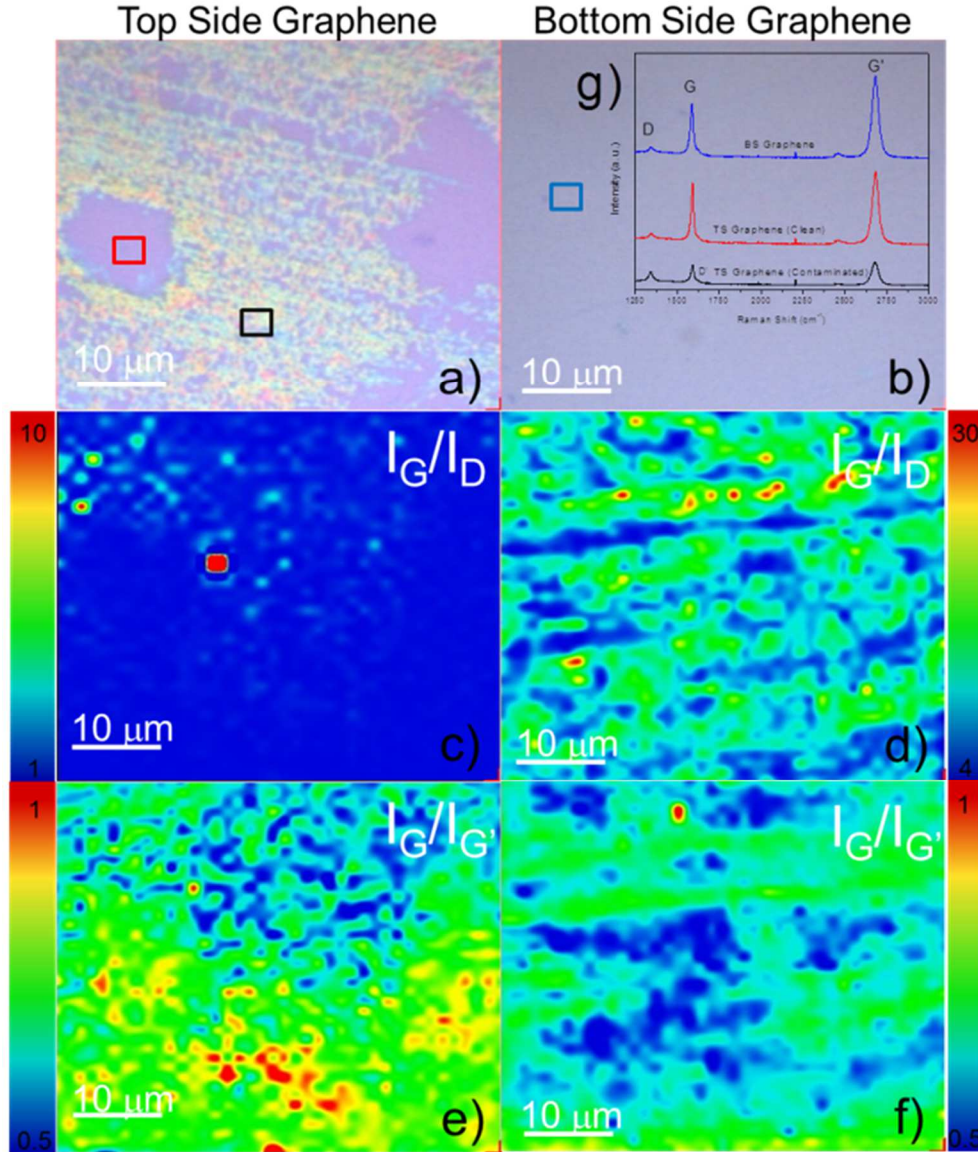
Figure 3.2: *Optical and Raman Spectroscopy comparison of topside versus*

bottom side graphene. Optical images of opposing graphene sides a) and b).

Raman mapping of I_G/I_D c) and d) and $I_G/I_{G'}$ e) and f) of opposing sides. g),

Raman Spectra of regions indicated by colored boxes in a) and b).

that the ratio of the G peak intensity and the G' Peak intensity (2690 cm^{-1}), which

has previously been used to determine the number of graphene layers present

[29-34]. The top side graphene has a slightly higher overall I$_G$ to I$_{G'}$ ratio

compared to the bottom across the whole sample but it is still mostly single layer

graphene with only a few regions which could be considered bilayer graphene.

The bilayer regions on the contaminated side may be caused by graphene which

folded in on itself due to the contamination. It is also apparent that a D' peak is

apparent on the contaminated graphene region, which is indicative of a highly

defected graphene, and sometimes even used to determine the edge structure of

graphene domains [35]. Lastly the Raman peaks displayed have not been

normalized or flattened but it is noticeable that the intensity signal of the

contaminated graphene is weaker than the non- contaminated graphene.

The type of heavy contamination shown in Figure 3.2a is not

characteristically common to most graphene growths but was achieved by doing

a long 2 hour growth, which allowed for prolonged contamination exposure. This

designed prolonged contamination procedure has allowed for the effects of the

contamination to be amplified and studied more carefully. SEM images of

various amounts of contamination are shown in Figure 3.3 as well as the

evolution of the contamination from light contamination to heavy contamination of

the Cu surface. The SEM image in Figure 3.3a shows the appearance of an

uncontaminated graphene/Cu growth by CVD. Figure 3.3b displays the initial

formation of the contamination on the graphene/Cu foil, which is what has been

more commonly seen in previous publications. The contamination appears as small white dots under SEM and this is the appearance of the contamination that most often appears in typical graphene synthesis by CVD. Figures 3.3c and 3.3d show the formation of a worm like structures, followed by a dendritic like structure, respectively, on the graphene/Cu foil as the exposure to the contamination is increased by either prolonging the CVD growth or by increasing the contamination source.
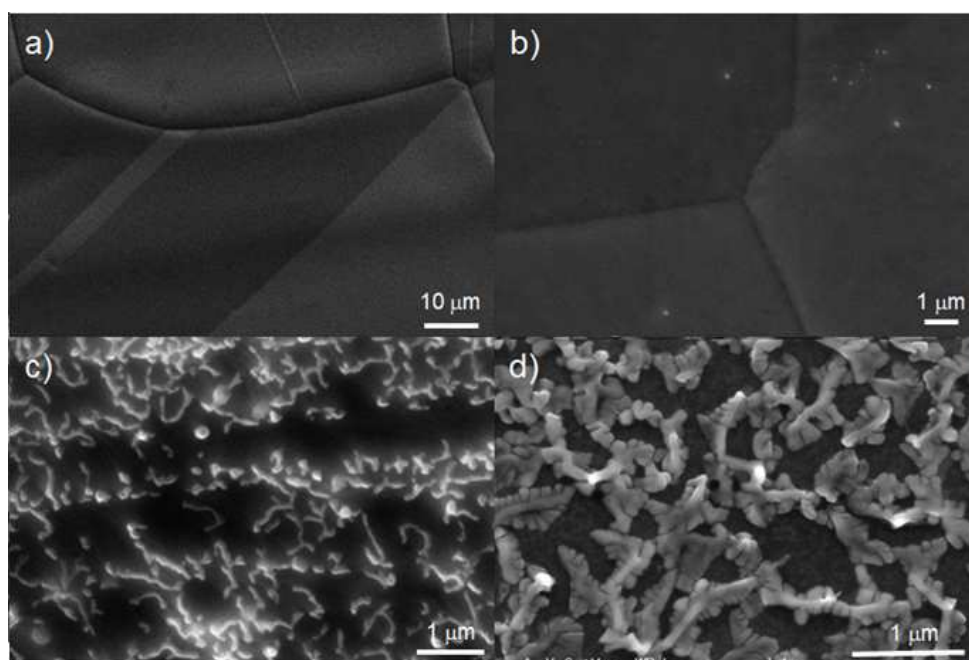
Figure 3.3. *Scanning electron microscopy images of evolution of contamination on graphene grown on Cu substrate. a) Clean pristine graphene and copper substrate. b) Beginning stages of contamination formation after complete graphene growth. c) Heavy surface area coverage of long tube contamination. d) Dendritic structure of the contamination after long period contaminate formation.*

Back gated graphene field effect transistors (GFET) were fabricated from pristine and contaminated graphene,as shown in figure 3.4a, in order test the affects that the contamination has on the graphene's electrical performance. Figure 3.4b shows the comparison of the drain current versus the drain voltage of both devices from -5 V to 5 V. The heavily contaminated sample has a drain current over one order of magnitude less than the pristine graphene's current at 5 V. Figures 3.4c and 3.4) show the difference in quality of the devices optically between both devices. The contaminated device shows how much more rough the surface is, which is even apparent through the 110 nm thick metal contacts(Titanium thickness: 10 nm, gold thickness: 100 nm), while the pristine graphene sample shows no such sign. While patterning the graphene by photolithography followed by the oxygen plasma etching, it was also noticed that it was impossible to pattern the contaminated sample into the appropriate shape in between the contacts. Raman spectroscopy confirmed that the graphene was in fact patterned but the contamination would be largely unaffected in the oxygen plasma, while the unprotected pristine graphene could be completely etched away in 1 min at 50 mW and an O_2 flow of 100 sccm. Figure 3.4b clearly showed the bright colored contamination compared to the light violet seen in figure 3.4c). When trying to sweep the drain voltage at voltages greater than 5 volts the contaminated GFET devices would burn up and fail as opposed to the pristine graphene that could be swept from -20 V to 20 V and up to -100 V to 100 V at

smaller currents as shown in Figure S1. We believe the failure of the FET device

based on contaminated graphene is due to the high resistance. Finally Atomic

force microscopy (AFM) was utilized in order to confirm the size of the

contamination on the surface of the devices. Figures 3.4e and 3.4f show the

AFM height profile of the contaminated device and the pristine device,

respectively. The contaminated device shows the typical dendritic structure with

heights reaching up to 550 nm. The pristine sample shows a very smooth

service with some sporadic debris, most likely caused during the

photolithography process.
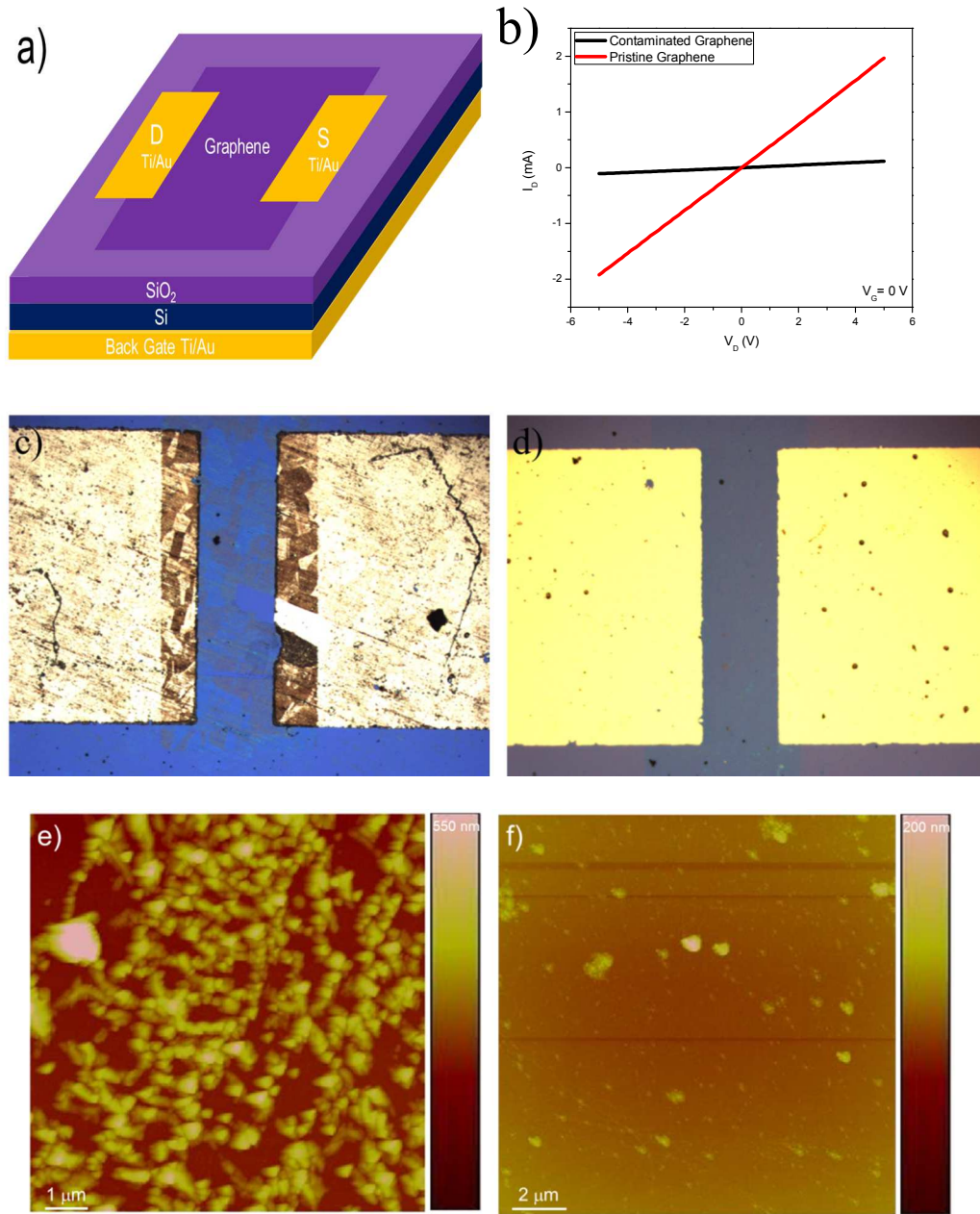
Figure 3.4. *Device performance comparison of top side versus bottom side graphene. a) Schematic of fabricated devices. b) Displays I_d vs. V_d of both devices from – 5 V to 5 V. c) and d) show the optical images of the contaminated graphene and the pristine graphene devices, respectively. e) displays the contaminated and f) pristine graphene AFM height profiles.*

3.4 Cause of Contamination

Energy dispersive X-ray spectroscopy was (EDS) conducted on a two heavily contaminated samples both from the same growths. One of the samples was directly analyzed on the Cu foil, while the second was graphene transferred onto a Si substrate with 300 nm SiO_2. The results are demonstrated in Figure 3.5a and 3.5b. Figure 3.5a shows that the expected carbon and copper on the surface but also a fair amount of silicon and oxygen. In order to confirm that the contamination is not a copper oxide or copper silicate Figure 3.5b) shows the EDS on the SiO_2 substrate and shows no trace of Cu. The common denominator between both samples is the silicon and oxygen (aside from the carbon), which confirms that the contamination is some silicon oxide. Additional EDS data is shown in 3.6. This explains why Raman spectroscopy would not reveal any information about the contamination since it was concealed by the SiO_2 peaks of the substrate used. The difference in $I_G/I_{G'}$ mapping may also be explained by the multiple reflection model since it has been shown that thin layers of can cause drastic changes in the I_G to $I_{G'}$ ratio. [36] It also reveals why the oxygen plasma used to pattern our devices could not pattern the contaminated samples into the appropriate shape, since silicate is not affected by oxygen plasma.
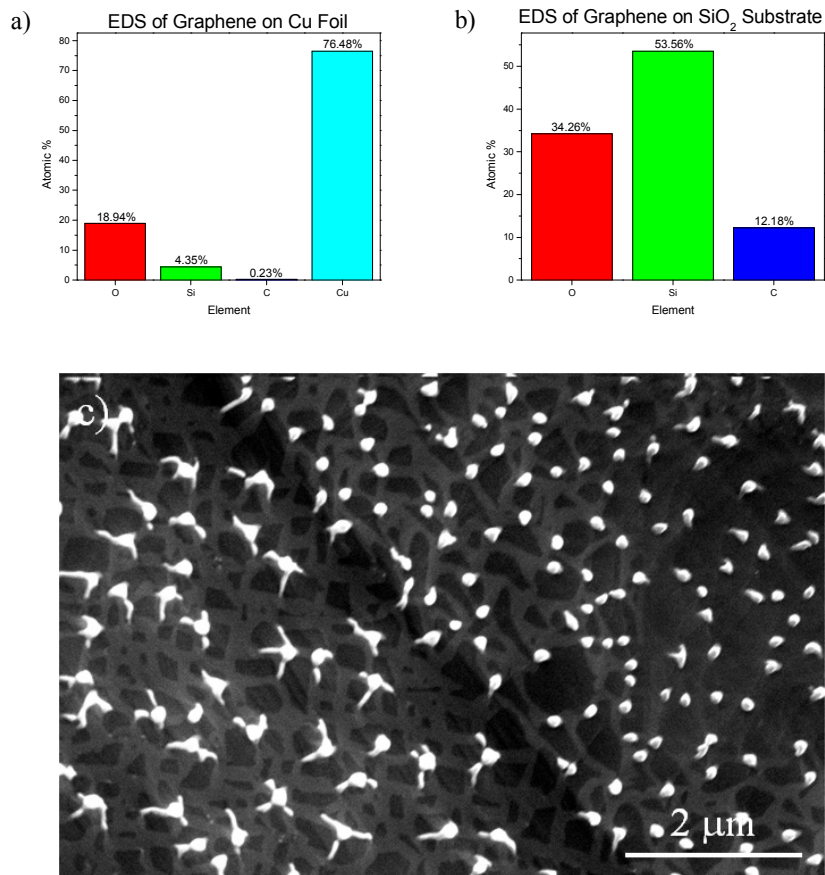
Figure 3.5: *Silicon oxide contamination EDS. EDS of contaminated samples on Cu foil a) and on SiO$_2$ substrate b). c) SEM image of intermediate growth stage of both the silicate contamination and the graphene crystals. It is apparent that the graphene and contamination are not over lapping during their growth and are growing around each other simultaneously.*
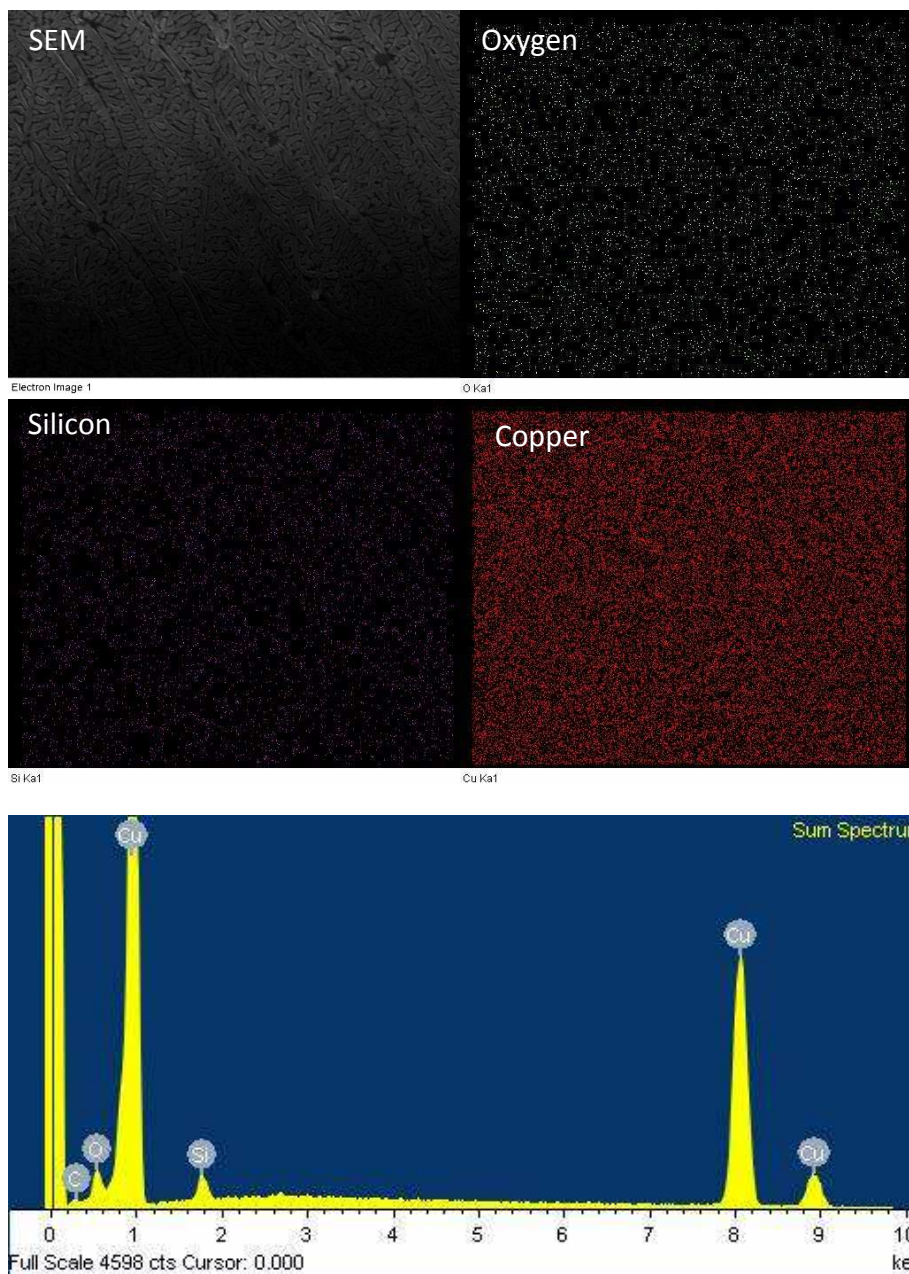
Figure 3.6: *EDS 2D maps on a contaminated Copper Substrate.*

The only possible source for the silicon oxide contamination is from the quartz tube that is used during the synthesis as well as possibly the quartz plate. Since only the top side of the graphene is heavily contaminated in our growths

then it was concluded that the quartz tube must be the culprit of the silicon oxide contamination. The question arises then, why does the quartz tube contaminate the copper foil and not the quartz plate? The explanation provided here stems from the phase transition of SiO_2 from α-quartz to β-quartz at temperatures between 550° C and 600° C, which causes non ordered crystal structure [37]. During the transition from α to β quartz the density of quartz the crystal structure changes from a rhombohedral (trigonal) to hexagonal and thus going from a density of 2.65 g/cm^2 to 2.53 g/cm^2 [38]. It has been noticed that along the quartz tube where the temperature has been measured to be in the range of 559° C and 600° C, there is a copper deposition into the quartz tube that ends up diffusing into the quartz tube itself as shown in Figure 3.7a. However regions above or below this threshold seem to be unaffected. It's believed that as copper diffuses into this unstable phase regions that silicon oxide gets evaporated and then redeposited onto the copper surface.

The quartz plate has also been shown to be able to contaminate the bottom of the graphene over if 1) the quartz plate is not fused polished quartz, and 2) the quartz plate is not kept smoothed and copper diffusion is observed after many growths. Figure 3.7b shows a quartz plate that has been lightly scratched by rough handling and it shows slight copper diffusion into the quartz where the Cu foil rest during the graphene synthesis. It is believed that during the ramping of the furnace from room temperature to 1000° C that copper diffuses into the plate while the plate is going from the α to β phase transition.

The copper was confirmed to be inside the quartz and not just melted Cu on the surface by placing the quartz plate in HCl solution for several days and observing no notable copper etching. Figure 3.7c) shows a quartz plate used for several growths while being handled very carefully handled and not scratched in any way. Bottom side graphene growths stay pristine with minimal to no contamination. Once deposition of the copper into an unpolished or scratched quartz plate has been observed it begin to contaminate the bottom of the graphene (although at much lower levels than the tube) if proper care of the quartz plate is not observed. This however can be remedied quite easily by either being careful when handling the quartz plate and not scratching it and by also leaving the quartz plate in HCl to etch any Cu on the surface of quartz plate. One could also just replace the quartz plate completely with a new one or not use a quartz plate at all as others have demonstrated before, however for large scale manufacturing this may not preferable as it will add to the manufacturing cost.

The mechanism at which the silicon oxide deposits on the surface of the Cu during the graphene growth seems to be very similar to that of graphene [39]. Graphene domains form at defects sites of the Cu foil and it seems that the same occurs with the contamination[40]. Figure 3.5c shows a SEM image of the intermediate stages of the silicon oxide contamination and the graphene formation. It appears that there is a competition between the graphene and the silicone oxide to see which will take up the most real estate on the copper foil. There is no overlap between the graphene and silicon oxide on the surface, so if
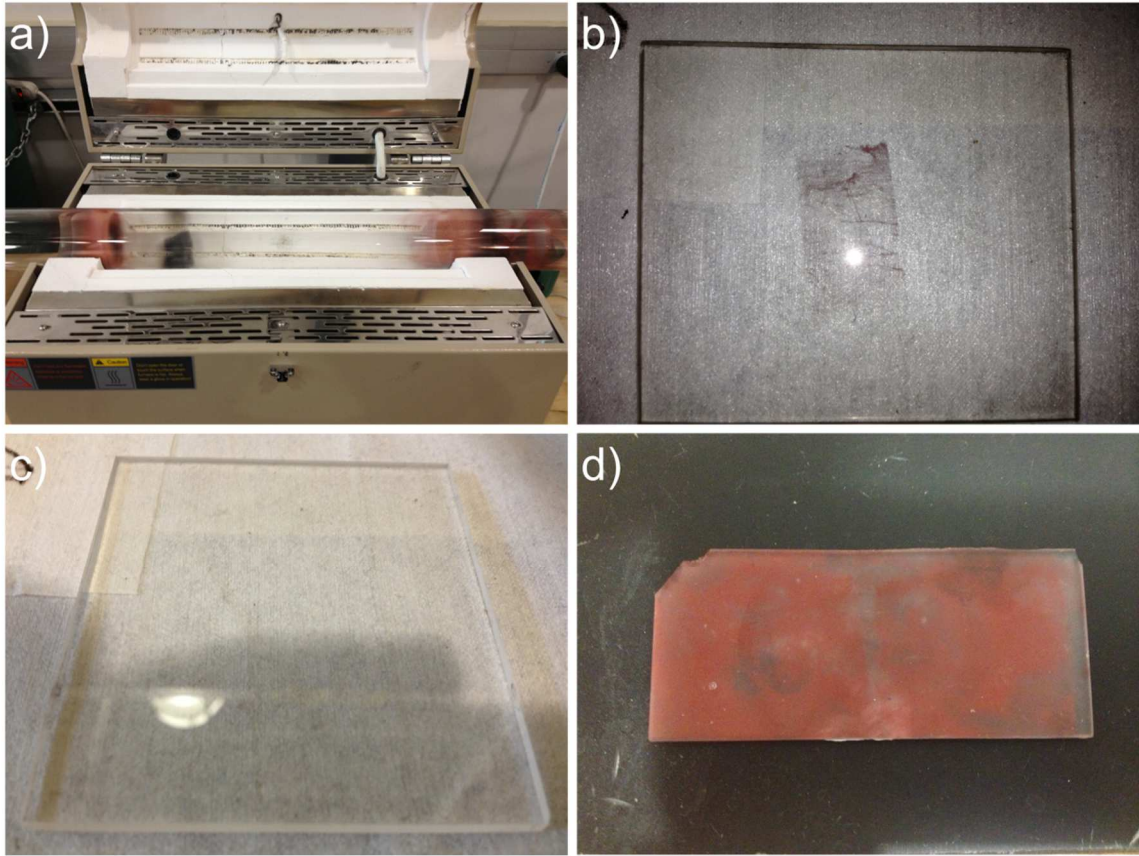
Figure 3.7: *Deposition of Cu into quartz. a) Quartz tube is contamination by Cu diffusion indicated by red rings around the edge of the furnace. b) Scratched quartz plate also begins to show signs of Cu diffusion. c) Clean Quartz plate after several dozen growths. d) Unpolished Quartz plate contaminated greatly after few growths.*

the graphene can be formed quickly on the copper surface the silicate contamination will remain only as small dots. We believe that is why the contamination problem was not been studied that much in previously reported literatures. However for CVD growth of graphene with large domain size as

reported lately [41-43], highly diluted carbon precursor and prolonged growth time are used, the contamination becomes a critical issue. If the graphene growth is slow, the silicon oxide will gain more surface area as it forms into a tube and then dendritic structure. This explains why the contaminated graphene FET was not able to go to high voltages compared to the pristine graphene, since the graphene was not a uniform sheet but more of a network of non-uniform ribbons which would not be able to handle the higher current densities. Finally this also reveals why the Raman spectra revealed a larger D and the inclusion of a D' peak due to the edge defects of the graphene which compared to the pristine graphene's uniform sheet.

The silicon oxide is preserved and is not affected throughout the transfer process at all by the $FeCl_3$ and is transferred to the substrate directly by the PMMA coating. It may be possible to remove the contamination by using an etchant such as HF or BOE before the removing the copper which would leave holes where the silicate was but it has yet to be tried. This could be used as a way to pattern small graphene ribbons, flakes or nanomeshes like previously reported depending on the amount of silicon oxide on the surface but it may be a bit uncontrollable.

3.5 Conclusion:

Graphene grown on both the top side and bottom side of a sheet of copper foil were compared. It was shown that the exposed top side is contaminated with either light dot like contamination or with heavy dendritic like

contamination, which is dependent on the time it is exposed to the contamination and the growth rate of the graphene. The protected bottom side of the copper foil is free of this contamination. It has been shown that the mystery contamination that is fairly common to graphene synthesized by thermal chemical vapor deposition in a quartz tube is in fact a silicon oxide, which is caused by the phase transition from α–quartz to β–quartz of the quartz tube itself, which occurs at 573° C. The contamination however can be avoided by using a quartz plate and laying your Cu foil flat on its surface, which will greatly reduce and even eliminate your contamination on the side of the copper that is in direct contact with the quartz plate, but still allow the formation of graphene. Raman Spectroscopy and SEM reveal that that the contamination is detrimental to the quality of the graphene as both the graphene and silicon oxide compete to grow on the surface of the copper foil, which if the silicate out grows the graphene on the surface of the copper, it will leave the graphene in either non-uniform ribbons or even isolated islands. This can have a negative impact on the device performance as demonstrated by graphene FET's fabricated and tested created by both pristine bottom side graphene and top side contaminated graphene. It was shown that the I_D was more than an order of magnitude large for the pristine graphene device, than the contaminated graphene device. Contaminated graphene FET's were also unable to be sweep at larger voltages than -5 V to 5 V's due to the non-uniform sheets created due to the contamination which compromises the integrity of the devices at larger drain voltage sweeps or higher currents.

Although the silicon oxide can be eliminated by the methods provided here it may be possible to use this contamination as a way of patterning the graphene grown by CVD. Although our group has not spent any time pursuing this idea, it is not hard to imagine a way to create a very specific arrangement of defect points on the Cu foil as has been shown before, do a short exposure growth of the silicon oxide contamination and then do a ultrafast graphene growth on the non-patterned regions. By removing the silicon oxide contamination you can be left with a specific graphene pattern such as a nanomesh, nanoribbons or quantum dots. This may be something to look into for future applications but as long as it is uncontrolled, the contamination is better avoided.

References

1. K. S. Novoselov, A.K.G., S. V. Morozov, D. Jiang, Y. Zhang, S. V. Dubonos, I. V. Grigorieva, A. A. Firsov Electric Field Effect in Atomically Thin Carbon Films. Science, 2004. 306(5696): p. 666-669.

2. Falkovsky, L.A., Optical Properties of Graphene. Journal of Physics: COnference Series, 2008. 129(1).

3. A. A. Balandin, S.G., W. Bao, I. Calizo, D. Teweldebrhan, Feng Miao, and Chun Ning Lau, Superior Thermal Conductivity of Single-Layer Graphene. Nano Letters, 2008. 8(3): p. 902-907.

4. C. Lee, X.W., J. W. Kysar, J. Hone, Measurement of the Elastic Properties and Intrinsic Strength of Monolayer Graphene. Science, 2008. 321: p. 385.

5. Castro Neto, A.H., et al., The electronic properties of graphene. Reviews of Modern Physics, 2009. 81(1): p. 109-162.

6. Virendra Singha, b., Daeha Jounga, c, Lei Zhaia, d, , , Soumen Dasa, b, Saiful I. Khondakera, c, e, , , Sudipta Seal, Graphene based materials: Past, present and future. Progress in Material Science, 2011. 56(8): p. 1178-1271.

7. Ki Kang Kim, A.H., Xiaoting Jia, Soo Min Kim, Yumeng Shi, Mildred Dresselhaus, Tomas Palacios, and Jing Kong, Synthesis and Characterization of Hexagonal Boron Nitride Film as a Dielectric Layer for Graphene Devices. ACS Nano, 2012. 6(10): p. 8583-8590.

8. Zhan, Y., et al., Large-Area Vapor-Phase Growth and Characterization of MoS2 Atomic Layers on a SiO2 Substrate. Small, 2012. 8(7): p. 966-971.

9.   Bolotin, K.I., et al., Ultrahigh electron mobility in suspended graphene. Solid State Communications, 2008. 146(9–10): p. 351-355.

10.   Reina, A., et al., Growth of large-area single- and Bi-layer graphene by controlled carbon precipitation on polycrystalline Ni surfaces. Nano Research, 2009. 2(6): p. 509-516.

11.   Gao, L., et al., Repeated growth and bubbling transfer of graphene with millimetre-size single-crystal grains using platinum. Nature Communications, 2012. 3: p. 699.

12.   Meng, L., et al., Multi-oriented moiré superstructures of graphene on Ir(111): experimental observations and theoretical models. Journal of Physics: Condensed Matter, 2012. 24(31): p. 314214.

13.   Li, H., et al., The influence of annealing temperature on the morphology of graphene islands. Chinese Physics B, 2012. 21(8): p. 088102.

14.   Schwierz, F., Graphene transistors. Nature nanotechnology, 2010. 5(7): p. 487-496.

15.   Zhu, W., et al., Structure and electronic transport in graphene wrinkles. Nano letters, 2012. 12(7): p. 3431-3436.

16.   Pirkle, A., et al., The effect of chemical residues on the physical and electrical properties of chemical vapor deposited graphene transferred to SiO< inf> 2</inf>. Applied Physics Letters, 2011. 99(12): p. 122108-122108-3.

17.   Petrone, N., et al., Superior Mobility in Chemical Vapor Deposition Synthesized Graphene by Grain Size Engineering. Bulletin of the American Physical Society, 2012. 57.

18.   Yan, Z., et al., Toward the Synthesis of Wafer-Scale Single-Crystal Graphene on Copper Foils. ACS nano, 2012. 6(10): p. 9110-9117.

19.   Chen, S., et al., Millimeter-Size Single-Crystal Graphene by Suppressing Evaporative Loss of Cu During Low Pressure Chemical Vapor Deposition. Advanced Materials, 2013.

20.   Zhang, B., et al., Low-temperature chemical vapor deposition growth of graphene from toluene on electropolished copper foils. ACS nano, 2012. 6(3): p. 2471-2476.

21.   Luo, Z., et al., Effect of substrate roughness and feedstock concentration on growth of wafer-scale graphene at atmospheric pressure. Chemistry of Materials, 2011. 23(6): p. 1441-1447.

22.   Losurdo, M., et al., Graphene CVD growth on copper and nickel: role of hydrogen in kinetics and structure. Physical Chemistry Chemical Physics, 2011. 13(46): p. 20836-20843.

23.   Colombo, L., et al., Growth kinetics and defects of CVD graphene on Cu. ECS Transactions, 2010. 28(5): p. 109-114.

24.   Li, X., et al., Large-Area Synthesis of High-Quality and Uniform Graphene Films on Copper Foils. Science, 2009. 324(5932): p. 1312-1314.

25.   Kim, H., et al., Activation energy paths for graphene nucleation and growth on Cu. ACS nano, 2012. 6(4): p. 3614-3623.

26.   Jorio, A., et al., Raman spectroscopy in graphene related systems. 2010: Wiley-VCH.

27.   Dresselhaus, M.S., et al., Perspectives on carbon nanotubes and graphene Raman spectroscopy. Nano letters, 2010. 10(3): p. 751-758.

28.   Jorio, A., et al., Measuring disorder in graphene with the G and D bands. physica status solidi (b), 2010. 247(11-12): p. 2980-2982.

29.   Gupta, A., et al., Raman scattering from high-frequency phonons in supported n-graphene layer films. Nano Letters, 2006. 6(12): p. 2667-2673.

30.   Kyle, J.R., et al., Centimeter-Scale High-Resolution Metrology of Entire CVD-Grown Graphene Sheets. Small, 2011. 7(18): p. 2599-2606.

31.   Wang, W., et al., Three dimensional few layer graphene and carbon nanotube foam architectures for high fidelity supercapacitors. Nano Energy, 2013. 2(2): p. 294-303.

32.   Wang, W., et al., Intertwined Nanocarbon and Manganese Oxide Hybrid Foam for High-Energy Supercapacitors. Small, 2013.

33.   Guo, S., et al., Photoinduced Electron Transfer Between Pyridine Coated Cadmium Selenide Quantum Dots and Single Sheet Graphene. Advanced Functional Materials, 2013.

34.   Wang, W., et al., Hybrid Low Resistance Ultracapacitor Electrodes Based on 1-Pyrenebutyric Acid Functionalized Centimeter-Scale Graphene Sheets. Journal of Nanoscience and Nanotechnology, 2012. 12(9): p. 6913-6920.

35.   Eckmann, A., et al., Probing the Nature of Defects in Graphene by Raman Spectroscopy. Nano letters, 2012. 12(8): p. 3925-3930.

36.   Yoon, D., et al., Interference effect on Raman spectrum of graphene on SiO_{2}/Si. Physical Review B, 2009. 80(12): p. 125422.

37.   Van Tendeloo, G., J. Van Landuyt, and S. Amelinckx, The α→ β phase transition in quartz and AlPO4 as studied by electron microscopy and diffraction. physica status solidi (a), 1976. 33(2): p. 723-735.

38.   Wright, A.F. and M.S. Lehmann, The structure of quartz at 25 and 590°C determined by neutron diffraction. Journal of Solid State Chemistry, 1981. 36(3): p. 371-380.

39.   Li, X., et al., Evolution of graphene growth on Ni and Cu by carbon isotope labeling. Nano letters, 2009. 9(12): p. 4268-4272.

40.   Han, G.H., et al., Influence of Copper Morphology in Forming Nucleation Seeds for Graphene Growth. Nano Letters, 2011. 11(10): p. 4144-4148.

41.   Wang, H., et al., Controllable Synthesis of Submillimeter Single-Crystal Monolayer Graphene Domains on Copper Foils by Suppressing Nucleation. Journal of the American Chemical Society, 2012. 134(8): p. 3627-3630.

42.   Li, X., et al., Large-Area Graphene Single Crystals Grown by Low-Pressure Chemical Vapor Deposition of Methane on Copper. Journal of the American Chemical Society, 2011. 133(9): p. 2816-2819.

43.   Chen, S., et al., Millimeter-Size Single-Crystal Graphene by Suppressing Evaporative Loss of Cu During Low Pressure Chemical Vapor Deposition. Advanced Materials, 2013. 25(14): p. 2062-2065.

44.   Guo, S., et al., Tuning Electron Transport in Graphene-Based Field-Effect Devices using Block Co-polymers. Small, 2012. 8(7): p. 1073-1080.

45.   Kyle, J.R., et al., Centimeter-Scale High-Resolution Metrology of Entire CVD-Grown Graphene Sheets. Small, 2011. 7(18): p. 2599-2606.

Chapter 4

Rapid Synthesis of Graphene

The synthesis of graphene with large-area uniformity is an essential requirement for their application in electronic and optical devices. Here, we have reported on fast and scalable synthesis of large-scale single layer graphene with no annealing and growth times of less than 1 minute by oversaturating Cu foils with a high precursor partial pressure via chemical vapor deposition (CVD). To understand the growth mechanisms involved, the effect of Cu foil properties (purity, manufacturer and surface morphology) and growth parameters (growth time, pressure, annealing pre-treatment time and precursor partial pressure) on fast synthesis of graphene films has been systematically investigated using Raman spectroscopy, atomic force microcopy, scanning electron microcopy and optical microcopy. We have showed that certain foils promote self-limited growth of graphene films without any pre-treatment, while other foils favor the growth of thick graphitic like films or single- and multi-layered graphene films by depending on the type and surface morphology of Cu foils. Furthermore, we have examined changes in the surface morphology of Cu foils using electropolishing. Microscopic observations reveal that surface polishing of inexpensive low purity Cu foil, which previously yielded a thick graphitic film, could promote the single layer growth of graphene with large-area uniformity.

4.1 Introduction

Since the first isolation of graphene by the Manchester group in 2004 [1] revealed the high potential for the material in countless applications due to its unique electrical, optical [2], thermal [3] and mechanical properties [4], scientists and researchers have been racing to discover and engineer methods for the fabrication of graphene sheets of both large area and high quality. Several approaches have been utilized to produce graphene sheets, including micromechanical exfoliation [5, 6], chemical oxidation of graphite [7, 8], graphitization of SiC [9, 10] and chemical vapor deposition (CVD) [11-14] using transition metals as catalysts. Although micromechanical cleavage, yielding single crystalline graphene sheets, is still the method of choice for fundamental studies, it is impractical for large scale applications due to the size limitations of the exfoliated flakes. The synthesis of graphene flakes with several microns in size has commonly been demonstrated by the reduction of graphene oxide, but the problem with this technique is poor quality graphene layers. Epitaxial growth of graphene on SiC has been among the most promising techniques for electronic applications. Nevertheless, the SiC wafer cost and the growth at only wafer scale are drawbacks for this method. CVD of graphene on transition metal catalyst has been one of the most widely studied growth methods and has proved to one of the most promising methods for large scale manufacturing. The CVD growth of graphene has been demonstrated on several metal catalysts such as Cu [15], Ni [16], Ru [17] and Ir [18], with different foils yielding varying results,

but with relative ease. The most promising metal catalyst is arguably Cu since it is relatively inexpensive compared to other commonly used foils (or evaporated films) and has been extensively studied for several year. Initially believed to be self-limiting, the deposition of graphene to a single layer offered great promise (and delivered) for roll to roll production [19] of graphene sheets of very large size. However, although the size of the sheets is only limited to your CVD chamber and Cu foil sheet size, the quality of the films were far below what had been demonstrated with exfoliated graphene, due to several factors such as defects, contamination, wrinkles, non-uniformity, small grain sizes and poly-crystallinity [20-23]. Some of these problems arise due to the CVD growth chamber, the Cu foil and the transfer process from the Cu foil to a different substrate. Over the last several years, many of these problems have begun to be address, and CVD graphene grown has been shown capable of having mobilities comparable to exfoliated graphene [24, 25], but at a price. Many of these advancements have come at a cost of long time processing times and annealing of Cu foils as well as long graphene deposition times and low vacuum pressures [26, 27].

In this study, high and ultra-high purity Cu foils by different manufacturers have been investigated for their effects on high rate deposition of graphene with minimal foil preparation and growth times. The growth mechanisms responsible for different graphene morphologies have been studied, and the conditions needed for self-limiting growth of graphene have been discussed. The results

reveal that if the Cu foil is treated by an electropolishing process before the growth, single layer graphene could form on any desired foil no matter if the sample is oversaturated for times much longer than needed to form complete coverage. Therefore, uniform single layer graphene synthesis can be achieved with precursor exposure times of less than 1 min on inexpensive Cu foil by over saturating the Cu samples with the graphene precursors, leading to CVD procedures towards an inexpensive, fast and scalable method for uniform single layer graphene synthesis.

4.2. Experimental

4.2.1 Cu foil

The various Cu foils used in this experiment were purchased directly from the manufacturer. The foils were labeled as AA1, AA2 and GF as shown in Table 1. A good range of relatively high purity and ultra-high purity were sampled with these 3 foils. The cost per cm^2 is subjective to this study since it is dependent to the amount of foil that is purchased. Bulk orders are subject to lower prices; however, the general trend still applies.

Table 1 – Copper Foils Types				
Type	Manufacturer/Part Number	Purity (%)	Thickness (μm)	Cost/cm^2 (US)
AA1	Alfa Aesar #46986	99.8	25	$0.012
AA2	Alfa Aesar #10950	99.999 (Puratronic®)	25	$1.238
GF	Goodfellow #LS413128	99.9	20	$0.241

4.2.2 Cu foil pretreatment

During these experiments, one of two Cu pretreatments were applied; a simple cleaning or electropolishing. The emphasis of these treatments was speed of treatment as well as ridding the Cu surface of any contamination such as particles or any organic matter. In the case of the polishing treatment minimization of the Cu foils, the surface roughness was also emphasized and optimized. All foils were kept in their original packaging when not in used and only handled by scissors and tweezers in order to minimize the contamination on the foils.

For the simple cleaning, the Cu foil was rinsed with acetone for 1 min and then quickly rinsed with isopropyl alcohol (IPA) for 1 min. Next, it was dried thoroughly with N_2 gas and inserted into the CVD chamber. For the electropolishing treatment, a homemade polishing cell was used with a thick Cu foil (Alfa Aesar Part #13380) plate as the cathode. The electropolishing solution was 250 mL of deionized water, 125 mL of ethanol, 125 mL of ortho-phosphoric acid, 25 mL of IPA and 2.5 grams of urea. The Cu foil was attached by alligator clip and used as the anode and held parallel to the cathode. While a voltage of 4.0 V and a current in the range of 0.8-1.0 A was applied for a time ranging from 30-180 s. After polishing, the Cu foil was rinsed carefully in deionized water followed by a thorough rinse with IPA and then dried with N_2 gas. Each polishing process requires a fresh electrochemical solution since multiple uses of the same solution could damage the Cu foil by forming pits and holes.

4.2.3 CVD

A single zone CVD furnace (MTI) with a horizontal quartz tube in the length of 1000 mm and inner diameter of 72 mm was used for the synthesis of the graphene. The Cu foils (25 mm X 25 mm) were placed into the central heat zone of the furnace, using a clean and polished quartz substrate holder (70 mm X 70 mm). To remove the oxygen, the chamber was pumped down to 100 mTorr for 5 min and then brought to 20 Torr and stabilized with a flow of 50 sccm Ar and 5 sccm H_2. The furnace was then heated to 1000 ^{o}C in 45 min. Ar flow was shut down, and H_2 flow was increased to 20 sccm 2 min before the growth starts. The growth was performed at this temperature with a flow of 5 sccm CH_4 and 20 sccm H_2. This flow rate and pressure were chosen since it had previously been determined to be enough to saturate the Cu foils quickly with graphene after only a couple of minutes. After the growth step was completed, CH_4 flow was shut down, and the furnace was cooled with a flow of 5 sccm H_2 and 50 sccm Ar in 40 min. To compare the graphene growth on 3 types of Cu foils under the same growth conditions, all foils were placed in the furnace, and grown simultaneously.

4.2.4 Etch and transfer

First, the graphene/Cu foils were spin-coated with PMMA. The PMMA/graphene/Cu foils were then left to stabilize for 25 min without any heat treatment. Third, the uncoated backside of the foils was etched in a solution of

0.3 M of FeCl$_3$ for 10 min, following a deionized water rinse in order to remove the graphene layer on the backside of the foils. Next, the foils were left floating in a solution of 0.1 M ammonium persulfate for up to several hours until the Cu was completely etched. The PMMA/graphene samples were then fished out of the etching solution and immersed into the deionize water to remove the etchant residue. Further, it was fished by the SiO$_2$/Si substrate. Finally, the PMMA layer was rinsed off with acetone for several min, then with IPA and blow dried with N$_2$ gas.

4.2.5 Characterization

Raman spectroscopy measurements were done on a Thermo Scientific DXR, using a 100X objective and a laser wavelength of 514 nm at 10 mW. Scanning electron microscopy (SEM) was performed using a Phillips XL-30 with a working distance of 10 mm and electron beam energy of 10 keV. A Veeco atomic force microscope (AFM) was used to study the surface morphology and composition under tapping mode.

4.3 Results and Discussion

4.3.1 Cu type

The three types of Cu foils have been compared in order to determine if Cu foil manufacturer and purity are a critical factor in the uniformity and quality of

graphene. Initially, the CVD furnace was ramped to 1000° C with no steady state

annealing step, and the precursor gases of CH_4 and H_2 have been introduced for

5 min. Fig. 4.1 shows the SEM images (a-c), optical images (d-f) and Raman

spectra (g) of the graphene samples grown on the tree types of Cu foils. It should

be noted that the graphene samples have been transferred to the SiO_2/Si

substrates for optical imaging and Raman spectroscopy analysis. For AA1, there

is a thick and uneven deposition of carbon as shown Fig. 4.1a and 4.1d. The

Raman spectra shows a large D peak and the absence of G' peak, revealing that

a graphitic film is formed. The precursor deposition seems to be highly

concentrated along the Cu foil striations, which can be observed as thick lines in

Fig. 4.1a and 4.1d. AA2 yields the growth of single layer graphene with a high

density of multilayer graphene domains as shown in Fig 4.1b and 4.1e. Fig.4.1g

shows the Raman spectra taken from a single-layer and a multilayer region of

AA2. The results confirm the growth of the graphene on AA2, but with non-

uniform thicknesses [28]. Moreover, a high D peak and additional D' peak are

observed on the single layer regions, indicating the poor quality of graphene

layers grown on AA2 [29]. For GF, SEM and optical images demonstrate the

growth of uniform single layer graphene with small or negligible multilayer points

across the substrate as seen in Fig. 4.1c and 4.1f. The Raman spectra reveal the

typical Raman bands [30] of a single layer graphene with a smaller D peak

compared to that of AA1 and AA2. The D peak is likely due to small graphene

domains caused by the saturation of the CVD precursors, which leads to a high density of grain boundary defects [29].
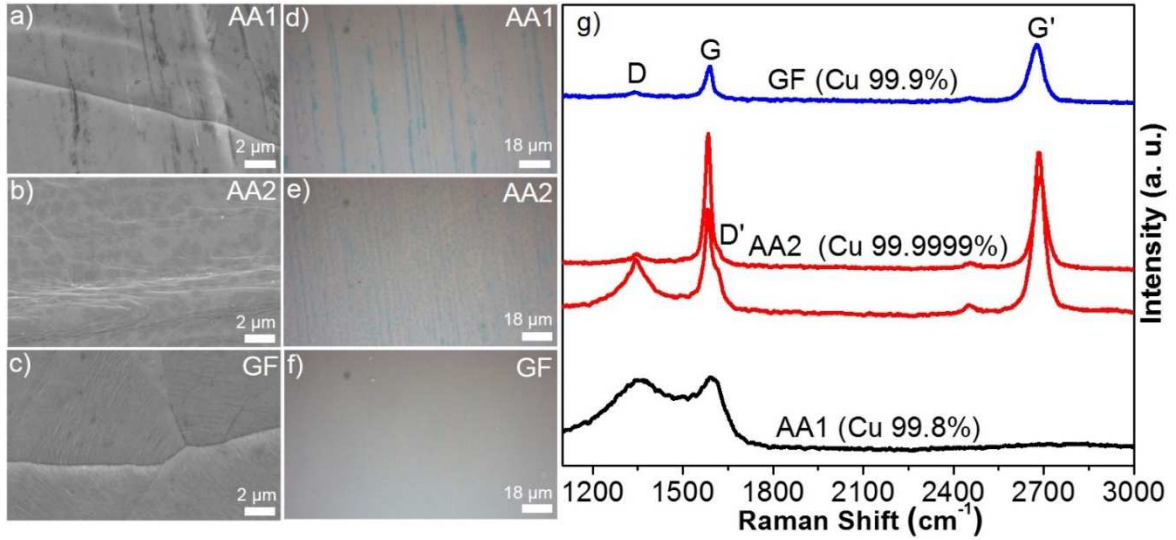
Figure 4.1. *SEM images (a-c), optical images (d-f) and Raman spectra (g) of the graphene samples grown on AA1, AA2 and GF with no annealing.*

The aforementioned experiment has been repeated with an additional 25 min steady state annealing step before the growth starts. The results reveal a similar trend to that of the growths without annealing as can be seen in Fig. 4.2. For AA1, the Raman spectra confirm the existence of the thick uneven graphitic layers with some single layer graphene regions. Annealing seems to promote the growth of thinner graphene films. In Fig. 4.2a-4.2c, the SEM images reveal clearly the detailed surface morphology of the Cu foils (Other than Cu grain boundaries), which is not visible in the case of the growth without annealing. For AA2, the growth of single layer graphene with some bilayer domains across the substrate is observed from the SEM and optical images in Fig. 4.2b and 4.2e,

and confirmed by the Raman spectra in Fig. 4.2g. The density of the bilayer domains is less than to the density of the multilayer domains of AA1. The low density of the multilayer graphene domains results in the growth of the large grains [31]. For AA2, the size of thicker domains is increased to the 2-3 µm as a result of annealing as shown in Fig. 4.2b. For GF, the similar trends are observed to the growth without annealing. As it is shown in Fig. 4.2g, the Raman spectra reveals that single layer graphene forms uniformly on GF. However, annealing also results in a high density of deep level defects at Cu grain boundaries (Fig. 4.2c and 4.2f), which is known to have a detrimental effect on the electrical properties of graphene [32-34].
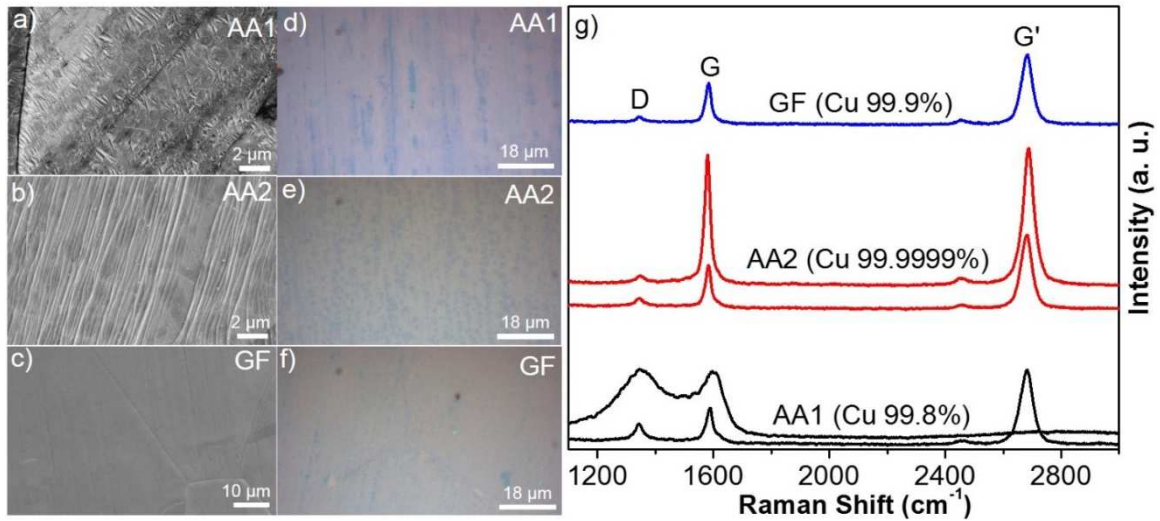

Figure 4.2: *SEM images **(a-c)**, optical images **(d-f)** and Raman spectra **(g)** of the graphene samples grown on AA1, AA2 and GF with 25 min annealing.*

In order to investigate the reason for the discrepancy of the graphene films on different types of Cu foils, AFM has been performed on the copper foils

without any pretreatment. Fig. S2 shows the AFM images of the Cu foils as purchased. The root mean square surface roughness value, R_q, of AA1, AA2 and GF has been measured from their AFM height profile images, which are given in Table 2. The results indicate that more expensive Cu foils have a smoother surface and higher purity, but it does not necessarily mean that more expensive copper foils result in the growth of high quality of graphene layers. As shown in Table 2, R_q of 0 min annealing growth demonstrates that the surface roughness of all Cu foils is improved during the heating [21, 22, 35, 36] even if there is no annealing. Although the surface roughness of AA1 and AA2 slightly decreases after the growth, the surface roughness of GF is improved by over 50% and comparable to that of AA2. Very little improvement is found in the surface morphology of the foils after annealing for 25 min. The results reveal that additional 25 min annealing does not dramatically affect the surface roughness of the Cu foils despite the fact that annealing improves the crystallinity of the Cu foils [37].

Table 2 – Copper Foils Surface Morphology			
Type	R_q (nm) As Received	R_q (nm) 0 min Annealing	R_q (nm) 25 min Annealing
AA1	68.3	55.7	53.3
AA2	25.6	23.8	20.4
GF	57.6	22.9	21.1

From the results, we conclude that GF is the most effective foil for promoting uniform self-limiting single layer graphene while AA1 and AA2 promote multilayer graphene formation. Fig 4.3 a and 4.3b show the surface morphology of AA1, AA2 and GF after the graphene growth without annealing and with annealing, respectively. Similar trends are observed in the surface morphology of the foils after graphene growth, and no significant change is found in the surface morphology of the foils by 25 min annealing. The AFM images of AA1 reveal the existence of high peaks and deep valleys, but with a fairly smooth surface. For AA2, it shows a commonly seen step morphology, which has been discussed in the previous works [26, 37]. GF shows a different morphology compared to AA1 and AA2. GF surface appears to have a higher density of the steps and is more wavelike across the surface. It has been reported [38] that the high and wide steps promote epitaxial growth of graphene, leading to multilayer graphene formation. However, this is not a case in the growth on GF due to the higher density of these surface steps. We show that the higher density of surface steps promotes self-limiting graphene growth.
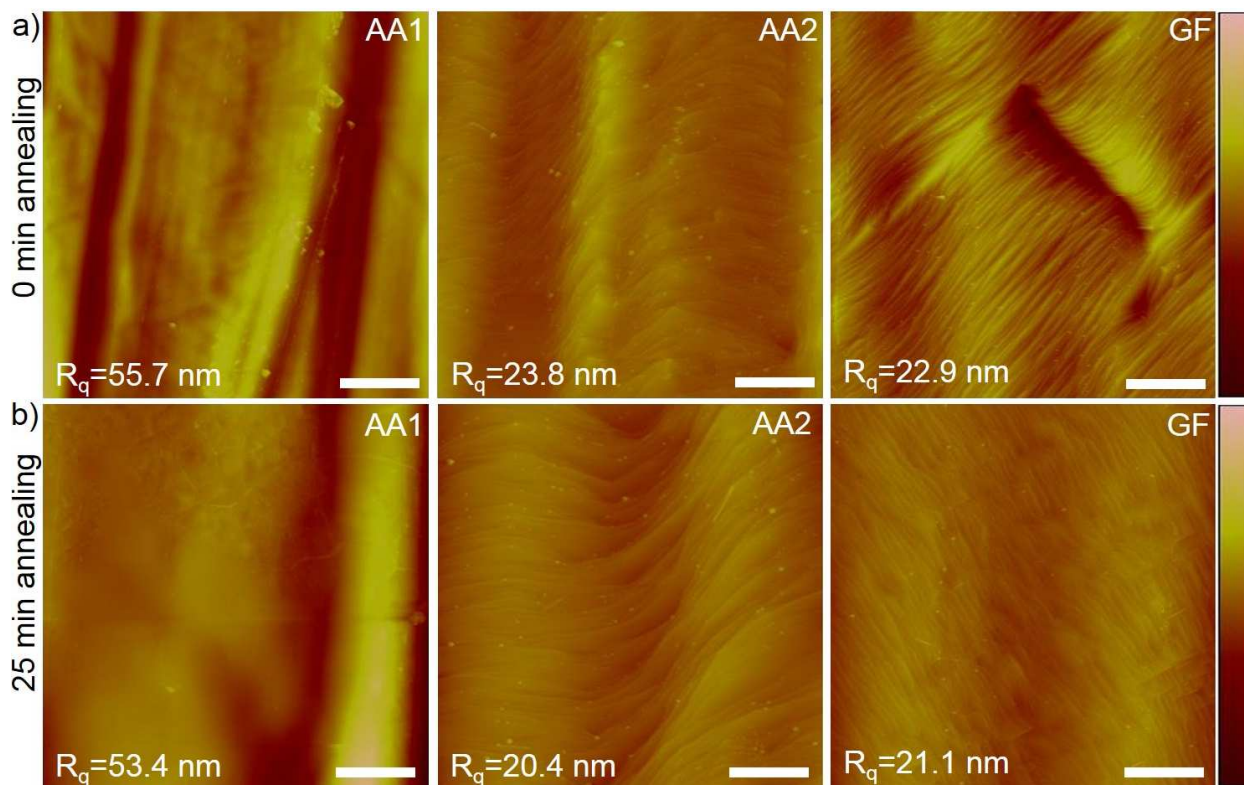
Figure 4.3 *AFM images of graphene grown on AA1, AA2 and GF without annealing (a) and 25 min annealing (b) for 5 minute growth time (The scale bar is 3 μm).*

Further insight can be gained by investigating the height profile across the surface of the Cu foils from the AFM images as shown in Fig. 4.3a and 4.3b for both 0 and 25 min annealed growths. The thick uneven graphitic layers grown on AA1 can be attributed to the relatively smooth surface of the Cu foil surface. This may seem counterintuitive, but it can be observed from the surface height line scans (Fig. 4.4a-4.4c) across the Cu foils perpendicular to their Cu striations (Fig. 4.5 and Fig. 4.6). Although AA1 has striations as much as 100 nm deeper,

its surface is smoother when compared to AA2 and GF as shown in Fig. 4.4a.

Moreover, the peak and valley count of AA1 appear to be much less when

compared to the other two foils, which is given in Fig. 4.4c. 25 min annealing

leads to the reduced striation depths and an increased peak and valley count,

which can be seen in Fig 4.4b and 4.4c. This can account for the formation of

graphene regions, which formed in the rougher regions with the smoother

regions occupying along the deep striations forming thick graphitic films.
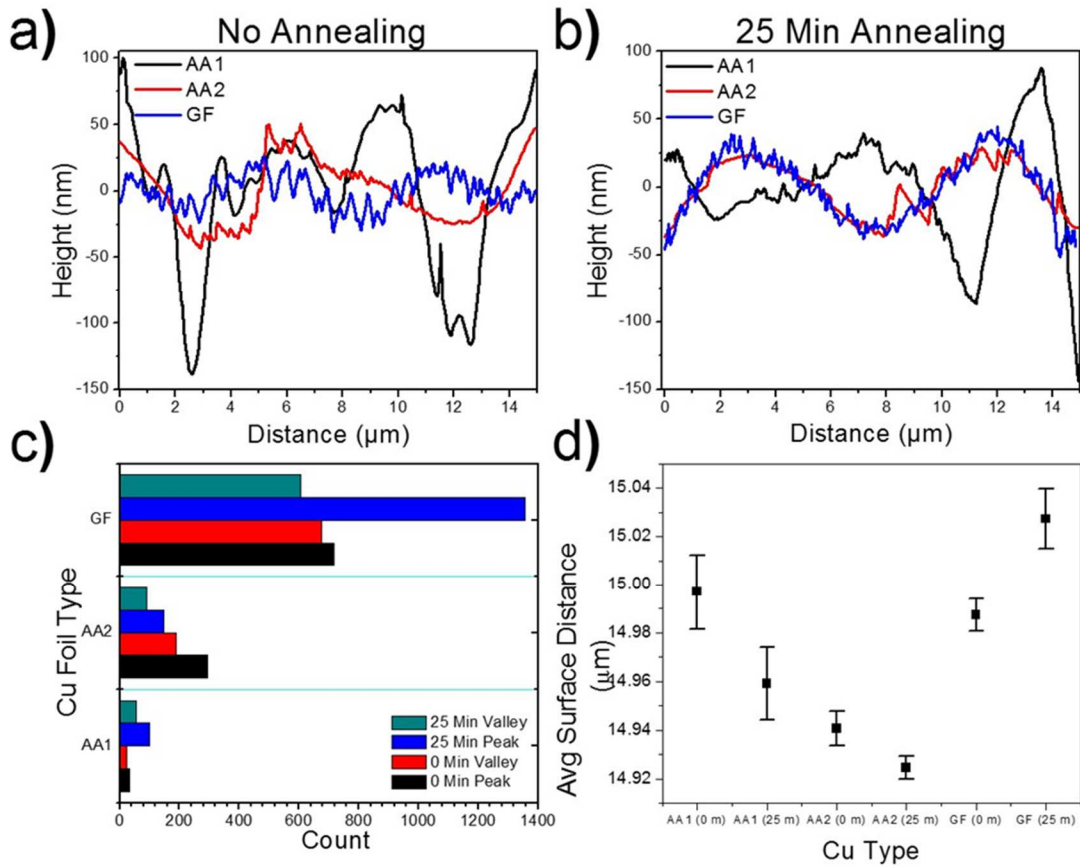
Figure 4.4: *Surface height scans of AA1, AA2 and GF without annealing (a) and*

25 min annealing (b). The peak and valley counts of the height scans (c) and

average surface distance across the surfaces (d).
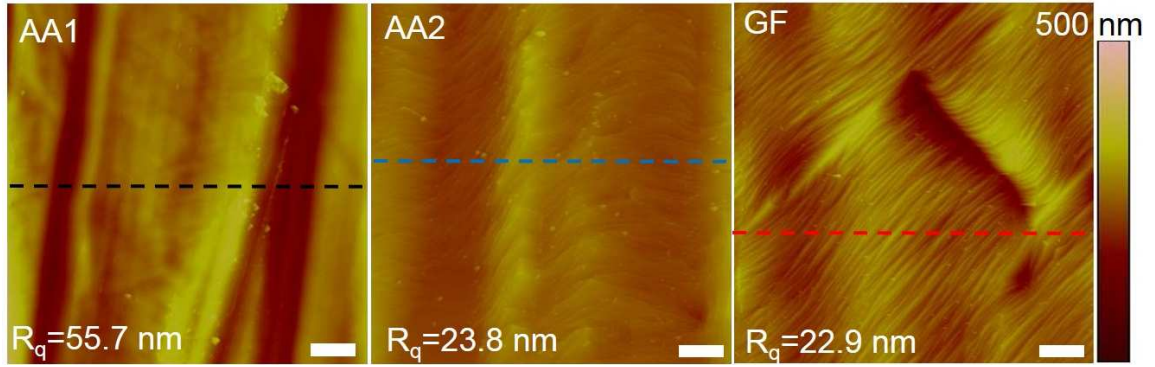
Figure 4.5. *AFM images of AA1, AA2 and GF after the graphene growth without annealing with scan lines. The scale bar is 2 μm.*
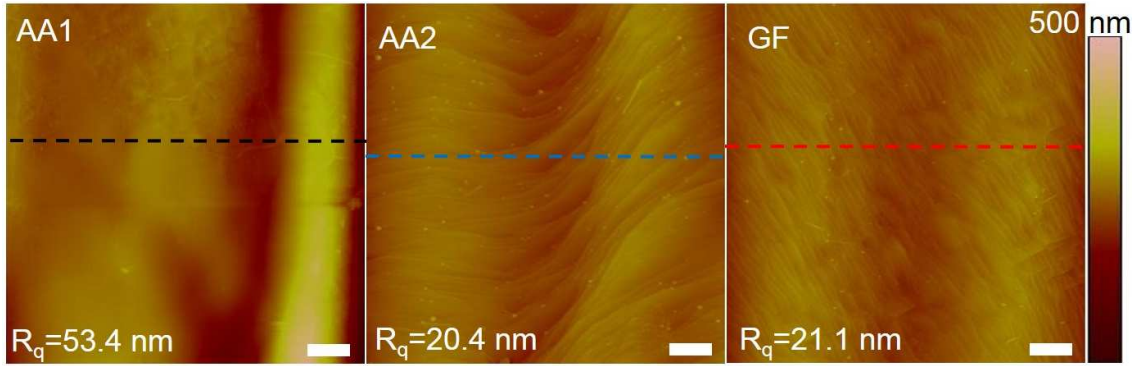
Figure 4.6. *AFM images of AA1, AA2 and GF after the graphene growth with 25 min annealing with scan lines. The scale bar is 2 μm.*

Further evidence to this discrepancy is found by comparing the surface morphology of AA1, AA2 and GF after growth. Although all foils have striations across the surface, the striations of AA2 and GF are much shallower. The striation depths for both AA2 and GF are almost identical, which is shown by the over lapping blue and red scans lines in Fig. 4.4 b. For AA2 and GF, similar striations on the surface lead to similar R_q after growth, but it is not the only

determining factor in providing an adequate surface for self-limiting high quality

graphene formation. By comparing the peak to valley count displayed in Fig. 4.4

c, we observe that there is a dramatic difference between AA2 and GF. The peak

to valley count of GF foil is several times larger than that of AA2. In the case of

25 min annealing, the peak to valley count of AA2 decreases, explaining why the

multilayer domains are larger [39]. The average surface distance of the scans of

all foils before and after annealing has been compared in order to confirm that

total surface area of the films is not a determining factor for single or few layer

graphene growth. Fig. 4.4d shows that the density of the peak to valley counts of

GF after annealing is higher than that of AA1 and AA2, making GF an ideal

substrate for self-limiting graphene synthesis.

Fig. 4.7 demonstrates the possible growth mechanisms involved for each foil. For

AA1 with its steep striations and continuous smooth and straight surface, the

growth of epitaxial graphene is promoted, and when it is saturated with high

levels of precursor gases, thick graphitic films are formed as shown in Fig. 4.7 a.

The wide and high steps of AA2 also promote epitaxial growth in these regions

as shown in Fig. 4.7b. However, for these experiments, it doesn't seem to grow

graphene thicknesses of more than a couple of layers. Finally, GF with its very

high density peak and valley count promotes the self-limiting graphene synthesis

across its surface, even if it is saturated with high levels of precursor gases,

which is shown in Fig. 4.7c.
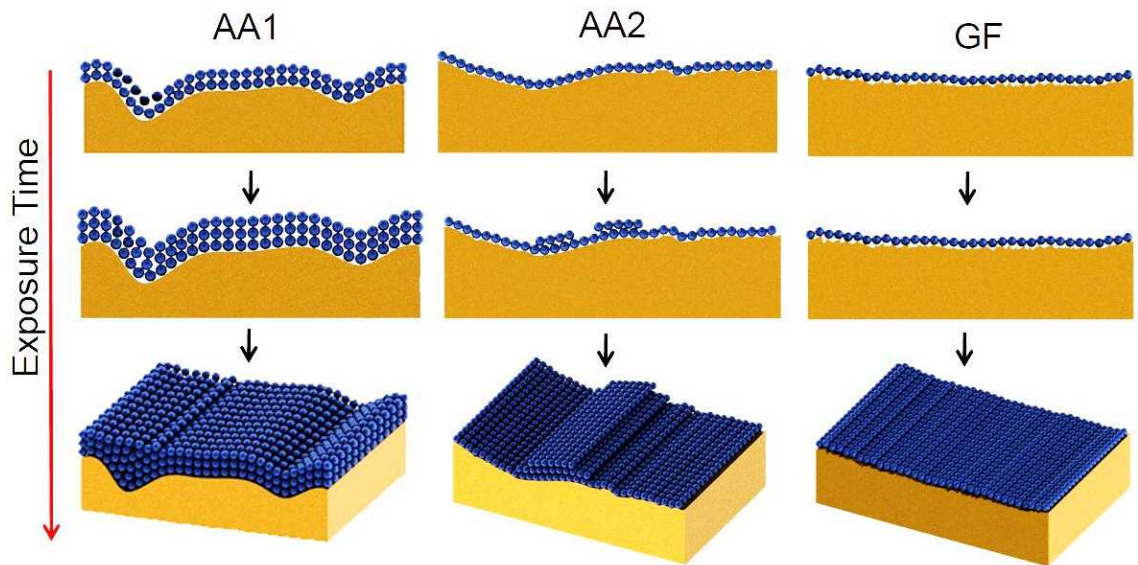
Figure 4.7: *Cu surface morphology effect on graphene layer formation comparison between AA1, AA2 and GF.*

We conclude that although GF naturally promotes the growth of single layer graphene without any special treatment, it does suffer from two main drawbacks. The first drawback is its high cost when compared to other foils. The second of these drawbacks is that deep grain boundaries are induced during the cleaning process. When electrochemical polishing, one of common surface treatment techniques, is applied in order to produce higher quality graphene films, GF develops very deep Cu grain boundaries. When GF is coated with the polymer during the transfer process, these deep grain boundaries of GF can fold over and trap the polymer within the graphene film, which is impossible to remove without damaging the continuous film. Cleaning GF with acetic acid before the growth also results in deep grain boundaries. Due to these problems in the use of GF,

we have focused on improving the self-limiting growth and the quality of the graphene film on AA1 by using electrochemical polishing.

4.4 Single layer optimization

Electropolishing has been utilized to improve the graphene growth on AA1. The effect of polishing duration on the surface morphology of AA1 has been systematically studied. Fig. 4.8 shows R_q and the peak to valley count versus polishing time for AA1. For 30 sec and 45 sec of polishing, AA1 still shows dramatic improvement in R_q, with the striations depths decreasing as shown in Fig. 4.8a-4.8c. After 60 sec of polishing, R_q decreased from 63 nm to less than 4 nm. Above 60 sec of polishing, there is no significant change observed in R_q, which displays asymptotic behavior with limit being near 3 nm. While R_q decreases with polishing time, the peak to valley count increases. For 60 sec of polishing, the peak to valley count is increased by three times compared to the initial value. For 180 sec of polishing, it reaches over 15000, which is 2 orders of magnitude greater than the initial value. We have noticed that long polishing times greater than 2 min results in etching of the edge of the foils.
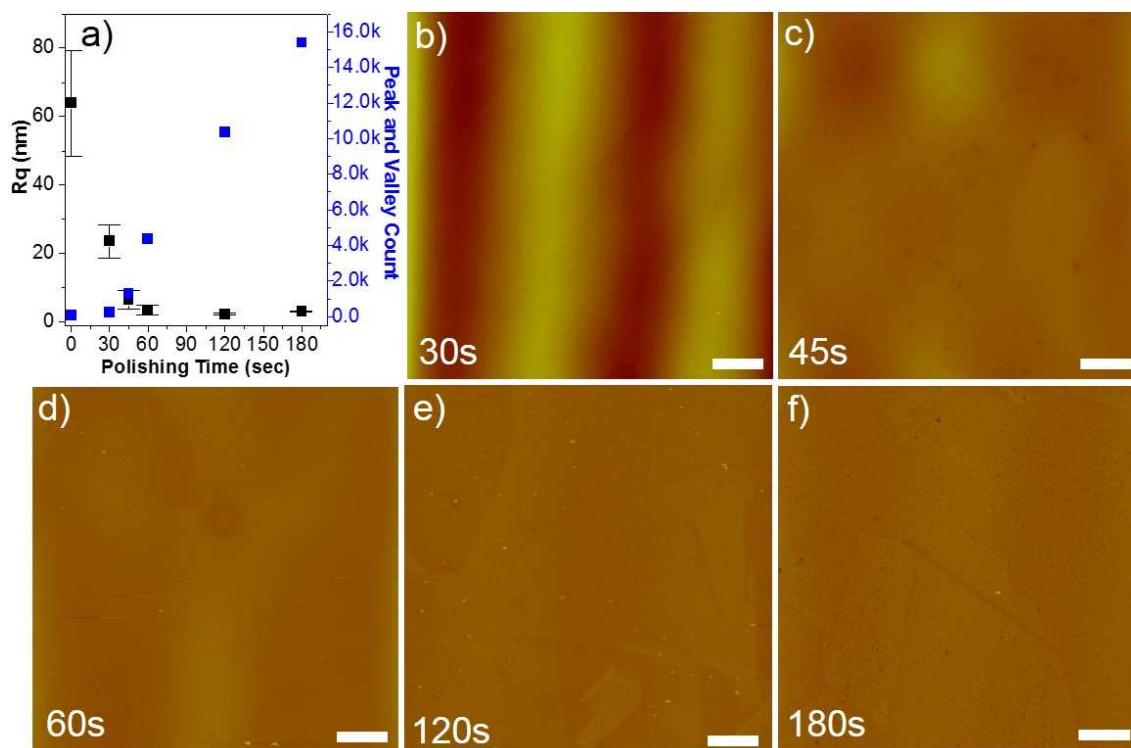
Figure 4.8: R_q *and peak to valley counts (a) and AFM height images (b-f) vs polishing time. (The scale bar is 2 μm.)*

The growth of graphene on the unpolished and polished AA1 has been simultaneously carried out to study the effect of polishing on the quality of graphene. The growth has been performed for 5 min without annealing. AFM has been used to study the surface morphology of the two foils after the graphene growth. From Fig. 4.9a and 4.9b, it is found that the surface of the polished foil is flatter with some little striations compared to the unpolished foil. Figure 4.9c displays the height scan profile comparison of polished and unpolished samples. While the unpolished sample shows high R_q of 73.4 nm and low peak to valley count of 55, the polished sample reveals low R_q of 8.49 nm and an extremely high

peak to valley count of 2530. The peak and valley count of AA1 is comparable to that of GF, which has shown above, thus promoting self-limiting graphene deposition as shown in the inset of Fig. 4.9c. The Raman spectra of the unpolished and polished AA1 has been compared in Fig. 4.9d. The Raman spectra of the unpolished sample shows large D and broad G peaks, indicating the growth of thick and damaged graphitic film [30]. The Raman spectra of the polished sample shows sharp small D and sharp G' peaks, indicating the growth of continuous single layer graphene with high crystallinity [29, 30, 40, 41].
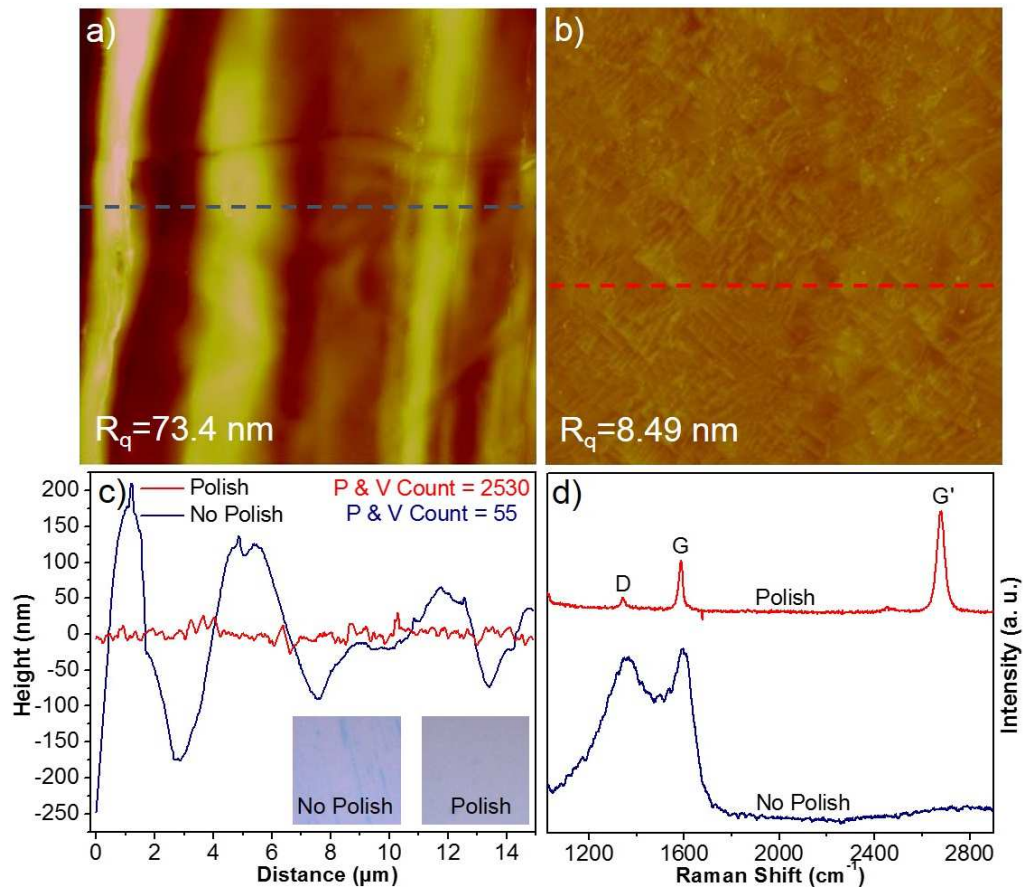
Figure 4.9 *AFM images (a,b), height scan profile (c) and Raman comparisons (d) of the unpolished and polished AA1 after the graphene growth.*

99

Finally, the graphene growth has been performed on AA1 polished for 90 sec by tuning growth times from 1 to 20 min. From the polishing experiments above, 90 sec of polishing has been determined to be the optimal polishing compromise time in order to get a low density of graphene domains and high peak to valley count. Fig. 4.10a shows the Raman spectra of the various graphene films that have been overexposed and underexposed to the precursor times from the original 5 min of exposure. The Raman spectra show very little variation throughout different exposure times. For all samples, the low ratio of G to G' peaks and small D peak have been observed, revealing that the grown film is single layer and contamination-free.
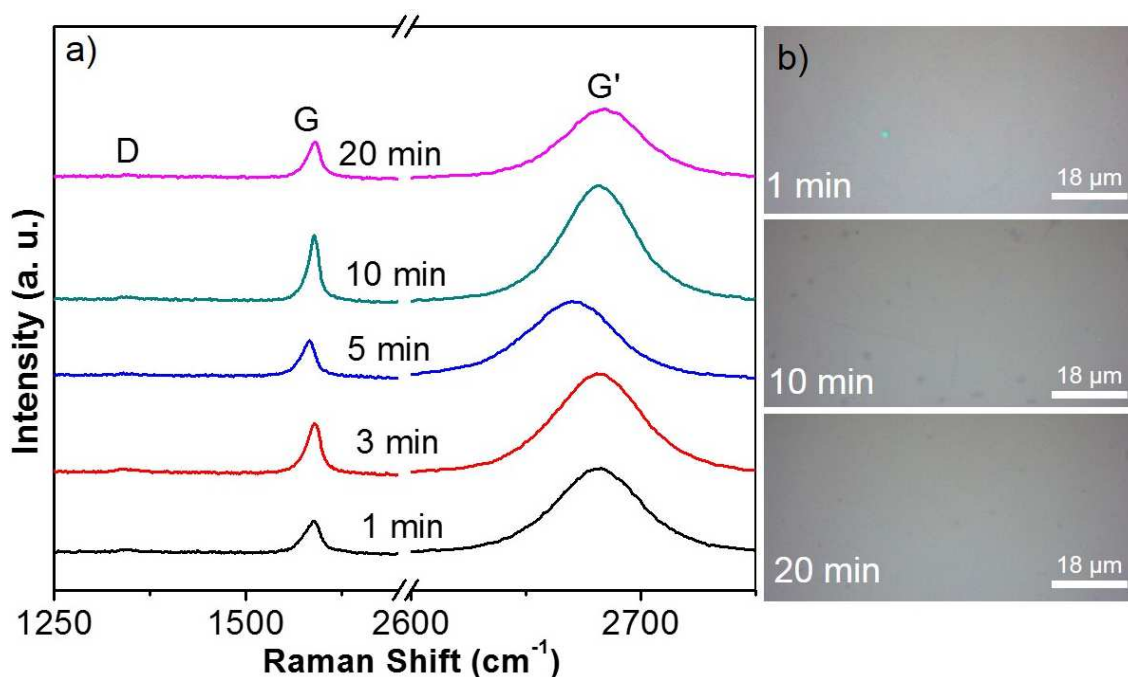
Figure 4.10:. *a) Raman spectra from the graphene for the growth times of 1, 3, 5, 10 and 20 min. b) Optical images of continuous graphene films for the growth times of 1, 10 and 20 min.*

The results reveal that the growth of uniform single layer graphene can be achieved for the short exposure time (1 min). A graphene growth for the exposure time less than 1 min has not performed. However, it is conceivable that the processing time could be less than 1 minute based on the experimental results. Fig. 4.10b displays the optical images of the graphene, transferred to SiO_2 substrates, for the growth times of 1, 10 and 20 min. It is clearly shown that all graphene films are clearly continuous and single layer. However, negligible amount of the bilayer domains can be seen on the graphene sample for the growth time of 10 min. This can be attributed to uneven polishing of the Cu foil and easily remedied by a more robust and consistent polishing setup. The bilayer domains shown here serve as an indication of how large the graphene domains grow, which are not able to be observed through SEM due to the continuous films growing so rapidly.

4.5. Conclusion

Although differences between two foil manufacturers, Alfa Aesar and Goodfellow, result in differences in graphene growth by CVD, it has been shown higher purity foils (or more expensive foils) do not necessarily provide higher quality single layer graphene. GF provided a self-limiting single layer graphene film, while the lower purity AA1 and higher purity AA2 provided thick graphitic films and single layer/bilayer films respectively, under the same growth conditions. By studying the surface morphology of the Cu foils before and after

the graphene synthesis it was shown that the determining factors in producing uniform single layer graphene sheets are the low surface roughness values and high peak and valley counts of the Cu foils. The GF foil had a naturally high peak and valley count straight from the manufacturer resulting in self-limiting single layer graphene formation. However it was shown that by electropolishing AA1 (the lowest purity and most inexpensive foil tested) for only 90 sec that the surface roughness could be decreased and the peak and valley count increased enough to promote self-limiting single layer graphene on the foil.

Finally it was demonstrated that the now self-limiting AA1 sample could be over exposed to the precursor gases for times up to 20 minutes and the single layer graphene surface would be passivized and not form anymore graphene layers. Thus by over exposing the AA1 foil to high amounts of precursor gas full single layer sheets of graphene were synthesized with growth times as short as 1 minute at a pressure of only 20 torr. Growth times of just a few seconds could be possible however they could not be explored here due the small flow rate limits of our current mass flow controllers. However synthesis of large graphene films would only be limited to the size of the polishing station and CVD chamber and how quickly, large amounts of the precursor gas could be introduced into the chamber. Thus a low cost, rapid and large scale method for high quality, uniform single layer graphene sheets is proposed.

References:

1. K. S. Novoselov, A.K. Geim., S. V. Morozov, D. Jiang, Y. Zhang, S. V. Dubonos, et al., Electric field effect in atomically thin carbon films. Science 2004; 306(5696):666-9.

2. L. A. Falkovsky, Optical properties of graphene. JPCS 2008; 129(1).

3. A. A. Balandin, S.Ghosh., W. Bao, I. Calizo, D. Teweldebrhan, F. Miao, et al., Superior thermal conductivity of single-layer graphene. Nano Lett. 2008; 8(3):902-7.

4. C. Lee, X. Wei., J. W. Kysar, J. Hone, Measurement of the elastic properties and intrinsic strength of monolayer graphene. Science 2008; 321(5887): 385-8.

5. Y. Hernandez, V. Nicolosi, M. Lotya, F. M. Blighe, Z. Sun, S. De, et al., High-yield production of graphene by liquid-phase exfoliation of graphite. Nat. Nanotechnol. 2008; 3(9):563-8.

6. Y. Si, E.T. Samulski, Exfoliated graphene separated by platinum nanoparticles. Chem. Mater. 2008; 20(21):6792-7.

7. S. Stankovich, D. A. Dikin, R. D. Piner, K. A. Kohlhaas, A. Kleinhammes, Y. Jia, Synthesis of graphene-based nanosheets via chemical reduction of exfoliated graphite oxide. Carbon 2007; 45(7):1558-65.

8. G. Eda, G. Fanchini, M. Chhowalla, Large-area ultrathin films of reduced graphene oxide as a transparent and flexible electronic material. Nat. Nanotechnol. 2008; 3(5):270-4.

9.   C. Virojanadara, M. syvajarvi, R. Yakimova, L. I. Johansson, A. A. Zakharov, T. Balasubramanian, Homogeneous large-area graphene layer growth on 6 H-SiC (0001). Phys. Rev. B 2008; 78(24):245403.

10.   Z. H. Ni, W. Chen, X. F. Fan, J. L. Kuo, T. Yu, A. T. S. Wee, et al., Raman spectroscopy of epitaxial graphene on a SiC substrate. Phys. Rev. B 2008; 77(11):115416.

11.   A. Reina, S. Thiele, X. Jia, S. Bhaviripudi, M. S. Dreselhaus, J. A. Schaefer, et al., Growth of large-area single- and bi-layer graphene by controlled carbon precipitation on polycrystalline Ni surfaces. Nano Res. 2009; 2(6):509-16.

12.   L. Gao, W. Ren, H. Xu, L. Jin, Z. Wang, T. Ma, et al., Repeated growth and bubbling transfer of graphene with millimetre-size single-crystal grains using platinum. Nat. Commun. 2012; **3**:699.

13.   L. Meng, R. Wu, L. Zhang, L. Li, S. Du, Y. Wang, et al., Multi-oriented moiré superstructures of graphene on Ir (111): experimental observations and theoretical models. J. Phys.: Condens. Matter. 2012; 24(31):314214.

14.   X. Li, W. Cai, J. An, S. Kim, J. Nah, D. Yang, et al., Large-area synthesis of high-quality and uniform graphene films on copper foils. Science 2009; 324(5932):1312-14.

15.   X. Mi, V. Meunier, N. Koratkar, Y. Shi, Facet-insensitive graphene growth on copper. Phys. Rev. B 2012; 85(15):155436.

16.   S. J. Chae, F. Güneş, K. K. Kim, E. S. Kim, G. H. Han, S. M. Kim, et al., Synthesis of large-area graphene layers on poly-nickel substrate by chemical vapor deposition: wrinkle formation. Adv. Mater. 2009; 21(22):2328-33.

17.   B. Borca, S. Barja, M. Garnica, J. J. Hinarejos, A. L. Vázquez de Parga, R. Miranda, Periodically modulated geometric and electronic structure of graphene on Ru (0 0 0 1). Semicond. Sci. 2010; 25(3):034001.

18.   P. Lacovig, M. Pozzo, D. Alfe, P. Vilmercati, A. Baraldi, S. Lizzit, Growth of dome-shaped carbon nanoislands on Ir (111): the intermediate between carbidic clusters and quasi-free-standing graphene. Phys. Rev. Lett. 2009; 103(16):166101.

19.   S. Bae, H. Kim, Y. Lee, X. Xu, J.-S. Park, Y. Zheng, et al., Roll-to-roll production of 30-inch graphene films for transparent electrodes., Nat. Nanotechnol. 2010; 5(8):574-8.

20.   W. Zhu, T. Low, V. Perebeinos, A. A. Bol, Y. Zhu, H. Yan, et al., Structure and electronic transport in graphene wrinkles. Nano Lett. 2012; 12(7): 3431-6.

21.   N. Petrone, C. Dean, I. Meric, A. van der Zande, P. Huang, L. Wang, Superior mobility in chemical vapor deposition synthesized graphene by grain size engineering, APS Meeting Abstracts 2012; 1:12007.

22.   H. Li, X.Wen-Yan, Q. Yan-De, P. Yi, G. Min, P. Li-Da, et al., The influence of annealing temperature on the morphology of graphene islands. Chin. Phys. B 2012; 21(8):088102.

23.   A. Pirkle, J. Chan, A. Venugopal, D. Hinojos, C. W. Magnuson, S. McDonnell, et al., The effect of chemical residues on the physical and electrical properties of chemical vapor deposited graphene transferred to SiO_2. Appl. Phys. Lett. 2011; 99(12):122108-3.

24.   W. Gannett, W. Regan, K. Watanabe, T. Taniguchi, M. F. Crommie, A. Zettl., Boron nitride substrates for high mobility chemical vapor deposited graphene. Appl. Phys. Lett. 2011; 98(24):242105.

25.   S. Lee, O. D. Iyore, S. Park, Y. G. Lee, S. Jandhyala, C. G. Kang, et al., Rigid substrate process to achieve high mobility in graphene field-effect transistors on a flexible substrate. Carbon 2014; 68:791-7.

26.   S. Chen, H. Ji, H. Chou, Q. Li, H. Li, J. W. Suk, et al., Millimeter-size single-crystal graphene by suppressing evaporative loss of Cu during low pressure chemical vapor deposition. Adv. Mater. 2013; 25(14):2062-5.

27.   Y. Hao, M. S. Bharathi, L. Wang, Y. Liu, H. Chen, S. Nie, et al., The role of surface oxygen in the growth of large single-crystal graphene on copper. Science 2013, 342(6159):720-3.

28.   Z. Mutlu, M. Penchev, I. Ruiz, H. H. Bay, S. Guo, M. Ozkan, et al., Effects of process tube position on properties of graphene layers. MRS Procs. 2012; 1451:57-62.

29.   A. Eckmann, A. Felten, A. Mishchenko, L. Britnell, R. Krupke, K. S. Novoselov, et al., Probing the nature of defects in graphene by Raman spectroscopy. Nano Lett. 2012; 12(8):3930.

30.   M. S. Dresselhaus, A. Jorio, M. Hofmann, G. Dresselhaus, R. Saito, et al., Perspectives on carbon nanotubes and graphene Raman spectroscopy. Nano Lett., 10(3) (2010): 751-8.

31.   X. Li, C. W. Magnuson, A. Venugopal, J. An, J. W. Suk, B. Han, et al., Graphene films with large domain size by a two-step chemical vapor deposition process. Nano Lett. 2010; 10(11):4328-34.

32.   L. Colombo, X. Li, B. Han, C. Magnuson, W. Cai, Y. Zhu, R. S. Ruoff. Growth kinetics and defects of CVD graphene on Cu. ECS Trans. 2010; 28(5):109-114.

33.   G. Hee, F. Güneş, J. J. Bae, E. S. Kim, S. J. Chae, H. -J. Shin, Influence of copper morphology in forming nucleation seeds for graphene growth. Nano Lett. 2011; 11(10):4144-8.

34.   P. Egberts, G. Han, X. Z. Liu, A. T. C. Johnson, R. W. Carpick. Frictional behavior of atomically-thin sheets: hexagonal-shaped graphene islands grown on copper by chemical vapor deposition. ACS nano 2014.

35.   P. Y. Huang, C. S. Ruiz-Vargas, A. M. van der Zande, W. S. Whitney, M. P. Levendorf, J. W. Kevek, et al., Grains and grain boundaries in single-layer graphene atomic patchwork quilts. Nature 2011; 469(7330):389-92.

36.   B. Zhang, W. H. Lee, R. Piner, I. Kholmanov, Y. Wu, H. Li, et al., Low-temperature chemical vapor deposition growth of graphene from toluene on electropolished copper foils. ACS nano 2012; 6(3):2471-6.

37.	Z. Luo, Y. Lu, D. W. Singer, M. E. Berck, L. A. Somers, B. R. Goldsmith, et al., Effect of substrate roughness and feedstock concentration on growth of wafer-scale graphene at atmospheric pressure. Chem. Mater. 2011; 23(6):1441-7.

38.	L. Fan, Z. Li, Z. Xu, K. Wang, J. Wei, X. Li, et al., Step driven competitive epitaxial and self-limited growth of graphene on copper surface. Aip Adv 2011, 1(3):032145.

39.	K. Hayashi, S. Sato, N. Yokoyama, Anisotropic graphene growth accompanied by step bunching on a dynamic copper surface. Nanotechnology 2013; 24(2):025603.

40.	C. Casiraghi, A. Hartschuh, H. Qian, S. Piscanec, C. Georgi, A. Fasoli, et al., Raman spectroscopy of graphene edges. Nano Lett. 2009; 9(4):1433-41.

41.	A. Jorio, M. S. Dresselhaus, R. Saito, G. Dresselhaus. Raman spectroscopy in graphene related systems. John Wiley & Sons, 2010.

Chapter 5

A New Variant of Graphene: Wafer Scale Graphene Oxide Sheets

For the first time, the synthesis of a uniform monolayer graphene oxide film is demonstrated by chemical vapor deposition on thin Cu foils using a simple 2 step precursor exposure at atmospheric pressure. The uniformity and continuity of the film is confirmed using optical and scanning electron microscopy, while the film thickness and monolayer deposition is demonstrated by atomic force microscopy. Regions of folded edge regions are shown to have monolayer, bilayer and multilayer regions are they are studied by Raman spectroscopy to confirm the presence of graphene oxide films, while X-ray photoelectron spectroscopy is carried out to confirm the carbon-oxygen bonds of the film. Fluorescent quenching microscopy demonstrates the presence of a uniform graphene oxide film by demonstrated a clear contrast compared to pristine graphene film. Finally the reduction of the graphene oxide film to graphene is demonstrated by laser light exposure, using Raman spectroscopy mapping. This synthesis method has much potential for large scale synthesis of uniform continuous graphene oxide films for semiconducting and transparent electrode applications.

5.1 Introduction

Graphene has had an extraordinary impact over the last decade since its discovery as the world first 2 dimensional (2D) material[1], including creating a feverish interest for other 2D materials[2-4] and their properties[5,6] and potential applications[7,8]. The graphene derivative, graphene oxide (GO)[9,10], long seen as an intermediary material to create graphene[11,12], has also garnered much attention due to its ease of production, scalability and ability to produce graphene through the reduction of graphene oxide (r-GO). A few of the more popular methods to produce GO include; Hummer's[13], Tour's[14], Staudenmaier's[15,16] and several others[17]. These methods consist of oxidizing bulk graphite using oxidants such as KClO3, NaNO3 and KMnO4,in which oxygen intercalates in between the graphite's graphene stacks and graphene oxide is produced by exfoliating the graphite oxide into GO. The various preparation methods create varying GO structures[9], which differ in terms of crystal structure and oxygen to carbon ratio. Interestingly, band gap engineering of GO has been shown to be possible through control of the oxygenation levels of GO[18]. GO's electrical properties have been shown to be range from insulating to semimetal[19-21], while also displaying photoluminescence in a wide range of wavelengths[22,23]. Thus control of GO synthesis and its oxygen concentration and structure may open up the door for semiconducting graphene.

Unfortunately, although the production of graphene oxide is facile, inexpensive and scalable for mass production, it has limitations in terms of future applications due to its physical nature. The aforementioned methods produce flakes of GO, consisting of varying flake sizes, layer thicknesses and uneven film distribution. This results in limited use of GO for semiconducting applications, which require very strict control of uniformity, thickness and chemical structure. In addition, the reduction of GO into r-GO oxide produces a low quality graphene film with many defects, resulting in graphene with only a fraction of its theoretical capabilities. Thus GO and r-GO are limited to applications in which uniform monolayer GO or r-GO films are not vital, such as energy storage, material coatings/composites, transparent conductors and etc. Fortunately the reduction of GO is not the only promising method for large scale graphene synthesis, with chemical vapor deposition (CVD) making great strides over the last several years.

CVD graphene quality has been steadily increasing over the last several years, producing graphene with charge carrier mobility's[24-26], which are beginning to rival that of exfoliated graphene, while producing large uniform monolayer sheets[27-30]. While some research has focused on oxygenating CVD graphene or graphitic materials through oxygen plasma treatments[34], these treatments suffer from surface structure damage, non-uniform functionalization and additional processing steps, which hinder its future applications. Here, for the first time, we report the direct synthesis of uniform monolayer GO sheets by CVD on Copper

foils. The GO films monolayer nature are demonstrated by optical microscopy (OM), scanning electron microscopy (SEM), transmission electron microscopy (TEM) and atomic force microscopy (AFM), while its chemical and electronic structure is confirmed using Raman spectroscopy, X-ray and ultraviolet photoelecton spectroscopy (XPS, UPS) and energy dispersive x-ray spectroscopy (EDS). The ability to grow uniform GO films, along with the potential to control its oxygenation levels, allows for a new perspective on this long standing material, resulting in a "new" 2D material with a very high range of applications and potential.

5.2 Experimental and Results

A uniform monolayer GO film was grown via CVD on Cu foil, using a two-step growth process as shown in figure 5.1. The Cu foil was initially electro-polished aggressively in order to promote a self-limiting single layer graphene film with only a short precursor exposure time, as demonstrated previously[34]. The foil was then ramped up to 800o C under a 1:4 ratio of H_2 and Ar gas, at 700 Torr. Once at 800° C, the foil was exposed to a gas mixture of O_2/H_2 at a ratio of 1:2 for 3 minutes, oxygenating the Cu surface. Next the Cu was oversaturated with the graphene precursor gases, CH_4 and H_2, at a ratio of 1:2 for 5 minutes, resulting in the synthesis of a monolayer film of graphene on the Cu foil. The foil was then cooled down at a rate of 50° C/min, until it reached ambient room temperature, under the flow of H_2 and Ar gas. The Cu foil was then coated in Poly(methyl methacrylate) (PMMA) and electro-chemically delaminated from the

Cu foil in a 1 M solution NaOH and then transferred onto a 300 nm SiO$_2$/Si substrate for characterization.

The resulting GO film bears a similar resemblance to graphene films when viewed with the naked eye or under optical microscope as shown in figure 5.2a and figure 5.2b. In figure 5.2a, a continuous GO film transferred onto the center of an approximately piece of SiO2 wafer (approximately 2cm x 3cm in size) is shown. The contrast between the bare substrate and the
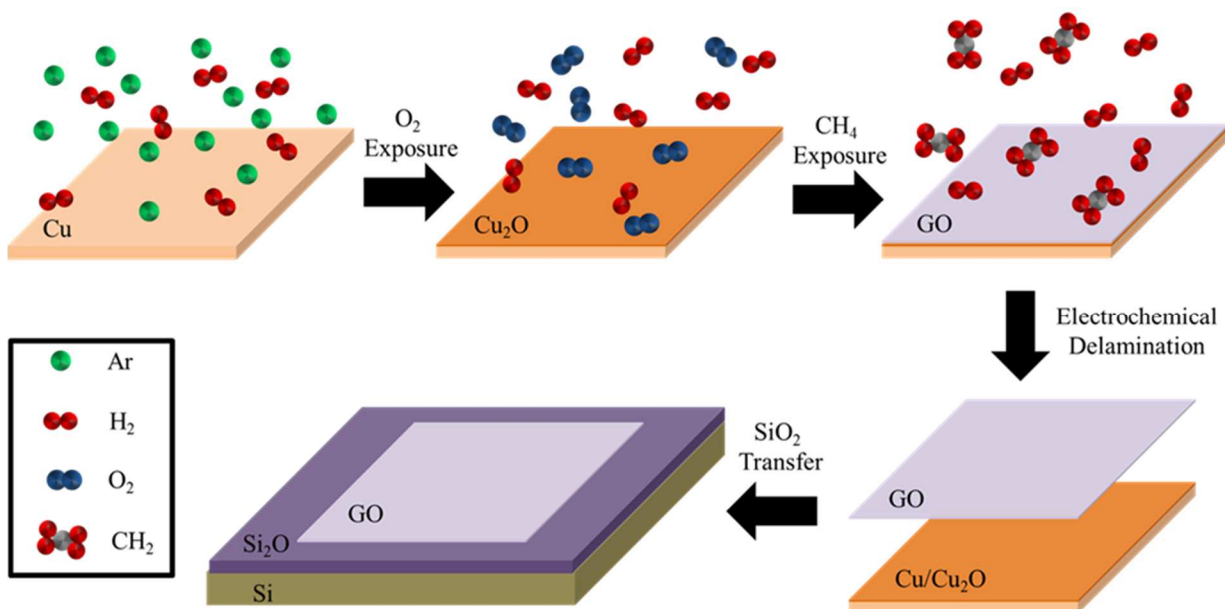
**Figure 5.1**: *Synthesis and transfer of graphene oxide film by Chemical vapor deposition.*

GO film is small but can be differentiated as with typical graphene films.   Figure 2b, shows the optical micrograph of the GO film and its edge at a magnification of 100 times. The contrast is more obvious now, but most importantly the film appears uniformly monolayer, while damaged and torn regions at the edge

appear to show bilayer and multilayer folds, which can be seen due to the increased contrast.

AFM was done on the edge of the GO film in order to determine the film thickness. Figure 5.2d shows the 2 dimensional mapping of the height profile of the film, as well as a sublet featuring the line height of the scan indicated by the red line. The sublet in 5.2d shows the average difference between the height of the substrate and the GO film was 1.33 nm. The thickness of pristine graphene has been measured to be 0.34 nm, while monolayer GO thicknesses measurements have been measured to be about 1.33 nm, which is higher than previously reported monolayer GO thicknesses[35,36] but still lower than bilayer GO. The line scan reveals an edge overshoot of almost 10nm as the tip scans from the bare substrate to the GO film. Since the region scanned was not on a folded region, it was initially believed to be an artifact of the AFM measurement. However after some consideration, there may be a second explanation for this height jump. It has been known that the edge of graphene and graphene oxide films can be highly defective, creating the presence of functional groups from the PMMA or the adsorption of water. This would result in physically creating a thicker edge or possibly disturbing the AFM cantilever with some other force. The AFM phase profile in the supplementary information suggest that the edges have a different chemical makeup than the bulk film or the substrate as shown in figure SI 1, however at this time were not able to determine the edge structure.
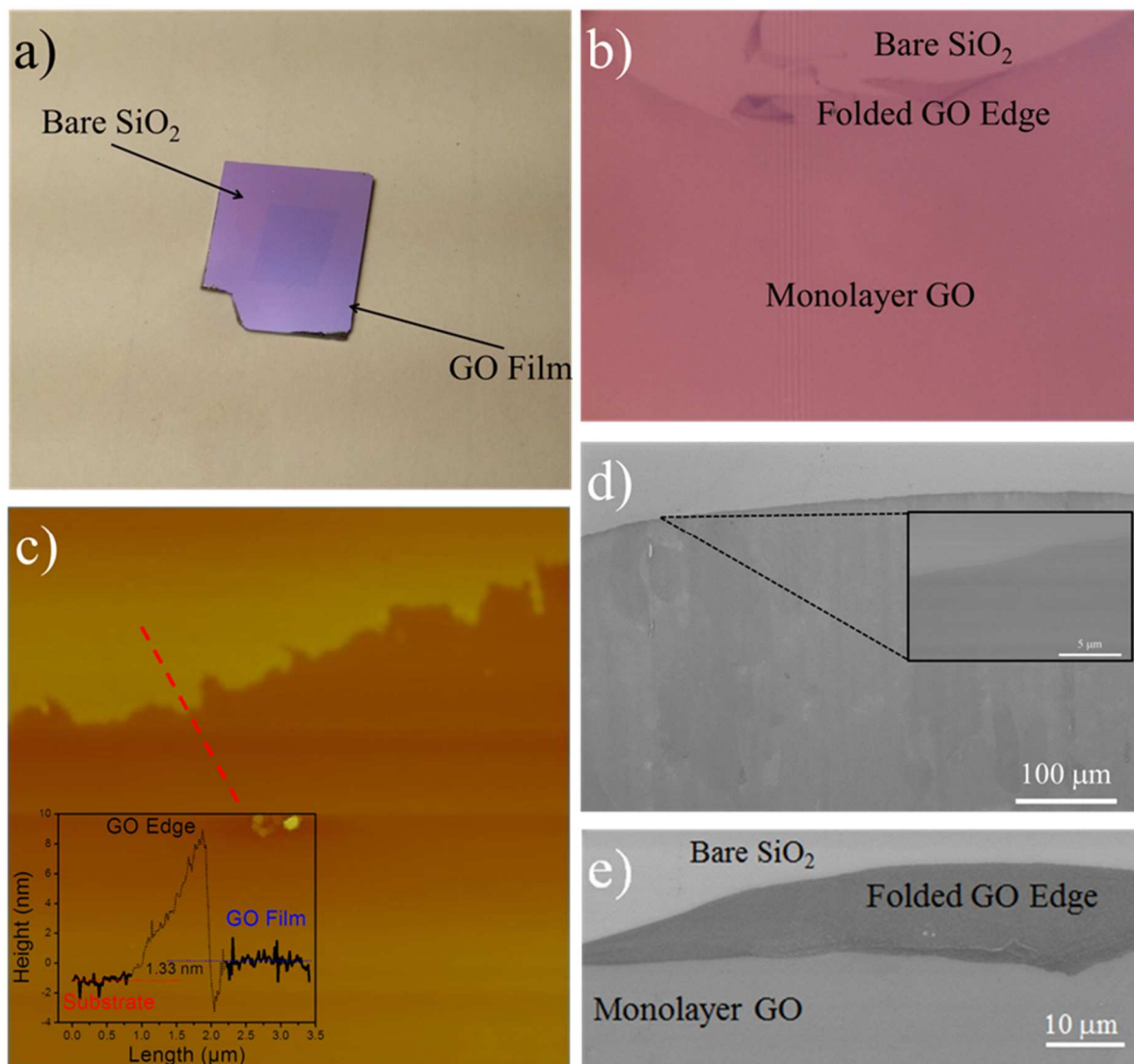
Figure 5.2: *Optical, atomic force and scanning electron microscopy images uniform GO films. a) Photograph of GO film on a SiO2 wafer. b) Optical image of GO film edge. c) AFM height scan of GO film edge, with line scan height inset (red dashed line). d) and f) SEM micrographs of GO edge and folded GO edge.*

In order to further confirm its continuity SEM was conducted at low and high magnification as shown in figure 5.2d and its inset. Again, SEM was taken at the edge of the film to show the contrast between the GO and the bare substrate. The film is continuous at low and high magnifications as seen in the sublet.   It can also be seen that the film transfer was relatively clean with no holes, tears or surface contamination. Interestingly at low magnification there were a lot of contrast differences within the GO film. Normally this could be attributed to an uneven graphene film, but since the monolayer nature of the film is confirmed through the optical microscopy and AFM, the contrast seen by SEM must be attributed to another phenomenon. Graphene is a conductive semimetal, however GO can range from insulator to semi-metallic depending on its oxygen concentration[19]. One possible explanation for the non-uniformity of the GO SEM image may be uneven surface charging due to different oxygenation levels or PMMA contamination. An SEM image of a folded edge of the GO film is shown in the figure 5.2e and the high degree of contrast between the few layer GO and the monolayer film demonstrates that the contrast variation seen in figure 5.2c could not possibly be due to uneven film deposition as the contrast between the single layer and bilayer GO is markedly striking, even more so than its optical counterpart. Figure 5.2e also shows the region which has folded over on itself several times, with the edge of the film pointing out of the substrate. The edge appears brighter than the monolayer or bilayer film, suggesting some charging of the edge of the film, possibly due to the presence of attached functional groups,

which would further provide evidence of the presence of some functional groups at the edge of the GO film.

Raman spectra of the GO film were taken at a film edge in which the edge had folded over on itself due to the transfer, resulting in multilayer regions. Point Raman spectra was taken in the bulk monolayer film, as well as double, triple and quadruple layer regions as shown in figure 3a, as indicated by the colored dots. Their spectra are shown in figure 5.3b, with each colored curve corresponding to its colored point in figure 5.3a. The Raman spectra show pronounced D and G peaks, centered around ~1342 cm-1 and ~1600 cm-1, respectively. For the monolayer region there is only the slightest hint of a G' peak at ~1700 cm-1 and a D+G peak at ~2900 cm-1. However as the number of layers increase from monolayer to 4 layers the G' and D+G peaks become more pronounced. The G peak is the signature peak of sp2 carbon structures, which indicates that this film is in fact graphitic; however the large D peak indicates very large disorder in the film[37]. The G' Raman peak is also a sp2 bond signature but in this case the presence of sp3 bonds dampens the intensity[38]. The pronounced D and G peaks with suppressed G' peaks measured here is the signature Raman characteristic and has been reported in previous literature[39,40]. It should be noted that the ratio of the intensity of the D and G peaks, ID:IG, for the monolayer GO is about 1.45, which has previously been a tool to measure the number of defects in graphene[41,42]. When compared to previous literature, a high ID:IG value such 1.45 is indicative of a high carbon to oxygen concentration

ratio, meaning there is a small concentration of (less than 15%) of C-O, C=O, and O=C-OH bonds in the GO.
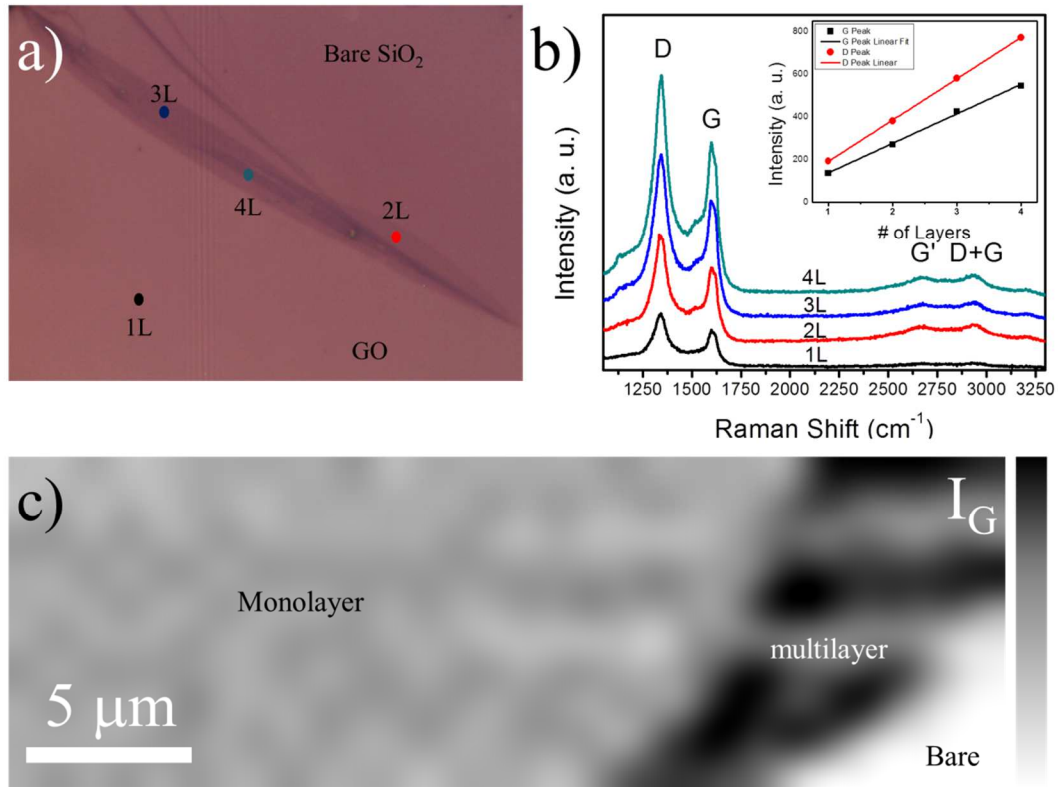
Figure 5.3: *Optical image of folded graphene oxide, Raman spectra and Raman mapping.*

The as the number of GO layers increases so does the intensity of the D and G peaks as well as the G' and D+G peaks as shown in figure 5.3b. The intensity increases linearly from 1 to 4 layers, as seen in the sublet of figure 5.3c, which is in agreement with previous literature. The intensity ratio, Id:IG, varies slightly between 1.39 and 1.46 between the 4 layers, but does not show any

significant trend (SI. 2). The G peak seems to vary between 1596-1600 cm-1, while the D peak varies from 1342-1346 cm-1, as the film is measured from 1 to 4 layers; however there is also no noticeable trend from one to 4 layers and could just as easily be an artifact of the Raman instrumentation. The shift data can be seen in the supporting information in figure SI. 3. Finally figure 5.3c shows the IG Raman mapping of and GO edge region with a bilayer/multilayer fold. The gray region indicates a uniform monolayer region, the dark grey and black regions indicated multilayer regions and the white region is bare SiO_2 substrate. The uniform intensity of the G peak in the monolayer indicates film is uniformly deposited.

Further spectroscopy was conducted using XPS in order to confirm the presence of oxygen in the graphene film. Figure 5.4 shows the XPS data taken of the monolayer GO film. The X's denote the experimental data, while the deconvoluted curves are shown by the solid colorful curves, and the sum of the curves is shown by the red dashed lines. The prominent peak (purple) located at 284.5 eV is the sp2 carbon peak, indicating the graphitic structure of the monolayer film9. There is also a peak (blue) at 285.6 eV, which corresponds to sp3 carbon bonds[43,44], which suggest that sigma bonding either with carbon or oxygen. The following three peaks in ascending intensity are at 286.5 eV (gold), 287.7 eV (green) and 288.9 eV (orange), which correspond to epoxide and hydroxyl groups, carbonyl groups and carboxyl groups, respectively[9,45]. This confirms the film is GO and not graphene. The C-O peak intensity is relatively

low compared to the C-C peak indicating a low concentration of oxygenation of the graphene surface. This is in agreement with our Raman data, which indicates the high ID:IG ratio would correspond to a low concentration of oxygen to carbon.
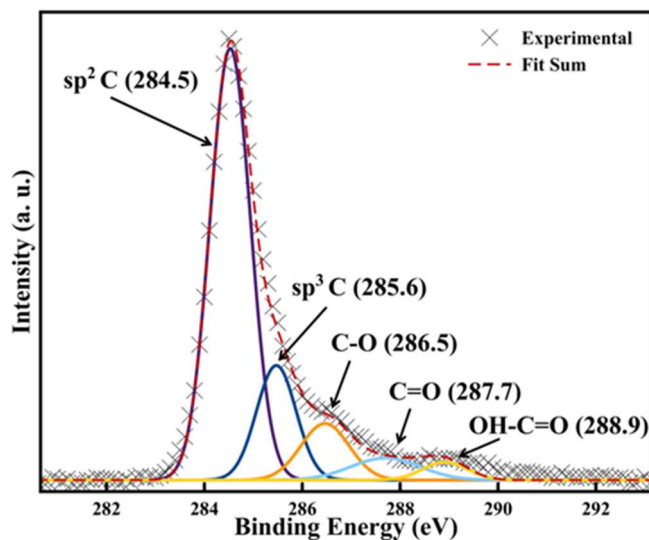
Figure 5.4: *XPS of monolayer graphene oxide film*.

5.3 Discussion

Although the exact growth mechanism cannot be determined in situ with our experimental setup, it is postulated that several competing reactions in the chamber are taking place in order to produce the GO film as shown in figure 6. Introducing O_2 and H_2 into the chamber, results in the oxygenation of the Cu surface, resulting in either a thin film of Cu_2O/CuO or just adsorbed oxygen on the Cu surface, as shown in figure 6a. However the presence of H_2 will have a two important roles in what happens to the oxygenated Cu. It may interact with

the oxygen to form OH groups on the surface, or it may begin to reduce the oxygen off of the Cu surface, leaving behind bare Cu or a hydrogenated Cu surface. With the consistent presence of O_2 and H_2 gases in the chamber during this step there is a competition of oxygen adsorption and reduction, continuously occurring until the CH_4 is introduced.

The use of O_2 gas in graphene synthesis has been demonstrated to produce large graphene crystal formation due to the passivation of the Cu defect sites, which would typically act as domain seeds for graphene growth as shown in figure 5.5b. This would result in a low domain density, thus resulting in graphene films with graphene crystals of up to several mm in size. Because these growths use low CH_4 exposure and long growth times of up to several hours, the oxygen on the Cu surface is readily consumed by several reactions including, hydrogen to form H_2O or carbon to form CO and CO_2. Thus, as shown by figure 5.5b, by the time the graphene film is formed there is little or no presence of oxygen on the Cu surface. This mechanism described above is the result of oxygen adsorption onto the Cu surface, but there has been previous research to demonstrate that oxidation of the Cu surface, can be utilized as a self-cleaning substrate once the copper oxide is reduced back to Cu at high temperatures. This has also resulted in large graphene domain synthesis and thus must be taken into consideration when trying to discuss the synthesis of GO.
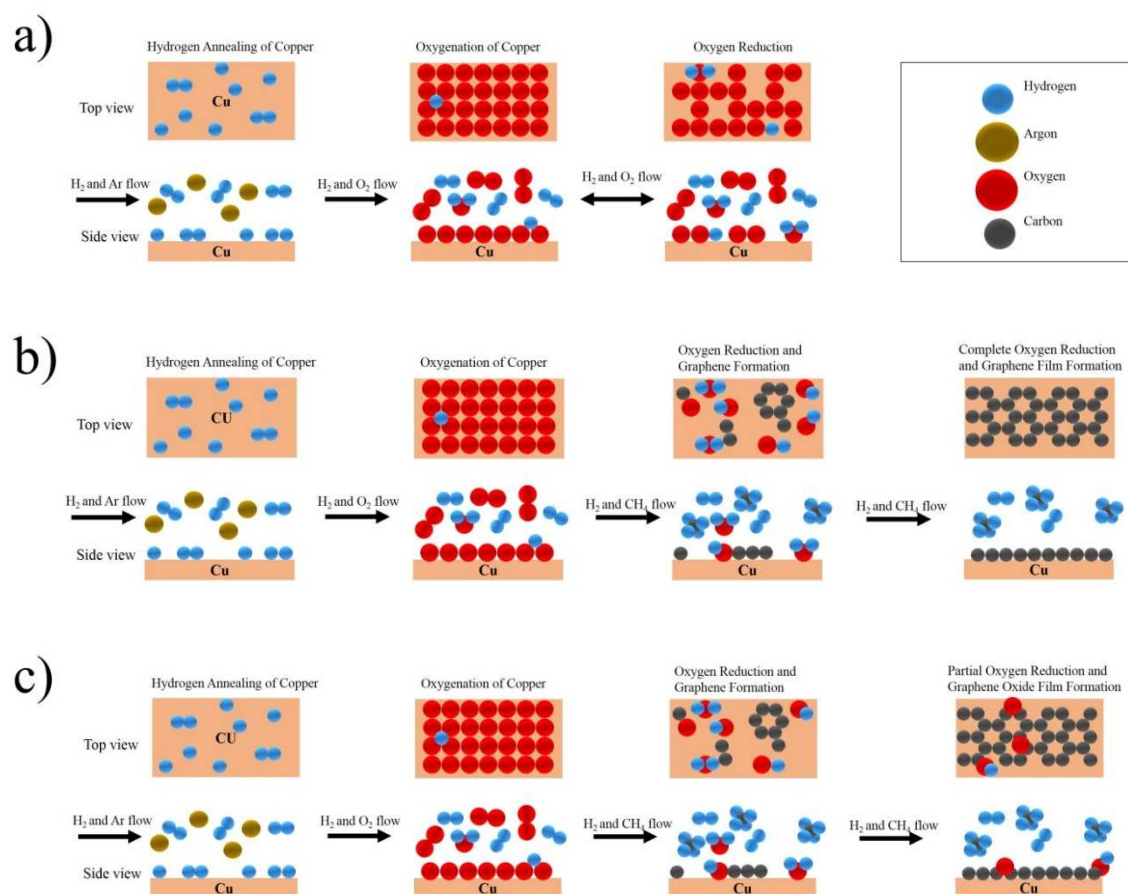
Figure 5.5: *Various Cu surface states. a) Surface of Cu when exposed to O2 and H2 at high temperature. b) Graphene synthesis after O2 exposure and slow and low CH4 exposure to form uniform graphene film. c) The formation of graphene oxide after Cu exposure to O2 and rapid and oversaturation of CH4.*

Figure 5.5c shows what is speculated to be the growth mechanism of the GO film. The introduction of O_2 and H_2, again, results in the formation of an

oxygenated surface, while simultaneously being reduced, with this action

repeated throughout the oxygenation step. Because the high exposure of

oxygen it is believed that the Cu surface will be highly oxygenated by the time the

CH4 is introduced. Because we saturate the Cu with a the graphene forming

precursors, the graphene film forms rapidly before the oxygen has had a time to

reduce completely. Thus the oxygen, OH groups and C-O groups are

incorporated into the graphene lattice resulting in the formation of GO. It is

unclear whether once the GO film is formed if the reduction of oxygen continues

or not, but if it does it may create a scenario where once the GO film is formed,

the any excess time afterwards may result in the reduction of the GO film, and

quite possibly the repair of the film to form elemental graphene. This may

possibly explain why the oxygen levels are low, but may also be a potential route

towards controlling the oxygen concentration.

5.4 Conclusion

Thus we have demonstrated the first synthesis of uniform monolayer

graphene oxide films by CVD. The uniformity and monolayer nature was

confirmed through OM, SEM and AFM, while the presence GO was

demonstrated by Raman spectroscopy and XPS. This is the first truly scalable

synthesis of uniform GO films, as well as the only scalable demonstration of

monolayer GO films. The potential of this material to open up new avenues of

applications for graphene is very high. Future work to advance this study will

concentrate on the growth mechanism of GO, controllable oxygen concentration

and its electrical properties. If direct understanding of the growth mechanism can provide a method for controlling the oxygen concentration in the GO film, then the realizable formation of a band gap is sure to follow thereafter.

References

1   Novoselov, K. S. et al. Electric field effect in atomically thin carbon films. science 306, 666-669 (2004).

2   Ionescu, R. et al. Oxygen etching of thick MoS 2 films. Chemical Communications 50, 11226-11229 (2014).

3   Kim, K. K. et al. Synthesis of monolayer hexagonal boron nitride on Cu foil using chemical vapor deposition. Nano letters 12, 161-166 (2011).

4   George, A. S. et al. Wafer Scale Synthesis and High Resolution Structural Characterization of Atomically Thin MoS2 Layers. Advanced Functional Materials 24, 7461-7466 (2014).

5   Mak, K. F. et al. Tightly bound trions in monolayer MoS2. Nature materials 12, 207-211 (2013).

6   Lee, G.-H. et al. Electron tunneling through atomically flat and ultrathin hexagonal boron nitride. Applied Physics Letters 99, 243114 (2011).

7   Wang, H. et al. Integrated circuits based on bilayer MoS2 transistors. Nano letters 12, 4674-4680 (2012).

8   Dean, C. et al. Boron nitride substrates for high-quality graphene electronics. Nature nanotechnology 5, 722-726 (2010).

9   Dreyer, D. R., Park, S., Bielawski, C. W. & Ruoff, R. S. The chemistry of graphene oxide. Chemical Society Reviews 39, 228-240 (2010).

10   Eda, G., Fanchini, G. & Chhowalla, M. Large-area ultrathin films of reduced graphene oxide as a transparent and flexible electronic material. Nature nanotechnology 3, 270-274 (2008).

11   Stankovich, S. et al. Synthesis of graphene-based nanosheets via chemical reduction of exfoliated graphite oxide. Carbon 45, 1558-1565 (2007).

12   Gómez-Navarro, C. et al. Electronic transport properties of individual chemically reduced graphene oxide sheets. Nano letters 7, 3499-3503 (2007).

13   Hummers Jr, W. S. & Offeman, R. E. Preparation of graphitic oxide. Journal of the American Chemical Society 80, 1339-1339 (1958).

14   Marcano, D. C. et al. Improved synthesis of graphene oxide. ACS nano 4, 4806-4814 (2010).

15   Staudenmaier, L. Verfahren zur darstellung der graphitsäure. Berichte der deutschen chemischen Gesellschaft 31, 1481-1487 (1898).

16   Staudenmaier, L. Verfahren zur Darstellung der Graphitsäure. Berichte der deutschen chemischen Gesellschaft 32, 1394-1399 (1899).

17   Lai, L. et al. One-step synthesis of NH 2-graphene from in situ graphene-oxide reduction and its improved electrochemical properties. Carbon 49, 3250-3257 (2011).

18   Huang, H., Li, Z., She, J. & Wang, W. Oxygen density dependent band gap of reduced graphene oxide. Journal of Applied Physics 111, 054317 (2012).

19   Eda, G., Mattevi, C., Yamaguchi, H., Kim, H. & Chhowalla, M. Insulator to semimetal transition in graphene oxide. The Journal of Physical Chemistry C 113, 15768-15771 (2009).

20   Mattevi, C. et al. Evolution of electrical, chemical, and structural properties of transparent and conducting chemically derived graphene thin films. Advanced Functional Materials 19, 2577-2583 (2009).

21   Loh, K. P., Bao, Q., Eda, G. & Chhowalla, M. Graphene oxide as a chemically tunable platform for optical applications. Nature chemistry 2, 1015-1024 (2010).

22   Eda, G. et al. Blue photoluminescence from chemically derived graphene oxide. Advanced Materials 22, 505-509 (2010).

23   Luo, Z., Vora, P. M., Mele, E. J., Johnson, A. C. & Kikkawa, J. M. Photoluminescence and band gap modulation in graphene oxide. Applied physics letters 94, 111909 (2009).

24   Chen, B. et al. How good can CVD-grown monolayer graphene be? Nanoscale 6, 15255-15261 (2014).

25   Gannett, W. et al. Boron nitride substrates for high mobility chemical vapor deposited graphene. Applied Physics Letters 98, 242105 (2011).

26   Calado, V. et al. Ballistic transport in graphene grown by chemical vapor deposition. Applied Physics Letters 104, 023103 (2014).

27   Ruiz, I., Wang, W., George, A., Ozkan, C. S. & Ozkan, M. Silicon Oxide Contamination of Graphene Sheets Synthesized on Copper Substrates via

Chemical Vapor Deposition. Advanced Science, Engineering and Medicine 6, 1070-1075 (2014).

28   Li, X. et al. Large-area graphene single crystals grown by low-pressure chemical vapor deposition of methane on copper. Journal of the American Chemical Society 133, 2816-2819 (2011).

29   Hao, Y. et al. The role of surface oxygen in the growth of large single-crystal graphene on copper. Science 342, 720-723 (2013).

30   Chen, S. et al. Millimeter-Size Single-Crystal Graphene by Suppressing Evaporative Loss of Cu During Low Pressure Chemical Vapor Deposition. Advanced Materials 25, 2062-2065 (2013).

31   Wang, W. et al. Improved functionality of graphene and carbon nanotube hybrid foam architecture by UV-ozone treatment. Nanoscale 7, 7045-7050 (2015).

32   Gokus, T. et al. Making graphene luminescent by oxygen plasma treatment. ACS nano 3, 3963-3968 (2009).

33   Nourbakhsh, A. et al. Bandgap opening in oxygen plasma-treated graphene. Nanotechnology 21, 435203 (2010).

34   Isaac Ruiz, Z. M., Robert Ionescu, Lauro Zavala, Cengiz Ozkan, Mihrimah Ozkan. Copper Surface Morphology Effect on Rapid and Uniform Synthesis of Graphene Sheets by Chemical Vapor Deposition (2015).

35   Gao, W., Alemany, L. B., Ci, L. & Ajayan, P. M. New insights into the structure and reduction of graphite oxide. Nature chemistry 1, 403-408 (2009).

36   Li, D., Müller, M. B., Gilje, S., Kaner, R. B. & Wallace, G. G. Processable aqueous dispersions of graphene nanosheets. Nature nanotechnology 3, 101-105 (2008).

37   Dresselhaus, M. S., Jorio, A., Hofmann, M., Dresselhaus, G. & Saito, R. Perspectives on carbon nanotubes and graphene Raman spectroscopy. Nano letters 10, 751-758 (2010).

38   Ferrari, A. et al. Raman spectrum of graphene and graphene layers. Physical review letters 97, 187401 (2006).

39   Cuong, T. V. et al. Photoluminescence and Raman studies of graphene thin films prepared by reduction of graphene oxide. Materials letters 64, 399-401 (2010).

40   Zhou, X. et al. In situ synthesis of metal nanoparticles on single-layer graphene oxide and reduced graphene oxide surfaces. The Journal of Physical Chemistry C 113, 10842-10846 (2009).

41   Eckmann, A. et al. Probing the nature of defects in graphene by Raman spectroscopy. Nano letters 12, 3925-3930 (2012).

42   Cançado, L. G. et al. Quantifying defects in graphene via Raman spectroscopy at different excitation energies. Nano letters 11, 3190-3196 (2011).

43   Pukha, V. et al. Growth of nanocomposite films from accelerated C60 ions. Journal of Physics D: Applied Physics 45, 335302 (2012).

44   Chidembo, A. T. et al. In situ engineering of urchin-like reduced graphene oxide–Mn 2 O 3–Mn 3 O 4 nanostructures for supercapacitors. RSC Advances 4, 886-892 (2014).

45   Yang, D. et al. Chemical analysis of graphene oxide films after heat and chemical treatments by X-ray photoelectron and Micro-Raman spectroscopy. Carbon 47, 145-152 (2009).